Development of a ‘tool box’ for generating designer nucleosomes in high throughput fashion

Dissertation

for the award of the degree

”Doctor rerum naturalium” (Dr. rer. nat.)

Division of Mathematics and Natural Science

of the Georg-August-Universität Göttingen

with the doctoral program:

GGNB Biomolecules - Structure - Function - Dynamics

submitted by

Henriette Mahler

born in Jena, Germany

Göttingen 2016

Thesis committee members:

Prof. Dr. Wolfgang Fischle (1st reviewer), Research Group of Chromatin Biochemistry, King Abdullah University of Science and Technology, Thuwal (SAU)

Prof. Dr. Heinz Neumann, Max-Planck-Institut für Molekulare Physiologie, Dortmund

Prof. Dr. Dirk Schwarzer, Interfakultäres Institut für Biochemie, Eberhard Karls Universität Tübingen

Extended thesis committee:

Prof. Dr. Henning Urlaub, (2nd reviewer), Research Group Bioanalytical Mass Spectrometry, Max-Planck-Institut für Biophysikalische Chemie, Göttingen

Prof. Dr. Claudia Hörbartner, Institute for Organic and Biomolecular Chemistry, Georg August Universität Göttingen

Prof. Dr. Steven Johnsen, Translational Cancer Research, University Medical Center Göttingen

Date of oral examination: December 22nd, 2016

I affirm that the presented thesis “Development of a ‘tool box’ for generating designer nucleosomes in high throughput fashion” has been written independently and with no other sources and aids than quoted.

Göttingen, November 10^{th}, 2016 Henriette Mahler

Acknowledgements

First and foremost, I would like to thank Prof. Dr. Wolfgang Fischle for his constant support and guidance as well as for his constructive criticism throughout my thesis.

I thank my thesis committee members Prof. Dr. Heinz Neumann and Prof. Dr. Dirk Schwarzer for their interest in my project, their time for fascinating discussions, and their helpful suggestions.

Many thanks go to my collaborators Prof. Dr. Dirk Schwarzer and Diego Aparicio Pelaz for the fruitful development of the nucleosome library and for the helpful and inspiring discussions.

I want to thank the GGNB for the constant support, informative lectures, and highly supportive method courses.

I am grateful to Prof. Dr. Henning Mootz for his support and discussions about protein *trans*-splicing.

My sincere thanks to all past and present lab members of the Chromatin Biochemistry group at the MPI as well as at KAUST. I enjoyed working with you. Thanks for the good atmosphere inside and outside the lab, for your support as well as for the endless discussions.

I want to thank Lydia Abdelhalim for running the daily lab business.

I especially thank my family for their constant encouragement, their belief in me, and unconditional support. None of this would have been possible without you.

Thank you, Jörg, for being there for me.

Contents

List of Figures

List of Tables

List of Abbreviations

aa	amino acid
ALPHA	amplified luminescent proximity homogeneous assay
ATP	adenosine triphosphate
a.u.	arbitrary units
BA-plates	binding assay plates
bp	base pair
Btn	biotin
°C	degree Celsius
Ci	Curie
cm	centimeter
CPM	counts per minute
CV	column volume
Cy5	cyanine 5 dye
d	optical path length
Da	Dalton in g/mol
ddH_2O	double-distilled water
DNA	deoxyribonucleic acid
ECL	enhanced chemiluminescence
e.g.	exempli gratia, for example
ε	extinction coefficient
eq	equivalent
FAM	carboxyfluoresceine
FL	full-length
Fwd	forward
g	gramme
GCN5	general control non-repressed 5
h	hour
H3um	histone H3 unmodified
HAT	histone acetyltransferase
HDAC	histone deacetylase
his-tag	polyhistidine-tag
HKMT	histone lysine methyltransferase
HP1	heterochromatin protein 1
HRP	horseradish peroxidase
INCENP	inner centromere protein
IntC	intein C-terminal part
IntN	intein N-terminal part
i.e.	id est, that is
k	kilo
KD	kinase domain
K_D	dissociation constant
L	liter
LSD	lysine specific demethylase
m	milli or meter
μ	micro
mol	mole
M	molar mol/L
MS	mass spectrometry
MW	molecular weight
MWCO	molecular weight cut off
n	nano
NaP_i	sodium phosphate buffer
ON	over night
PADI	peptidylarginine deiminase
PAGE	polyacrylamide gel electrophoresis

PCR	polymerase chain reaction
PDB	protein data base
p	pico
PRMT	protein arginine methyltransferase
PTM	post-translational modification
rcf	relative centrifugal force
Rev	reversed
rpm	rounds per minute
RS	restriction site
RT	room temperature
SD	standard deviation
sec	second
SP	splice product
SPPS	solid phase peptide synthesis
ssDNA	sonicated salmon sperm DNA
STA	streptavidin
TAMRA	carboxytetramethylrhodamine
Tg	tetraethylene glycol
TR-FRET	time resolved Förster resonance transfer
UV	ultra violet
V	volt
WB	wash buffer
WT	wild type

1 Introduction

1.1 Chromatin

A 'blueprint' of any organism is encoded in the DNA of every one of its cells. During development, cells differentiate and become specific. The regulation of development, maintenance of a certain state, and reaction to external impacts take place on chromatin. Chromatin describes the organization of DNA, histones, and non-histone proteins[1]. Chromatin can be separated into euchromatin and heterochromatin. Euchromatin describes areas with loosely packed DNA, available for chromatin remodelers, transcription factors, and polymerases; these regions are transcriptionally active. In contrast, heterochromatin describes well-ordered and densely packed DNA in fibers that is in general transcriptional silent[2]. The nucleosome is known to be the smallest building block of chromatin's highly complex and dynamic structure[1].

1.2 Chromatin structure

1.2.1 The nucleosome core particle

The nucleosome core particle (NCP) is a complex of DNA wrapped in 1.65 turns around an octameric core composed of a H3-H4 tetramer and two H2A-H2B dimers. Histones are small, highly basic proteins that are conserved among species. All four histone types have the histone fold in common that describes the folding of three α-helices connected by a short loop region, together referred to as the globular domain. The α-helices form a 'u'-like structure with the 1^{st} and the 3^{rd} α-helices stretching out of the plane in opposite directions, slightly skewing the 'u' shape (figure 1.1)[3].

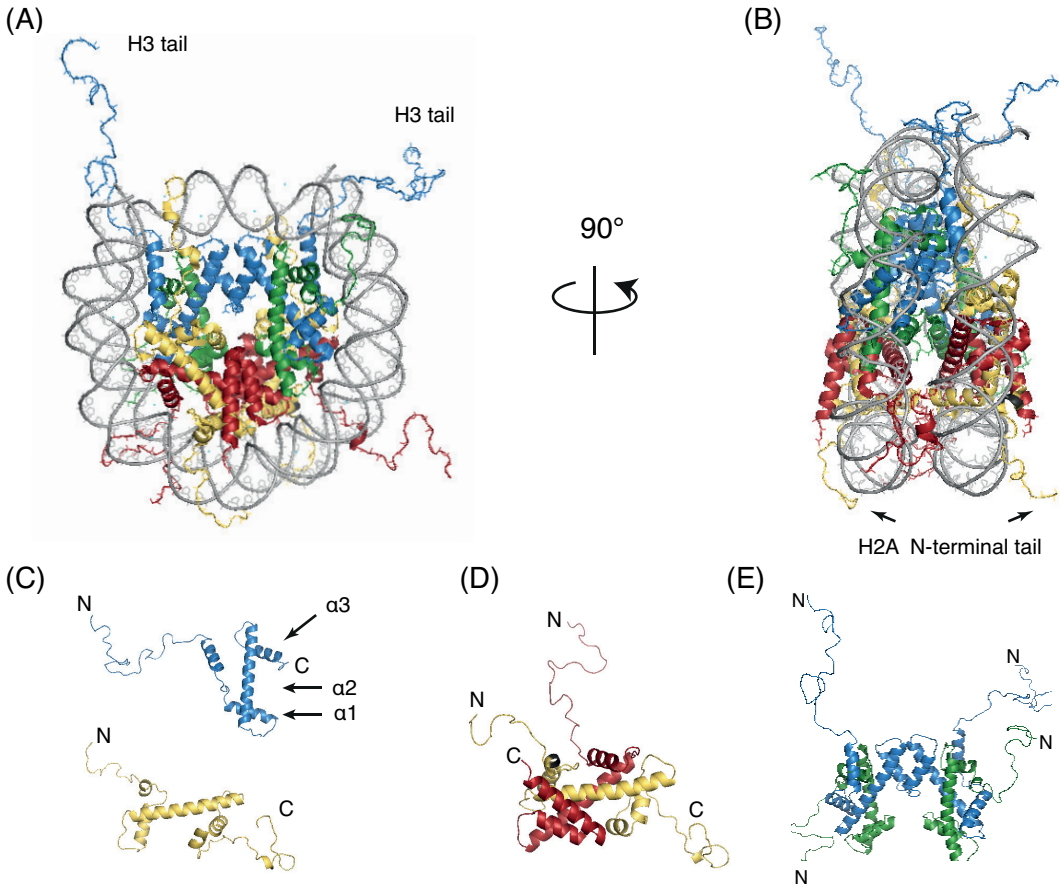

Figure 1.1: Crystal structure of the nucleosome core particle
Crystal structure of nucleosome core particle[3], PDB identification number: 1KX5. Histones and DNA are shown in yellow (H2A), red (H2B), blue (H3), green (H4) and gray (DNA). (A) frontal view on the NCP. (B) 90° rotation of (A). (C) Histone fold of H3 (blue) and H2A (yellow), α-helices 1-3 are shown on the example of H3; N- and C-terminus are marked with N and C, respectively. (D) Structure of H2A-H2B dimer within the NCP based on 1KX5. (E) Structure of H3-H4 tetramer within the NCP based on 1KX5.

Several interactions between histones and DNA keep both components in place. For example, ionic interactions of the phosphodiester backbone of the DNA, with lysine residues of the histone globular domain. Hydrogen bonds stabilize the complex between DNA phosphates and α-amides of amino acids within the α-helices of the histones, as well as non-polar interactions of the deoxyribose with the histone[3;4].

The N-termini of all four histones and C-termini of H2A and H2B stick out of the nucleosome core and can be accessed by nuclear proteins[3;4]. These histone tails are 20-30 amino acids long, unstructured and carry a wide range of post-translational modifications[5].

In vivo, the NCP assembly process is regulated by chromatin assembly factors and histone chaperones[6;7]. *In vitro*, the NCP can assemble without such factors and is thought to proceed via an all components detached state (DNA + H2A/H2B dimer + H3/H4 tetramer) over an intermediate DNA-H3/H4 tetrasome, for which the H2A/H2B dimer associate to form the NCP.

1.2.2 Chromatin folding in higher-order structures

The nucleosome has been found to be the smallest building block of chromatin and its highly complex and dynamic structure. Here, the first layer of compaction is achieved by linear arrangement of NCPs separated by 10-80 bp of linker DNA into a 11 nm high structure like 'beads on a string'[8;9]. For the further organization of the 11 nm high structure based on *in vitro* studies, two models have been proposed to form a 30 nm high fiber. The 'selenoid' model describes a scenario where the 11 nm high fiber is coiled around an axis of symmetry with slightly tilted NCPs connected by a DNA linker, thereby forming a 'tube' of 30 nm high[10;11]. Another model proposes a zig-zag ribbon-like structure that forms a compact helical ribbon with NCPs arranged face-to-face[12;13]. However, a variety of 30 nm high structures have been proposed based on *in vitro* and *in situ* studies. Less clear, however, is the picture of chromatin folding beyond the 30 nm fiber, though it likely contains long-range interactions and looping of chromatin fibers[14].

1.3 Post-translational modifications of histones

Up to date, there are many different known PTMs, e.g. modifications with rather small moieties such as acetylation, methylation, phosphorylation and deamination, or larger moieties such as ubiquitinylation, sumoylation, ADP-ribosylation, propylation and butylation[5]. Amongst the histones, H3 and H4 carry the most PTMs, whereas H2A possesses only few modifications on its N-terminus. In addition, H2A and H4 have the first 5 amino acids in common, which makes the investigation of the biologic purpose of modifications at these sites especially challenging[15].

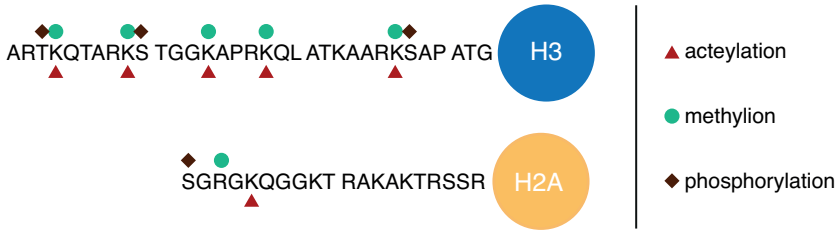

Figure 1.2: Selected histone modification of H3 and H2A
Globular domain of H3 (blue) and H2A (yellow) with sequence of N-terminal histone tail. Modification sites used in this study are marked for acetylation, methylation and phosphorylation with triangle, circle and diamond respectively.

1.3.1 Acetylation and phosphorylation

The acetylation of lysine residues is one of the longest known and most studied histone modification[16;17]. It has been found to disrupt higher-order chromatin structure and to facilitate transcription[18;19]. It is predominant in euchromatin and almost absent in heterochromatin[20]. The existing positive charge is transformed via acetylation of the basic lysine ε-amino group in the N-termini of histones, thus changing the affinity of the DNA to the histones and generating loosely packed DNA that is available for transcription factors and polymerases[21–23]. Additionally, the introduction of an acetyl-group provides a recognition mark for proteins to interact with[20]. This mark is set by HATs, removed by HDACs, and read by the bromo- and certain tandem-PHD-domains[24;25]. Acetylation of histones can be carried out in two different modes. Some HATs acetylate nucleosomes target specific lysines, while others acetylate rather globally, in an untargeted manner[26].

Table 1.1: Histone H2A and H3 modification and their associated function adapted from Lawrence *et al.*[5]

Histone modification	Associated function
H2AS1ph	Mitosis
H2AK4/5 ac	Transcriptional activation
H2AK7ac	Transcriptional activation
H3K4me2	Permissive euchromatin
H3K4me3	Active euchromatin
H3K9me3	Heterochromatin, transcriptional repression
H3K27me3	Transcriptional silencing
H3K36me3	Transcriptional elongation
H3K4ac	Transcriptional activation

Table 1.1 – continued from previous page

Histone modification	Associated function
H3K9ac	Transcriptional activation
H3K14ac	Transcriptional activation
H3K18ac	Transcriptional activation
H3K23ac	Transcriptional activation
H3K27ac	Transcriptional activation
H3T3ph	Mitosis
H3S10ph	Mitosis, meiosis and transcriptional activation
H3T11ph/S28ph	Mitosis

Abbreviatons:
H2A/H3 – histone H2A/H3
S – serine; K – lysine; T – threonine (followed by the residue number)
me2/3 – di-/tri methylation; ph – phosphorylation; ac – acetylation

H2A carries post-translational modification on the N-terminus: α-N-acetylation of H2AS1 and ε-acetylation of H2AK5, H2AK9, H2AK13 and H2AK15[27;28]. Whereas acetylation are observed on H3 tails on basically every lysine residue, H3K4, H3K9, H3K14, H3K18, H3K23 and H3K27 are associated with transcriptional activation as summarized in table 1.1[5]. While acetylation neutralizes the positive charge of lysine residues, the phosphorylation of serines or threonines introduces a negative charge. This influences the interaction with DNA, but also provides an additional recognition mark for interacting with effector proteins[29]. Phosphorylation sites are in general serines, threonines and thyrosines. The mark is placed by kinases and removed by phosphatases[30]. In the context of phosphorylated histones, the only domains known to interact with phosphorylated serines and threonines are 14-3-3 proteins and the BRCT domain[25;31]. Phosphorylations on histone H3 play a key role during mitosis by regulating its neighbor availability for binding partners. Phosphorylation has been associated with both transcription activation and silencing[29]. For example, HP1 binds H3K9me3, but the phosphorylation of H3S10 disrupts this interaction[32;33]. During mitosis, the serine 1 of H2A and H4 were found to be highly phosphorylated and less during S-phase[34]. Although histone H2A and H4 have the first 5 amino acids in common, it was shown that S1ph of H4 and H2A occurred at different stages during the development of *Xenopus laevis*[15]. Furthermore, phosphorylation together with acetylation on the same histone tail seems to have an enhancing effect on the activity on HAT. For GCN5, an enhanced acetylation activity on H3K14 was observed when H3S10 was phosphorylated[32].

1.3.2 Methylation

Methylation on lysine residues

Whereas acetylation is mainly found in transcriptionally active regions, methylation marks are common in both eu- and heterochromatic structures[35]. In contrast to acetylation and phosphorylation, methylation does not change the overall charge of the residue, but rather provides different handles by mono-, di-, or tri-methylation of the ε-amino group of lysines. Methyl marks are placed site-specifically by HKMTs. The first discovered HKMT was the human SUV39H1, which methylates H3K9, the docking site for HP1[36;37]. Almost every HKMT contains the catalytic SET domain which activates the methyl group from SAM and transfers it to the lysine residue of histones[38]. The site selectivity and methylation degree is thereby conveyed by the enzyme. Whether a HKMT only catalyzes the mono-methylated state or the di- and tri-methylated states as well depends on the spatial properties of the catalytic domain[37].

Removal of methylation marks is carried out by LSD, which are only able to remove mono- and di-methyl marks, whereas Jumonji demethylases are able to remove all three methylation states on lysines[38;39]. The mark is read by protein domains belonging to the royal superfamily consisting of chromo, double chromo-, double and tandem tudor-, as well as MBT-domains and the PHD-finger family. Whether these domains bind higher or lower methylation states of lysines depends on their binding pocket. Here, selective recognition of tri-methylated lysine residues is facilitated by stabilizing the target methylammounium group in an aromatic cage, thus stabilizing its positive charge via π-interaction by these aromatic residues and additional hydrophobic interactions[31]. In contrast, lower methylation states are stabilized within the binding pocket via hydrogen bonds. Additionally, the binding pocket is rather small, guaranteeing the binding of lower modification states. Consequently, tri-methylated lysines that demand large binding pockets are not recognized[31].

Abundant methylation sites on the histone H3 tail are K4, K9, K27, and K36[40]. Methylation of H3K4 hallmarks transcriptionally active chromatin. Nonetheless, in embryonic stem cells the euchromatic mark H3K4me3 and the heterochromatic mark H3K27me3 are found to coexist in silenced chromatin and form bivalent domains[35].

Different methylation states seem to have different purposes. It was shown in mice for

the methylation on lysine 9 of histone H3 that H3K9me3 is localized at pericentric heterochromatin, whereas H3K9me1/2 are found in silenced euchromatin[41–43]. Additionally, H3K27me2 is the predominant modification state in mouse embryonic stem cells, and is mutually exclusive with the H3K27me1 that is present in the core of expressed genes and the H3K27me3 that is connected to gene repression[44].

Methylation on arginine residues

Arginine residues can also be mono- and di-methylated at their guanidino group. The dimethylated state occurs either on the same (asymmetric) or on two different (symmetric) nitrogens of the guanidino group. The mark is placed by PRMTs using SAM as the methyl donor. There are two types of PRMTs; both types are able to mono-methylate arginines. They differ in their dimethylation product, whereas PRMT type I dimethylates arginines asymmetric (R_{2A}), type II PRMTs catalyze symmetric dimethylation marks (R_{2S})[38]. How the mark is removed is not yet entirely clear. Unmethylated arginines can be deiminated by PADIs, resulting in citrulline, thus preventing methylation. Whether Jumonji6 also has demethylase activity for arginine was debated for quite some time. Recently, it was found that certain Jumonji lysine demethylases are also able to demethylate arginines of histone peptides[45;46].
Asymmetric methylation of R3 of histone H2A and H4 is placed by PRMT1&6. This mark has been linked to gene activation. In contrast, symmetric methylation of H2A/H4-R3 by PRMT5&7 has been related to gene repression[45]. A study focusing on H2A arginine methylation could show that only H2AR3me was incorporated into chromatin after fertilization but not H2AR3me$_{2S}$, both PTMs are placed by PRMT5 in the oozyte of *Xenopus laevis*[47].

1.4 Chromatin effector proteins

Post-translational modifications on histones can act in two ways on chromatin. Firstly, by directly changing chromatin structure, and secondly, by recruiting effector proteins to chromatin, which in turn can have an indirect impact on chromatin structure[23;48;49]. Effector proteins are classified by their impact on chromatin: (1) Chromatin remodeling complexes

which are able to slide nucleosomes along the DNA in an ATP dependent manner. (2) Complexes mediating stability for higher order chromatin structure and (3) Enzymes 'writing' or 'erasing' post-translational modifications[35;50].

1.4.1 Histone acetyltransferase: GCN5

Histone acetyltransferases have been studied since the 1970s and categorized into HATs type A and B. While HATs type B are present in the cytoplasm and are acetylating free, *de novo* synthesized histones, type A HATs are found in the nuclei of acetylated histones within the nucleosome and are connected to transcriptional activation[20]. GCN5 is an A-type HAT and the eponyme of the GNAT family (GCN5 related N-acetyltransferases) that shares highly conserved features such as the HAT domain and an C-terminal bromo domain[26;51]. In *Saccharomyces cervisiae* GCN5 plays a role as a transcriptional co-activator in the activation of certain genes by acetylating histones within the promotor region of target genes[52;53].

Figure 1.3: Domain organization of GCN5
Localization of histone acetyl transferase domain (HAT) 100-255 aa and the acetylated–lysine-recognizing bromo domain (Bromo) 344-414 aa of GCN5 from yeast with N- and C-terminus labeled with N and C, respectively.

The HAT domain of GCN5 catalyzes the transfer of the acetyl group from AcCoA to the ε- amino group of the lysine residue via a tetrahedral intermediate. The nucleophilic attack of AcCoA is initiated by deprotonation of the ε- amino group by E173 of GCN5[54]. GCN5 first binds AcCoA, and only then it does gain an affinity for H3 binding[26].
The bromo domain of GCN5 binds to acetylated lysine residues with rather low affinity ($K_D = 1$ mM), thereby favouring positively charged residues neighboring the binding site[55]. GCN5 binds 11 amino acids of the histone H3 tail from R8 to Q19. When H3S10 is phosphorylated H3T11 makes additional contacts with GCN5. On the H3 peptide level, GCN5 from *Tetrahymena* prefers substrates phosphorylated on H3S10 and acetylates H3K14[56]. H3S10ph and H3K14ac together enhance the activity of GCN5. Certain promotors require the independent binding of both the kinase responsible for phosphorylation and the HAT for acetylation of histones for activation, while other promotors recruit the HAT in an H3S10ph-

dependent manner[29;57].

In vitro GCN5 is found to be solely active on nucleosomes when it forms the SAGA (Spt-Ada-GCN5 acetyltransferase) or the ADA complex (Ada-GCN5-acetlytransferase)[52]. Under certain experimental *in vitro* conditions, however, recombinant GCN5 is found to acetylate nucleosomes[58]. The SAGA complex preferentially hyperacetylates H3K4me3 nucleosomes over unmodified H3K4. This has not been observed on the H3 peptide level. Within the SAGA complex, recognition is carried out by the tandem Tudor domain of Sgf29. Enhancement in H3K4me2-dependent hyperacetylation was only observed on the histone H3, whereas the acetylation rate of histone H4 was unaffected[59]. A study by Cieniewicz *et. al*[60] with the ADA complex revealed preferred histone acetylation: H3K14 $>$ H3K23 $>$ H3K9 $\approx$ H3K18 $>$ H3K27 $>$ H3K36. Based on this study, a 'two-step reader/writer' model was suggested by first acetylating H3K14, thereby recruiting the bromo domain of GCN5 to the histone tail and then continuing acetylation of the remaining acetylation sites[60].

1.4.2 Kinase: Aurora B

The serine/threonine kinase Aurora was first identified in *Drosophila melanogaster* and is conserved from yeast to mammals. Three Aurora kinases are known in mammals: Aurora A, B, and C. Aurora A is localized to mitotic spindle poles while Aurora C functions similarly to Aurora B and is mainly expressed in testis[61;62]. Aurora B together with INCENP, Borealin and Survivin form the chromosomal passenger complex (CPC). Aurora B localizes during mitosis with centromers, then moves to the midzone of the central spindle and finally positioning itself on the midbody of dividing cells[63;64]. In addition to its regulating role during mitosis and cytokinesis, Aurora B has been found to be an active promoter in quiescent B and T cells. By phosphorylating H3S28, Aurora B maintains transcription in quiescent B and T cells[65].

Figure 1.4: Domain organization of Aurora B kinase
Localization of kinase domain (KD) between 76-251 aa[67], N: N-terminus, C: C-terminus.

In general, kinases are built in their catalytic domain either for the phosphorylation of serine/ threonine, or for tyrosine[66]. The catalytic domain accommodates the S/T or Y substrate and ATP. With the help of Mg^{2+}, ATP is orientated towards the substrate-enabling catalysis of the transfer of the γ-phosphate to the hydroxy moiety of the substrate[66]. Aurora B is activated by the binding to its complex partner INCENP and by phosphorylation of itself and INCENP on its C-terminal TSS motif. Autophosphorylation is thought to occur in *trans*, thus high concentration of Aurora B enhances the activation process[64]. The consensus target sequence of Aurora kinases is [R/K]-X-[T/S]-[I/L/V]. On histone H3, Aurora B phosphorylates accordingly within the RKS motif, although [I/L/V] are missing[63;68]. The CPC containing Aurora B is recruited to chromatin via Survivin that recognizes H3T3ph[69]. Aurora B phosphorylates H3 site-specifically at H3S10 and H3S28. In addition to histone H3, Aurora B has a variety of non-nucleosomal substrates[70;71].

1.4.3 Heterochromatin protein 1

The HP1 family is conserved from yeast to human. In several organisms, HP1 homologs come in isoforms. In humans, three isoforms are known: HP1α, β, and γ. While HP1γ is found in euchromatic regions, HP1α and β localize on chromosomes to pericentric heterochromatin[33;72]. HP1s are considered a key player of regulating heterochromatin[73]. At the beginning of mitosis, Aurora B phosphorylates H3S10 thus evicts HP1 from the preceding methyl mark[32;33]. HP1 has two folded domains separated by a naturally unstructured

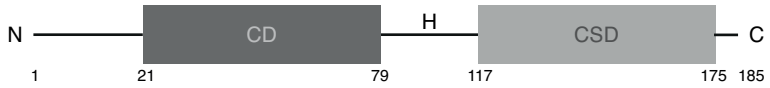

Figure 1.5: Domain organization of heterochromatin protein 1
Localization of chromo domain (CD) 21-79 aa, hinge region (H) 79-117 aa and chromo shadow domain (CSD) 117-175 aa of human HP1 β. N: N-terminus, C: C-terminus.

hinge region. The N-terminal chromo domain recognizes H3K9me3, whereas the chromo shadow domain is responsible for dimerization, hereby stabilizing and regulating higher order chromatin structure. In addition, HP1 tethers other proteins via the chromo shadow domain to chromatin containing a P-X-V-X-L recognition motif[74]. For example, HP1 recruits the methyltransferase Su(var)3-9, which methylates H3K9 on proximate nucleosomes[75;76].

Beside the two binding domains, the very N-terminal stretch of HP1β aids binding via unspecific electrostatic interactions. Moreover, the flexible hinge region can interact unspecifically with DNA, depending on its overall charge, which can be altered through post-translational modification, overruling the H3K9um/H3K9me3 specific binding[75;77]. The binding of HP1 to H3K9me3 is regulated by the phosphorylation of its neighbor H3S10[33;78].

1.5 PTM cross-talk and multivalent readout

In order to shed light on the versatile post-translational modified histone tails and their different modification patterns, Strahl *et al.*[49] and Jenuwein and Allis[79] proposed the histone code, envisioning that a specific set of PTMs on the histone tails lead to a distinct biologic outcome by providing a platform for effector proteins. In addition to the histone code hypothesis, Schreiber *et al.*[48] highlighted the similarities between the mechanisms of histones conveying nuclear regulation and models of signal transduction that rely on robust signaling by feedback loops and redundant signaling.

Histone PTM pattern are interpreted by effector proteins that determine the biologic outcome[25]. PTM patterns on the histone tails are modified by enzymes that 'write' or 'erase' histone marks[80]. 'Writer' and 'eraser' need to be guided to the place of action; this is accomplished indirectly by effector proteins or directly by a binding domain of the enzyme that can be recruited to specific areas of the chromatin depending on the PTM pattern displayed on the histone tails[79]. For instance, H3K4me has been found in both activating and repressing contexts. The idea was thus put forward that the trigger for recruiting activating or repressive factors are multiple PTMs acting together, thereby influencing the recognition of effector proteins in a synergistic or antagonistic manner[31;48]. The effector proteins/ complexes in turn carry multiple domains/proteins which allow interaction with histone PTMs in a combinatorial manner. For example, human TAF1 (TATA-binding protein associated factor-1) is composed of multiple domains that recognize acetylated lysines, thereby gaining its affinity for hyperactelyated histone tails[35].

Taking a close look at histone modifications and their possible combinations, several layers of complexity would be possible. The most basic PTM cross-talk is observed between modifications that target the same amino acid residue, e.g., the mutual exclusive modifica-

tion of lysine residues by methylation or acetylation. Histone marks on the same histone tail (cross-talk in *cis*) may influence each other. The special case of cross-talk between adjacent amino residues has been found to be a general phenomenon and is termed as a 'binary switch', such as the 'methyl/phos' switch. This mechanism was first found for H3K9 and H3S10[33;78]. Upon phosphorylation of H3S10, the binding of HP1 to H3K9me3 is abolished. Consequently, more binary switches have been discovered, e.g. H3S28 and H3K27. The phosphorylation of H3S28 disrupts the recruitment of its binding partner to methylated H3K27 and induces the placement of acetylation[32;81;82]. Additionally, a methyl/phos-switch was also observed for H3T3 regulating the availability of H3K4me1[83]. Hence, recognition 'cassettes' have been defined for which a maximum of 5 and minimum of 3 modified residues are separated by only one unmodified amino acid. For example, the 'RKS' motif in H3 represents the immediate environment of H3K9 and H3K27 and is highly modified[23;84]. In addition, the presence of one modification may enhance the activity of an enzyme for placing another modification as it was observed for *Tetrahymena* GCN5 displaying enhanced H3K14 acetylation when H3S10 was phosphorylated[56].

Cross-talk of PTM residing on different histone tails (*trans*) is also possible, e.g. for BPTF (bromodomain PHD finger transcription factor), part of the NURF (nucleosome remodeling factor) complex, has been shown to interact simultaneously with H3K4me and H4K16ac. All three components are associated with the regulation of transcriptional activity[85]. The complexity of PTM cross-talk in *trans* can involve several histone modifications and effector proteins. For instance, the serine/threonine kinase Haspin phosphorylates H3T3, thereby recruiting the CPC containing Aurora B kinase that leads to the phosphorylation of H3S10. H3S10ph recruits HDACs that remove the acetyl group on H4K16. This induces the H4 tail to interact with the acidic patch of H2A and leads to condensed chromatin[86].

The investigation of asymmetric PTM cross-talk, i.e. the study of differentially modified histone tails of the same histone type within the same nucleosome, revealed that the heterochromatic mark H3K27me3 and the euchromatic mark H3K4me3 in bivalent chromatin are located on different histone tails within the same nucleosome[87]. Recent single molecule *in vivo* studies in embryonic stem cells refined the picture of bivalent chromatin. They found that the majority of bivalent modification patterns occur in an asymmetric manner but a small fraction of NCPs present symmetric modification patterns[88].

Here, only a few examples for PTM cross-talk in *cis* and in *trans* were mentioned, already

indicating a direction of high complexity within one histone tail. The complexity potentiates within the nucleosome that is eventually responsible for the regulation of life.

1.6 Techniques for studying histone PTMs

There are several tools available in the field for studying histone marks *in vitro* and *in vivo*. They can be distinguished by the choice of chromatin template and what sort of information they deliver. Most *in vitro* studies work with the histone tail peptide. They are the simplest archetype of the chromatin system when only histone modifications in *cis* are of interest. Here, PTMs are easy to introduce by SPPS. Thus, combinatorial studies are feasible. For studying PTM in *cis* and *trans*, suitable surrogates of chromatin are mono-nucleosomes or nucleosome arrays. The modified templates are more difficult to procure. In general, the modification is introduced at the histone level, followed by nucleosome reconstitution.

1.6.1 Generating modified histones – semisynthetic approaches

Native chemical ligation (NCL) has been the most powerful tool in synthesizing a wide range of proteins[89;90]. It has been applied on histones for introducing site-specific modified histone tails. NCL works in aqueous solvents, neutral pH environments and under denaturing conditions. The only requirement is an N-terminal cysteine that requires recombinant integration at the desired ligation site on the histone. The PTM decorated histone tail with a C-terminal thioester is synthesized by SPPS[89;91].

Mechanistically, expressed protein ligation (EPL) works similarly to NCL. Both techniques rely on the formation of a thioester, a transesterification, and a native peptide bond. By means of EPL, it is however possible to work with native, fully folded proteins. Here, a protein (intein) is expressed between two other protein domains (exteins) that catalyse the ligation and formation of a native peptide bond between both terminal exteins (figure 1.6 (A)). The mechanism relies on the formation of a thioester via an N $\rightarrow$ S acyl shift at the C-terminus of the N-terminal extein (Ext_n), followed by a nucleophilic attack of the cysteine of the C-terminal extein (Ext_c), thereby transferring the ester. The subsequent irreversible rearrangement of the asparagine within the intein cuts it loose. The intein departs, leaving behind two exteins

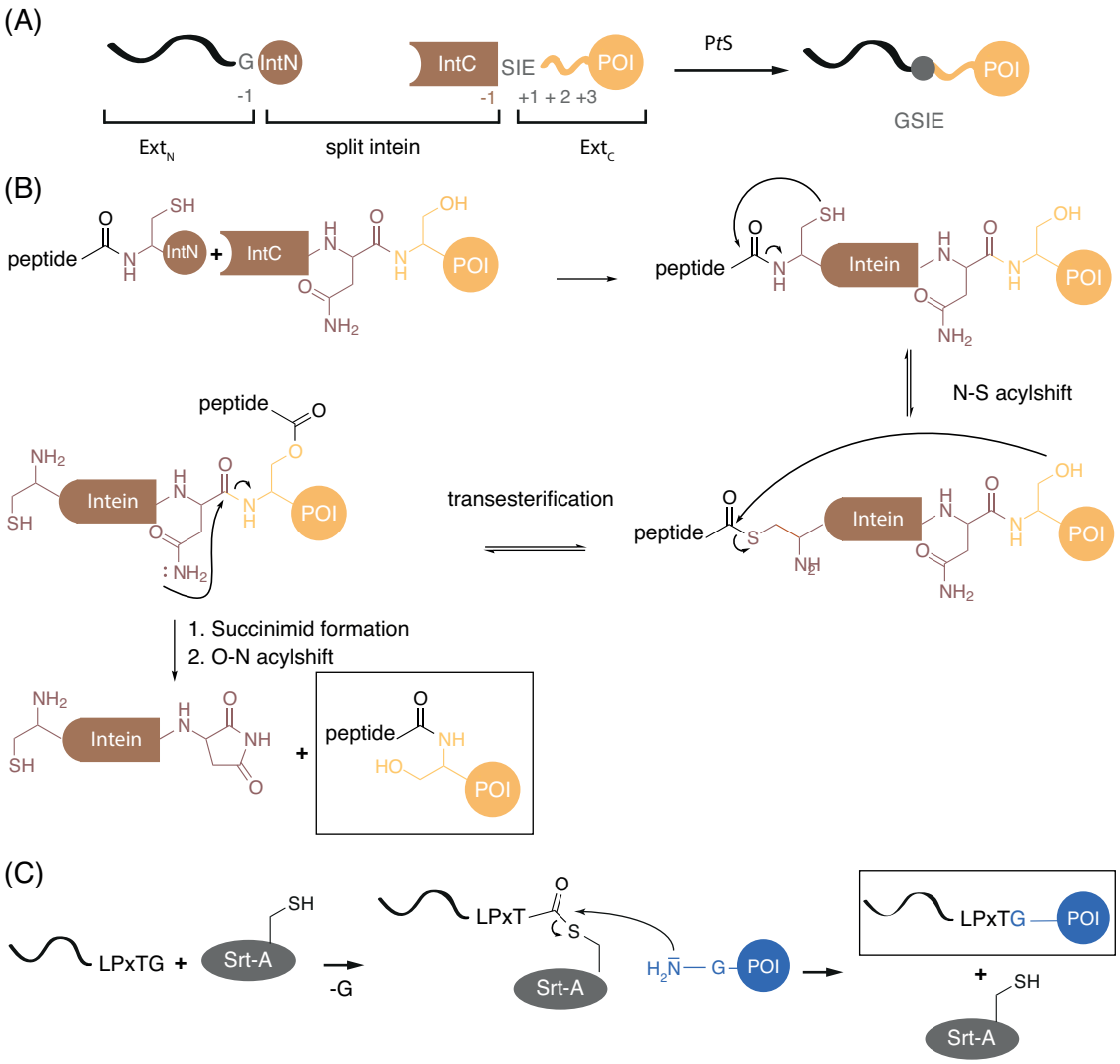

Figure 1.6: Protein *trans*-splicing and Sortase A mediated ligation
Reaction mechanism of protein *trans*-splicing and Sortase A (SrtA) mediated ligation. (A) Peptide and POI (protein of interest) requirements for protein *trans*-splicing (P*t*S) and resulting splice product. Abbreviations are for Ext$_N$: N-terminal extein, Int$_N$: N-terminal intein, Int$_C$: C-terminal intein and Ext$_C$: C-terminal extein. Sequence requirements are at position -1: G, +1: S, +2: I and +3: E. Ligation scar depicted in grey: GSIE. (B) Mechanism of P*t*S in 5 steps: intein formation, N-S acylshift, transesterification, irreversible succinimid formation and final restoring of the native peptide bond by O-N acylshift. (C) Mechanism of SrtA mediated ligation and requirements for peptide: LPxTG sequence and POI: N-terminal G. Threonine of the peptide is activated by formation of SrtA-peptide thiosester that is attacked by the N-terminal nucleophile (glycin) of POI.

connected via a native peptide bond (figure 1.6 (B))[92].

This technique became interesting for protein engineering by the discovery and development of mini split inteins[93]. As the name implies, the intein also works when it is split in two; upon combining both parts, it catalyses the formation of the native peptide bond in *trans* between its flanking exteins. Hence, it is referred to as protein *trans*-splicing (P*t*S). Naturally occurring inteins have their split site in the middle, close to the homing endonuclease domain, which is a common feature among inteins, but is dispensable for the ligation. Split mini inteins were engineered in such a manner so that either the N- or C- terminus has a short peptide sequence that can be easily synthesized via SPPS to label proteins with dyes or short peptide sequences[93;94]. P*t*S has also been used *in vivo* for labeling histone H2B C- terminal with a dye, peptide-tag or for introducing it into isolated nuclei the C-terminal tail of H2B ubiquitinylated at K120[95]. Appleby-Tagoe *et al.*[96] set out to optimize the splicing efficiency and sequence requirements for the *Ssp* DnaB mini intein (intein from *Synechocystis species* within the DnaB gene) using sequentially directed evolution. They found a mutant (M86) with mutations throughout the entire intein that led to improved splicing and accepted different amino acids at the -1 position (last amino acid of Ext_N, one before the intein, see figure 1.6 (A)). This is of special importance because it remains in the final splice product. Nevertheless, some extein site requirements remain. At the -1 position of Ext_N, amino acids with small side chains are favored (G, A). In contrast, at the Ext_C at +1, the catalytic S is indispensable. Additional I and E at +2 an +3 are a great benefit for effective splicing[96;97].

Another semisynthetic strategy to ligate peptides to proteins via a native peptide bond relies on the use of enzymes. One of these enzymes is the transpeptidase Sortase A (SrtA) of *Staphylococcus aureus*. In *S. Aureus* SrtA mediates the attachment of surface proteins to the cell wall by the recognition of a short peptide sequence LPxTG within the target. Srt A activates the carboxy-group of the threonine via the formation of a thioester by generating a substrate-enzyme intermediate. In a second step, the N-terminal glycine of the protein (or peptide) to be ligated serves as a nucleophile and forms the native peptide bond[98;99]. SrtA was subjected to optimization in terms of the recognition sequence by phage display. The F40 mutant selectively recognized a new motif APxTG, which happens to be native within histone H3. However, efficient ligation is only achieved after 24 hours[99].

1.6.2 Advances in studying PTMs in the context of histone tail peptide or full-length proteins

Several techniques have been developed for studying the binding properties of either specific histone tail modifications or specific PTM binding domains. For the screening of binding domains on several histone PTMs, the high-throughput screening method SPOTblot was developed. Using this, modified histone peptides are immobilized on a membrane. The membrane is probed with the his-tagged binding domain of interest and binding events are detected using antibodies against the his-tag of the bound domain[100;101].

Chromatin associated domain array (CADOR) is a complementary approach in studying binding partners of specific histone marks. Here, reader domains are fused via GST onto a glass slide, probed with synthetic histone tails carrying different modifications and a fluorogenic probe is used for the readout[102;103].

A homogeneous enzymatic assay using LANCE and ALPHA technology was adopted for studying methyltransferase activity on modified H3 peptide and full-length protein[104–106]. Both techniques rely on antibody recognition of the substrate. Using LANCE technology, the readout depends on TR-FRET. Hence, the antibody against the modification of interest is modified with Europium that serves as a FRET Donor. The substrate, e.g. histone peptide, is linked to a FRET acceptor bead. If the modification of interest has been placed by the enzyme to be investigated, an antibody against this modification coupled to the FRET donor would recognize it. This way, the FRET donor and acceptor are localized within the FRET radius, which allows upon excitation of the donor bead detection of the signal emitted by the FRET-acceptor. Similarly, ALPHA depends on two antibodies against the substrate, each against a different epitope. The antibodies are additionally linked either with the acceptor bead or a biotin-tag, thereby inserting a handle for the donor bead. In contrast to FRET-based assays, the donor bead here releases singlet oxygen that emits light from the acceptor bead that is of shorter wave length than is used for the excitation of the donor bead. Using this readout technology, beads can be up to 200 nm apart from each other before singlet oxygen relaxes[104].

Garske *et al.*[107] developed an 'on bead screening' assay. The authors synthesized a H3-peptide[108] and H4-peptide[107] library with 50000 and 800 different modification patterns immobilized on beads, respectively. The whole library is then presented a GST-tagged reader

domain in direct competition for all modifications. Using the dimerization property of GST, GST-tagged alkaline phosphatase is added, which upon the addition of bromo-4-chloroindlyl phosphate results in a blue precipitate. Such detected positive hits are selected for mass spectrometry in order to determine the PTM pattern of the histone tail.
As these techniques used histone peptides or full-length protein, precise but only limited information could be gained. More importantly, several chromatin effector proteins have been shown to interact differently with histone peptides than with nucleosomes[59;109;110].

Techniques for studying PTM cross-talk

Mass spectrometry has been a very powerful tool in detecting PTMs on histones in an unbiased manner. Using top-down (analyzing intact histones/proteins), middle-up (large fragments of ~ 5 kDa are subjected for MS analysis) and bottom-up (analyzing small fragments of histones/proteins via MS) MS strategies identify an ever growing number of PTMs on histones[5;42]. Top down experiments using SILAC (stable isotope labeling by amino acids in cell culture) provide a great overview of proteins that interact with a specific set of modifications. This has been accomplished on the histone peptide level as well as on mono-nucleosomes and the nucleosome array level by performing a pulldown experiment in heavyisotope labeled and unlabeled nuclear extract[110–113]. Thus, it is possible using SILAC to screen for modifications within a chromatin array in a combinatorial manner, but this is very costly and time-consuming and requires advanced instrumentation. Nevertheless, this has been performed for selected modifications[110;112].
A very interesting technique named BICON (biotinylation assisted isolation of co-modified nucleosomes) was developed by Lau and Cheung[114]. As the name implies, BICON searches for nucleosomes modified *in vivo* using an enzyme of interest (in this study, MSK1 (mitogen- and stress-activated protein kinase-1)). Using the enzyme BirA, which biotinylates a short recognition sequence of 15 amino acids, they were able to introduce the recognition sequence C-terminal to H3.3, the target of MSK1. The fusion of both enzymes MSK1 and BirA leads to biotinylation of those H3.3 histones that are targeted by MSK1, which facilitates extracting modified nucleosomes, which are analyzed using antibodies against the modification of interest.
Nguyen *et al.*[115] developed a technique for studying PTM cross-talk in *cis*. They introduce

a method for studying the combinatorial readout of histone modifications within the context of nucleosomes by chromatin ‘readers’ and ‘writers’. The authors develop a shortcut for the reconstitution of NCP in order to build up an NCP library of 40 members with different modification patterns on all four histone types. In addition, they introduce a ’bar code’ label at the DNA coded for the modification patterns of the NCP. After incubation of the whole NCP library with a ‘reader’ or ‘writer’ protein, the authors perform immunoprecipitation against a modification placed by the ‘writer’ of interest for analyzing its NCP modification. Affinity purification is used for the identification of preferred NCP modification patterns for ‘reader’ proteins. Subsequent DNA sequencing of immunoprecipitated or affinity purified NCP reveal the ’bar code’ and thereby the nucleosome modification pattern.

These techniques are very powerful in their analysis of PTM in the context of nucleosomes, but they either require high-end instrumentation or depend on antibodies recognizing PTMs in the context of nucleosomes. In addition, working with predefined chromatin templates (NCP or nucleosome arrays) requires they be separately assembled for each modification pattern.

1.7 Objective of this study

In recent years, several *in vivo* and *in vitro* techniques were developed for studying the dependence of PTM on chromatin function. These combinatorial studies were conducted using histone peptides and selected PTM patterns were investigated *in vitro* using recombinant mono- and oligo- nucleosomes as well as chromatin arrays. These studies revealed that in several cases, effector proteins act differently on isolated histone peptides as compared to mono-nucleosomes and chromatin arrays. However, several techniques relied on the use of antibodies that limited the application because of their performance and availability or depended on sophisticated equipment. For these reasons, we set out to develop tools for studying combinatorial histone PTM patterns in the context of nucleosomes in a high-throughput approach. In addition, we hypothesized that the interaction of 'reader' and 'writer' with NCP is fine-tuned by certain PTM patterns presented by the NCP.

To address this, we set up an NCP library consisting of histone modification patterns in a combinatorial manner. We thus aimed to reduce the number of NCP assemblies necessary for the generation of modified NCP libraries to one single assembly. To do so, we developed a ligation-ready nucleosome to which histone tails can be attached in a histone type- and site-specific manner, thus allowing the introduction of various modifications. Moreover, we intended to establish a workflow which would allow us to perform the attachment of PTM-decorated histone tails to the immobilized, ligation-ready NCP directly in the plate. To address the question of whether additional modifications on NCPs would fine-tune the interaction with chromatin 'reader' and 'writer', we derived an assay with a fluorescence readout for 'reader' and a radioactive proximity readout for 'writer' using the immobilized, combinatorial post-translational modified NCP library.

The work presented here is the first attempt to generate an immobilized, combinatorial modified NCP library by introducing the modification to the assembled NCP and the development of an assay for analyzing the impact of histone PTM on the chromatin 'reader' and 'writer'. This study provides a potentially powerful tool for gaining insight into the complex regulation of chromatin by PTM cross-talk.

2 Material and methods

2.1 Material and reagents

Laboratory equipment used in this study is listed in table 2.1. Chemicals and media used for experiments and protein expression are listed in table 2.2. Radiochemicals for biochemical assays are listed in table 2.3. Commercial enzymes used for cloning and enzymatic experiments are found in table 2.4. Consumables, commercial kits and chromatographic equipment are listed in table 2.5. Primary and secondary antibodies including used dilutions are sorted in table 2.6. Peptides used for peptide pull-down and initial H2A ligation experiments are listed in table 2.7. Information for plasmids an their source are summarized in table 2.8. Details of bacterial strains for cloning and expression can be found in table 2.9.

Table 2.1: Laboratory equipment

Equipment	Supplier
ÄKTA Purifier/ Explorer	GE Healthcare, Buckinghamshire (UK)
Balances	Mettler-Toledo, Gießen
Centrifuge Sorvall Discovery M150	Thermo Scientific, Braunschweig
Centrifuge Sorvall Evolution RC	Thermo Scientific, Braunschweig
Centrifuges 5415R/ 5810R	Eppendorf, Hamburg
EmulsiFlex-C5 High Pressure Homogenizer	Avestin, Ottawa (Canada)
ChemiDoc	Bio-Rad, München
Heraues Kelvitron Incubator	Thermo Scientific, Braunschweig
Hybridization oven	GE Healthcare, Buckinghamshire (UK)
Infinite M1000Pro	TECAN, Männedorf (CHE)
MiniTrans-Blot	Bio-Rad, München
NanoDrop ND-1000	Peqlab, Erlangen
PCR thermocycler epgradientS	Eppendorf, Hamburg
Peristaltic pump	Ismatec, Glattbrugg (CHE)
pH meter	Mettler-Toledo, Gießen
Plate reader Chameleon V	Hidex, Turku (FIN)
Power supplies	Bio-Rad, München
SpeedVac Savant SPD131DDA	Thermo Scientific, Braunschweig
Stuart Gyrorocker SSL3	Sigma, Steinheim

Table 2.1 – continued from previous page

Equipment	Supplier
Sub-Cell-GT Agarose gel electrophoresis	Bio-Rad, München
Thermomixer comfort	Eppendorf, Hamburg
UV Transilluminator	Bio-Rad, München
Waterbath TW12	Julabo, Seelbach

Table 2.2: Chemicals and media used for experiments and protein expression

Chemical	Supplier
2 x YT medium	Roth, Karlsruhe
2-[4-(2-hydroxyethyl)piperazin-1-yl]ethanesulfonic acid (HEPES)	VWR, Radnor PA (USA)
2-Mercaptoethanol	Sigma, Steinheim
3-(N-Morpholino)propanesulfonic acid (MOPS)	VWR international, Poole (UK)
β-glycerophosphate	AppliChem, Darmstadt
Acetic acid	Merck, Darmstadt
Acetyl coenzyme A (AcCoA)	Roche, Mannheim
Acrylamid/ Bisacrylamid solution (37.5:1)	Merck, Darmstadt
Adenosine 5'-triphosphate, disodium salt (ATP)	Sigma, Steinheim
Agar	Roth, Karlsruhe
Agarose	Serva, Heidelberg
Amberlite MB3 resin	Merck, Darmstadt
Ammonium persulfate (APS)	AppliChem, Darmstadt
Ampicillin	Roth, Karlsruhe
Benzamidin hydrochloride	Sigma, Steinheim
Boric acid	Merck, Darmstadt
Bovine serum albumin (BSA)	Sigma, Steinheim
Bromphenol blue	Serva, Heidelberg
Chlormaphenicol	Sigma, Steinheim
Coomassie brilliant blue (CBB)	Bio-Rad, Hercules CA (USA)
Deoxynucleoside-5'-triphosphate (dATP, dCTP, dGTP, dTTP)	Roth, Karlsruhe
Di-sodium hydrogen phosphate (Na_2HPO_4)	Merck, Darmstadt
Dimethylsulfoxide (DMSO)	Sigma, Steinheim
Dithiothreithol (DTT)	AppliChem, Darmstadt
Ethanol	Merck, Darmstadt
Ethidium bromid solution (EtBr)	Roth, Karlsruhe
Ethylendiamine tetraacetate (EDTA)	Roth, Karlsruhe
Ethylene glycol-bis(2-aminoethylether)-N,N,N',N'-tetraacetic acid (EGTA)	Roth, Karlsruhe
Glucose	Merck, Darmstadt
Glycerol	Merck, Darmstadt
Glycine	Merck, Darmstadt
Guanidine hydrochlorid	Sigma, Steinheim
Hydrochloric acid (HCl)	Merck, Darmstadt
Imidazole	Roth, Karlsruhe
Isopropyl-βD-thiogalacto-pyranoside (IPTG)	AppliChem, Darmstadt
LB Broth	Dianova, Hamburg
Magnesium chloride hexahydrate ($MgCl_2$ 6·H_2O)	Merck, Darmstadt
Methanol	Merck, Darmstadt

Table 2.2 – continued from previous page

Chemical	Supplier
Milk powder	Roth, Karlsruhe
Nonident P-40 (NP-40)	Roche, Mannheim
Phenylmethylsulfonylfluorid (PMSF)	Sigma, Steinheim
Polyethylen glycol 6000 (PEG 6000)	Merck, Darmstadt
Ponceau S	Sigma, Steinheim
Potassium chloride (KCl)	Merck, Darmstadt
Potassium di-hydorigen phosphate (KH_2PO_4)	Roth, Karlsruhe
Protease inhibitor EDTA free	Roche, Mannheim
Sodium azide (NaN_3)	Alfa Aesar, Massachusetts (USA)
Sodium chloride (NaCl)	Merck, Darmstadt
Sodium di-hydrogen phosphate (NaH_2PO_4)	Merck, Darmstadt
Sodium dodecyl sulfate (SDS), ultra pure	Roth, Karlsruhe
Tetramethylethylendiamine (TEMED)	Sigma, Steinheim
Triethanolamine ($N(EtOH)_3$)	VWR, Fontenay-sous-Bois (F)
Tris(hydroxymethyl)amino-methane (TRIS base)	Roth, Karlsruhe
Triton X-100	Merck, Darmstadt
Tryptone/Peptone	Roth, Karlsruhe
Tween20	Sigma, Steinheim
Urea	Roth, Karlsruhe
Yeast extract	MOBIO, Hamburg

Table 2.3: Radiochemicals used in activity assays

Chemical	Specific activity [mCi/mmol]	Concentration [mCi/mL]	Supplier	Order Number
[acetyl-1-14C]-acetyl coenzyme A	60	0.02	Perkin Elmer	NEC313050UC
[γ-32P]-ATP	3000	10	Perkin Elmer	BLU002A001MC

Table 2.4: Commercial enzymes used for cloning and enzymatic experiments

Name	Supplier
Antarctic phosphatase	New England Biolabs, Frankfurt/Main
DNase I	New England Biolabs, Frankfurt/Main
Pfu DNA polymerase	Fermentas/Thermo Fischer, Schwerte
PfuUltra II Fusion HS polymerase	New England Biolabs, Frankfurt/Main
Q5 High-Fidelity DNA Polymerase	New England Biolabs, Frankfurt/Main
Restriction enzymes	New England Biolabs, Frankfurt/Main
T4 DNA ligase	New England Biolabs, Frankfurt/Main
Taq polymerase (home made)	purified by Sebastian David (MPI für biophysikalische Chemie)

Table 2.5: Consumables, commercial kits, and chromatographic equipment

Name	Supplier
1 Kb Plus DNA ladder	Invitrogen, Karlsruhe
Amberlite MB3 resin	Merck, Darmstadt
Amicon Ultra centrifugal filter devices (MWCO 3,10,30 kDa)	Millipore, Tullagreen (IRL)
ECL Plus Western Blotting Detection System	GE Healthcare, Buckinghamshire (UK)
ECL Western Blotting Detection Reagent	GE Healthcare, Buckinghamshire (UK)
FlashPlate Plus, Streptavidin 96-well scintillant coated microplate	Perkin Elmer, Shelton CT (USA)
HiLoad Superdex 200 PG 16/60	GE Healthcare, Little Chalfont (UK)
Ni^{2+}-NTA agarose	Qiagen, Hilden
Nitrocllulose membrane	GE Healthcare, Little Chalfont (UK)
NucleoBond Xtra Midi Plus	Machery & Nagel, Düren
NucleoSpin® Gel and PCR Clean-up	Machery & Nagel, Düren
NucleoSpin® Plasmid	Machery & Nagel, Düren
Pierce™ Streptavidin Coated High Capacity Plates, Black, 96-Well	Pierce, Thermo Fischer Rockford IL (USA)
Q-Sepharose XK26/20	GE Healthcare, Little Chalfont (UK)
SeeBlue Plus2 prestained protein standard	Invitrogen, Karlsruhe
Slide-A-Lyzer dialysis units (MWCO 3,500 and 10,000; volume 0.5 mL)	Thermo Fisher, Rockford IL (USA)
SP-Sepharose XK26/20	GE Healthcare, Little Chalfont (UK)
Spectra/Por Dialysis Membrane (MWCO 3,500 and 6-8,000)	Spectrum Laboratories, Inc., Rancho Dominguez CA (USA)
Streptavidin MagneSphere® Paramagnetic Particles	Promega, Mannheim
Superdex 200 10/300 GL	GE Healthcare, Little Chalfont (UK)

Table 2.6: Primary and secondary antibodies used for western blot analysis

Name	Host	Vendor/Catalog #	Dilution
Primary antibodies			
α-GFP	mouse, monoclonal	Santa Cruz / sc9996	1:5000
α-histone H2A	rabbit, polyclonal	Abcam / ab88770	1:1000
α-histone H3	rabbit, polyclonal	Abcam / ab1791 and ab1781	1:10000
α-histone H3K9me2	mouse, monoclonal	Abcam / ab1220	1:5000
α-histone H3K9me3	rabbit, polyclonal	Upstate/Millipore / 07-442	1:1000
α-histone H4	rabbit, polyclonal	Active Motif / 39269	1:1000
α-HP1β	mouse, monoclonal	Millipore / MAB3448	1:5000
Secondary antibodies			
α-mouse Alexa 488	goat, polyclonal	Invitrogen / A11001	1:5000
α-mouse HRP	goat, polyclonal	Dako / P0447	1:5000
α-rabbit Alexa 488	donkey, polyclonal	Invitrogen / A21206	1:5000
α-rabbit HRP	swine, polyclonal	Dako / P0399	1:5000

Table 2.7: Peptides used for peptide pull-down experiments and ligation of H2A

Name	Sequence	Source
FAM-IntN	FAM-KKESGCISGDSLISLA	D. Schwarzer, Eberhard Karls Universität Tübingen
H2A-IntN	SGRGKQGGKTRAKAKTRS GCISGDSLISLA	P. Henklein, Charité, Berlin
H3-Btn	ARTKQTARKSTGGKA PRKQL-Btn	P. Henklein, Charité, Berlin
H3K9me3-Btn	ARTKQTARKme2STGGKA PRKQL-Btn	P. Henklein, Charité, Berlin

Table 2.8: Plasmids used for PCR and bacterial expression

Vector-Insert	Restriction site	Purpose	Source
pBluescript II KS(+) 1x601	*Not*I/*Eco*RV	template for *Hin*dIII-*Eco*RI-*Eco*RV-147	A. Stützer, MPI für biophysikalische Chemie, Göttingen
pBluescript II KS(+) *Hin*dIII-*Eco*RI-*Eco*RV 1x601	*Bam*HI/*Xho*I	template for '147'-DNA	H. Mahler
pET16b His_6-Aurora B	*Nde*I/*Bam*HI	bacterial expression	H. Mahler
pET16b His_6-Cerulean-HP1β	*Nde*I/*Bam*HI	bacterial expression	H. Mahler
pET16b His_6-eCFP-HP1β	*Nde*I/*Bam*HI	bacterial expression/ template for mutagenesis	S. Szabolcs, MPI für biophysikalische Chemie, Göttingen
pET16b His_6-eCFP-HP1W42Aβ	*Nde*I/*Bam*HI	bacterial expression	S. Szabolcs, MPI für biophysikalische Chemie, Göttingen
pET16b His_6-mCFP-HP1β	*Nde*I/*Bam*HI	bacterial expression	H. Mahler
pET3a H2A	*Nde*I/*Bam*HI	bacterial expression	K. Luger, Colorado State University, Fort Collins (USA)
pET3a H2B	*Nde*I/*Bam*HI	bacterial expression	K. Luger, Colorado State University, Fort Collins (USA)
pET3a H3	*Nde*I/*Bam*HI	bacterial expression	K. Luger, Colorado State University, Fort Collins (USA)
pET3a H3Δ1-32	*Nde*I/*Xho*I	bacterial expression	D. Schwarzer, Eberhard Karls Universität Tübingen
pET3a H4	*Nde*I/*Bam*HI	bacterial expression	K. Luger, Colorado State University, Fort Collins (USA)
pET3a IntC-H2A	*Nde*I/*Bam*HI	bacterial expression	H. Mahler
pIT021 IntC *Ssp*DnaB M86	*Nco*I/*Hin*dIII	template for InteinC	H. Mootz, Westfälische Wilhelms-Universität, Münster

Table 2.8 – continued from previous page

Name	Restriction site	Purpose	Source
yGCN5 full-length[116]		bacterial expression	P. Selenko, Leibniz Institut für Molekulare Pharmakologie, Berlin

*Dpn*I

Table 2.9: Bacterial strains used for expression and cloning

Strain	Genotype	Supplier
Nova Blue	*E.coli end*A1 *hsd*R17 (r_{K12}^- m_{K12}^+) *sup*E44 *thi*-1 *rec*A1 *gyr*A96 *rel*A1 lac F'[*pro*A$^+$B$^+$ *lacI*^{q}ZΔM15::Tn10] (Tet^R)	Novagen/Merck Millipore, Darmstadt
BL21 (DE3) RIL	*E. coli* B F-*omp*T *hsd*S(r_B^- m_B^-) *dcm*+ Tet$_r$ *gal l* (DE3) *end*A The [argU ileY leuW Cam^R]	Stratagene, La Jolla (USA)
Rosetta pLysS	*E.coli* F$^-$ *omp*T *hsd*S$_B$(r_B^- m_B^-) *gal dcm* (DE3) pRARE (*Cam^R*)	Novagen/Merck Millipore, Darmstadt

2.2 Molecular biology methods

2.2.1 Determination of DNA concentration

The concentration of DNA was determined by measuring the absorbance at 260 nm against a blank control with the NanoDrop ND1000. The relation of $A_{260} = 1 = 50\,\mu$g/mL double stranded DNA was applied[117].

2.2.2 Transformation of *E. coli* strains

Chemically competent cells were transformed as described by Sambrook *et al.*[118]. 50 μL of chemically competent cells were thawed on ice and incubated on ice with 0.5-5 μL DNA plasmid for 20 min. Heat shock was applied for 45 sec at 42°C and subsequently placed on ice for 2 min. 250 μL SOC media (2 % [w/v] tryptone, 0.5 % [w/v] yeast extract, 10 mM NaCl, 2.5 mM KCl, 20 mM glucose) was added and incubated for 1 h at 37°C. In case of a transfor-

mation with fresh ligated material, all cells were taken otherwise only 20-50 μL and spread out on a selection plate carrying ampicillin and incubated over night at 37°C.

2.2.3 Agarose gel electrophoresis

For analyzing the quality of PCR products or NCP, agarose gel electrophoresis was performed[119]. The gel was prepared with 1 % agarose [w/v] in 1 x TBE (89 mM TRIS base, 89 mM boric acid, 2 mM EDTA pH 8.0) supplemented with EtBr or 0.2 x TB (18 mM TRIS base, 18 mM boric acid) without EtBr. Samples were set up by adding 6 x DNA loading buffer (18 % [v/v] glycerol, 6 mM EDTA, 0.15 % [w/v] bromophenol blue) to final 1 x concentration. Running along with 7 μL of 1 kb plus DNA ladder, samples were separated depending on their size by applying 100-120 V for 35 min at RT (PCR products) or at 100-120 V for 90-120 min at 4°C (NCPs). In case of NCP analysis, agarose gels needed to be stained post run with 0.1 μg/mL EtBr in 0.2 x TB buffer for 10 min at RT, washed for 15 min with ddH_2O. EtBr stained agarose gels were analyzed under UV using an photo imager system. The efficiency of the PCR for generating '147' Widom 601 nucleosome positioning sequence was evaluated by in-gel Cy5-fluorescence. This way, surplus Cy5-labeled oligonucleotides can be detected.

2.2.4 Site-directed mutagenesis

For obtaining the eCFP-HP1 derivatives mCFP- (eCFP A206K, monomeric) and Cerulean-HP1 (eCFP S72A/Y145A/H148D, weak dimer), their DNA coding sequence was generated by site directed mutagenesis[120] of pET16b-eCFP-HP1 for bacterial expression. The PCR was performed in total volume of 50 μL with 1xQ5 polymerase buffer, 50 μM dNTPs, 20 nM of each primer and 25 ng DNA template (pET16b eCFP-HP1) and 1 U Q5 polymerase using the in table 2.10 described PCR program. With this strategy, pET16b mCFP-HP1 was generated in one step, pET16b-Cerulean HP1 was performed in two. First step, site directed mutagenesis was performed for obtaining pET16b eCFP-Y145H Y148D and pET16b eCFP. The PCR product was purified using the commercial NucleoSpin Gel and PCR Clean Up kit. Purified plasmids were digested with the restriction enzyme *Dpn*I for 1 h at 37°C to destroy the template produced originally by *E.coli*. Chemically competent *E.Coli* were transformed with the mutation bearing, PCR generated plasmid as described before (chapter 2.2.2). Three to five

colonies were picked and raised in mini culture of 5 mL LB medium (1:1000 ampicillin, stock 100 μg/mL) at 37°C, ON and 130 rpm shaking. From these mini cultures, plasmids were isolated using the NculeoSpin Plasmid kit and sent for sequencing (SeqLab Göttingen). In the second step, the final mutation was inserted for obtaining pET16b Cerulean-HP1. Herefor, positive pET16b eCFP-Y145H Y148D clones served as DNA template for the final eCFP-Y145H/Y148D/S72A mutation to obtain pET16b-Cerulean-HP1 using site directed directed mutagenesis as described.

Table 2.10: PCR program mutagenesis - Q5 polymerase

Temperature	Time	Cycle
98°C	3’	
98°C	10”	25x
68-72°C	10-30”	
72°C	40-50”/kbp	
72°C	2’	
6°C	∞	

Table 2.11: Primer for site-directed mutagenesis

Name	Sequence
Fwd eCFP A206K	5’-GCACCCAGTCCAAACTGAGCAAGACCCCAACGAGAAGCG-3’
Rev eCFP A206K	5’-CTTTGCTCAGTTTGGACTGGGTGCTCAGGTAGTGGTTGTC-3’
Fwd eCFP S72A	5’-GCAGTGCTTCGCCCGCTACCCCGACCACATGAAGCAGCAC-3’
Rev eCFP S72A	5’-CGGGGTAGCGGGCGAAGCACTGCACGCCCCAGGTCAGGG-3’
Fwd eCFP Y145A H148D	5’-GAGTACAACGCCATCAGCGACAACGTCTATATCACCGCC-3’
Rev eCFP Y145A H148D	5’-GACGTTGTCGCTGATGGCGTTGTACTCCAGCTTGTGCCCC-3’

2.2.5 Fusion PCR

In order to obtain IntC-H2AΔ_{1-18} fusion protein for bacterial expression, DNA constructs coding for IntC-H2A were generated by two step fusion PCR[121]. In the first step, DNA constructs coding for each protein IntC (template vector: pIT021 IintC *Ssp* DnaB) and H2AΔ_{1-18} (template vector pET3a H2A) were generated separately with a sequence overlap at the joint (IntC 3’ overlap H2A and H2A 5’ overlap with IntC) using the primer listed in table 2.13 and

the PCR program shown in table 2.12. DNA insert IntC and H2AΔ_{1-18} were purified from PCR reaction mix using NucleoSpin Gel and PCR Clean Up kit.

In a second step, both DNA constructs IntC and H2AΔ_{1-18} were mixed equal molar and served as DNA template for the fusion DNA construct IntC-SIE-H2AΔ_{1-18} using the primer listed in table 2.13 and the PCR program shown in table 2.12. The DNA fusion insert IntC-SIE-H2AΔ_{1-18} and the target vector (pET16b) were digested with the restriction enzymes *Nco*I and *Bam*HI-HF for 1 h at 37°C. The vector was additionally dephosphorylated with antarctic phosphatase for 1 h at 37°C. Then, DNA insert and vector were gel purified and set up for ligation by T4 DNA ligase ON at 16°C in a 4:1 molar ratio (insert:vector).

Table 2.12: Fusion PCR program

Temperature	Time	Cycle
95°C	3’	
95°C	30”	35x
60°C	30”	
72°C	120”/kbp	
72°C	5’	
6°C	∞	

Table 2.13: Primer for fusion PCR

Name	Sequence	Insert
Fwd *Nco*I M86	5’-GAGATCCCATGGGCACTAGTAGC-3’	IntC
Rev M86 H2A 2	5’-GAGATTCGATGGAGTTATGGACAATGATGTC-3’	
Fwd M86 H2A	5’-CTCCATCGAATCTCGGGCTGGGCTAC-3’	H2AΔ_{1-18}
Rev *Bam*HI H2A	5’-GATCTCGGATCCTCACTTGCTCTTGGC-3’	
Fwd *Nco*I M86	5’-GAGATCCCATGGGCACTAGTAGC-3’	IntC-SIE-H2AΔ_{1-18}
Rev *Bam*HI H2A	5’-GATCTCGGATCCTCACTTGCTCTTGGC-3’	

Chemically competent cells were transformed with 5 μL of the ligation mix as described in chapter 2.2.2. 3-5 colonies were cultured in 5 mL LB supplemented with ampicillin at 37°C, ON and 130 rpm shaking. Plasmids were isolated from mini-culture (NucleoSpin Gel and PCR Clean Up kit) and the DNA digest was performed with 800 ng plasmid and 0.5 μL of each restriction enzyme (*Nde*I/*Bam*HI) for 30-60 min at 37°C and analyzed using agarose

gel electrophoresis as described in chapter 2.2.3. Plasmids carrying the expected insert size were sent for sequencing to Seqlab Göttingen using primer from their standard primer list (T7term).

2.2.6 Generation of biotinylated and Cy5-labeled '147' Widom 601 DNA template

The DNA template used in this study had several modifications from the original 147 base pair Widom 601 positioning sequence[122]. Firstly, it was extended at the 5'- end containing the sequence for three different restriction enzymes: *Hin*dIII, *Eco*RI and *Eco*RV using the fwd-template primer. Secondly, a Btn-tag was linked via a Tg-linker to the 5' end of the '147' sequence and thirdly, the fluorogenic probe Cy5 was attached to the 3'- end of the '147' sequence. Biotin- and Cy5-labeled oligo nucleotides were commercially available (table 2.14) and incorporated into the '147' sequence by PCR.

Table 2.14: Primer for 147 PCR

Name	Sequence
Fwd template	5'-GAGATCGGATCCAAGCTTGAATTCGATATCsCTGGAGAATCCCGGTGCC-3'
Fwd BtnTg	5'-BtnTg-CAAGCTTGAATTCGATATCCTGGAGAATC-3'
Rev Cy5	5'-Cy5-ACAGGATGTATATATCTGACA CGTGCCTG-3'

In order to generate labeled '147'-Widom 601 nucleosome positioning DNA sequence, PCR was performed in 96-well plate, in a reaction volume of 50 μL per well. Each reaction contained 1x Taq buffer (10 mM TRIS-HCl pH 8.8, 50 mM KCl, 0.8 % [v/v] NP-40), 240 μM dNTPs, 0.6 μM forward primer (Fwd BtnTg or Fwd template), 0.6 μM reversed primer (Rev Cy5), 1.5 mM $MgCl_2$, 10 ng DNA template and 5 U Taq polymerase. In order to check the quality of PCR, 5 μL of the raw PCR mix was analyzed by agarose gel electrophoresis (chapter 2.2.3).

Table 2.15: PCR program '147'-DNA

Temperature	Time	Cycle
94°C	2'	
94°C	30"	40x
57°C	30"	
72°C	30"	
72°C	5'	

2.2.7 PEG precipitation of biotinylated and Cy5-labeled '147' Widom 601 DNA template

The PCR amplified, biotin- and Cy5-labeled '147' Widom 601 DNA sequence was pooled and precipitated with polyethylene glycol (PEG 6000)[123] by adding a 2 x PEG solution (28 % PEG 6000, 1M NaCl) to give final concentration 1 x. After 15 min incubation at 37°C DNA was precipitated by centrifugation at 40000 rcf, 4°C for 15 min. The DNA pellet was washed with 5 mL 80 % EtOH, air dried and resuspended in ddH_2O. Quality control was performed by analyzing 200, 400 and 800 ng of purified DNA on an agarose gel observing intensities of EtBr and Cy5-fluorescence as described in chapter 2.2.3.

2.3 Protein biochemistry methods

2.3.1 Techniques for analyzing proteins

Determination of protein concentration

The concentration (c) of proteins was determined by measuring the absorbance (A) at 280 or 276 nm using NanoDrop ND 1000 (optical path length d = 0.1 cm, but internally corrected to d = 1 cm). According to the law of Lambert and Beer (equation 2.1) the protein concentration was calculated using extinction coefficients retrieved on the base of protein sequence by the tool ProtParam[124].

$$A = \varepsilon_{nm} \cdot c \cdot d \tag{2.1}$$

Table 2.16: Physical parameters of recombinant proteins

Protein	MW [kDa]	ε [$M^{-1}cm^{-1}$]
H2A	13.950	4470
IntC-H2A	28.679	23950
H2B	13.493	7450
H3	15.270	4470
H3Δ1-32	11.950	4470
H4	11.236	5960
His_6-Aurora B	42.522	42860
His_6-Cerulean-HP1	52.299	53860
His_6-eCFP-HP1	52.429	55600

Table 2.16 – continued from previous page

Protein	MW [kDa]	ε [$M^{-1}cm^{-1}$]
His_6-GCN5	52.310	49280
His_6-mCFP-HP1	52.487	55600

Polyacrylamide gel electrophoresis

The purity of proteins was assessed by SDS-PAGE[125]. In general, 15 % SDS polyacrylamide gels were handcasted. Proteins were denatured in 1 x Lämmli buffer (62,5 mM Tris-HCl pH 6.8, 2 % [w/v] SDS, 10 % [v/v] glycerol, 0.1 % [w/v] bromphenol blue) and boiled for 5 min at 95°C in SDS running buffer (25 mM TRIS base, 192 mM glycine, 1 % [w/v] SDS) with 200 V for 50 min at RT. If not meant for western blot analysis, SDS-gels were stained with coomassie solution (0.1 % [w/v] Coomassie brilliant blue R250, 10 % [v/v] acetic acid, 50 % [v/v] methanol) for 5 min and destained using destaining buffer (10 % [v/v] acetic acid, 7.5 % [v/v] methanol)[126].

Western blot analysis

For the analysis of proteins in low pmol amount or to visualize a specific protein, western blot analysis was performed[127]. Samples and SDS-PAGE were prepared and executed as described above. Proteins were transferred to nitrocellulose membrane (0.45 μm) for 1 h with 100 V in transfer buffer (25 mM TRIS base, 192 mM glycine, 0.1 % [w/v] SDS, 20 % [v/v] methanol). To the membrane transferred proteins were stained with Ponceau solution (5 % [v/v] acetic acid, 0.1 % [w/v] Ponceau S) for 5 min at RT and rinsed with ddH_2O until protein bands were visible. Further, membrane was blocked for 1 h at RT with 5 % [w/v] milk powder in PBST (137 mM NaCl, 2.7 mM KCl, 4.3 mM Na_2HPO_4, 1.4 mM KH_2PO_4, pH 7.3, 0.1 % [v/v] TWEEN20), primary antibody (dilution according table 2.6, 5 % milk, PBS, 0.01 % NaN_3) was incubated with the membrane over night at 4°C, washed 3 x 5 min with PBST and incubated for 1 h at RT with secondary antibody (1:5000 in PBST). The secondary antibody was removed and the membrane washed 3 x 15 min with PBST. Membranes incubated with secondary antibody conjugated to HRP were treated with ECL western blotting detection

reagents, resulting chemiluminescence was detected using the ChemiDoc imager system. In case of membranes were incubated with secondary antibody conjugated to Alexa488, fluorescence of Alexa488 was detected upon excitation at 488 nm by the ChemiDoc imager system.

2.3.2 Expression of recombinant proteins

Expression of core histones

Expression of histones was carried out as described by Luger *et al.*[128]. Briefly, 1.5 L of 2xYT media supplemented with ampicillin (0.1 μg/mL) was inoculated 1:100 with a pre-culture grown in LB with ampicillin (100 μg/L), chloramphenicol (34 μg/L) over night (ON) at 37°C. The final culture was grown until an OD_{600} of 0.4 -0.6 was reached, 0.3 mM IPTG was added and proteins were expressed for 3 h at 37°C. Cells were collected by centrifugation at 6200 rcf, 4°C for 15 min and stored at -80°C.

Expression of His_6-CFP-HP1-fusion proteins

His_6-eCFP-HP1β, His_6-mCFP-HP1β and His_6-Cerulean-HP1β were expressed in *E. coli* BL21 Rosetta cells. For the pre-culture, a single colony was picked and grown in 40 mL LB medium supplemented with ampicillin (100 μg/L) and chloramphenicol (34 μg/L) for 5 h at 37°C and 130 rpm shaking. 1.5 L 2xYT medium supplemented with ampicillin (100 μg/L) and chloramphenicol (34 μg/L) was inoculated 1:75 or 1:100 with the pre-culture and grown at 37°C and 125 rpm shaking until an OD_{600} of 0.3-0.5 was reached. Expression was induced with 0.3 mM IPTG ON at 18°C. Cells were collected by centrifugation at 6200 rcf, at 4°C for 15 min. Cells were either stored at -80°C or expressed proteins were immediately purified.

Expression of His_6-yGCN5 and His_6-Aurora B

Expression of His_6-tagged GCN5 from yeast and His_6-tagged Aurora B was performed in *E. coli* BL21 RIL cells. For the pre-culture, a single colony was picked and grown in 200 mL LB medium supplemented with ampicillin (100 μg/L) and chloramphenicol (34 μg/L) ON at 37°C

and 130 rpm shaking. For expression, 1.5 L 2xYT supplemented with ampicillin (100 μg/L) was inoculated 1:100 with the pre-culture and grown at 37°C, 125 rpm shaking to an OD_{600} of 0.3-0.5. Expression was induced with 0.3 mM IPTG at 30°C for 3 h.

2.3.3 Purification of recombinant proteins

Purification of core histones

Cells were resuspended in 50 mL wash buffer (50 mM TRIS-HCl pH 7.5, 100 mM NaCl, 1 mM EDTA, 2 mM DTT, 1 mM PMSF, 1 mM benzamidin). Resuspended cells were lysed using the EmulsiFlex 5C. Insoluble inclusion bodies were collected by centrifugation at 23000 rcf at 4°C for 20 min. Inclusion bodies were washed three times by resuspending the inclusion body pellet in 100-200 mL TW buffer (50 mM TRIS-HCl pH 7.5, 100 mM NaCl, 1 mM EDTA, 2 mM DTT, 1% v/v Triton X-100) and centrifugation at 23000 rcf at 4°C for 20 min. Triton X-100 was removed by another two wash steps using 200 mL wash buffer. Inclusion bodies were stored at -20°C.

Histones were extracted form inclusion bodies by adding 2 mL DMSO and incubation at RT for 30 min. In a first round, histones were solubilized with 30 mL of unfolding buffer (20 mM TRIS-HCl pH 7.5, 7 M guanidine hydrochloride, 10 mM DTT) for 1 h at RT. Then, separated from insoluble matter by centrifugation at 23000 rcf, 4°C for 20 min. In a second round, extraction of histones was performed by incubating the remaining pellet with 10 mL unfolding buffer for 30 min and centrifugation. Supernatants were pooled and dialyzed against SAU200 (20 mM sodium acetate pH 5.2, 7 M urea freshly deionized, 1 mM EDTA, 200 mM NaCl, 2 mM DTT). Histones were purified from DNA by loading them onto in SAU200 pre-equilibrated Q-Sepharose XK26/20 and SP-Sepharose XK26/20 column combination connected in series. When the input had reached the SP-Sepharose column, the Q-Sepharose column was disconnected and the SP-Sepharose column was washed with SAU200 until baseline of protein detection (absorbance at 280 nm or 276 nm) was reached. Histones were eluted with SAU600 (20 mM sodium acetate pH 5.2, 7 M urea freshly deionized, 1 mM EDTA, 600 mM NaCl, 2 mM DTT) from the SP-Sepharose column using a step gradient 30 % SAU600 for 1 CV followed by a linear gradient from 30-100 % SAU600 over 1 CV. Fractions were ana-

lyzed by SDS-PAGE (chapter 2.3.1). Histone containing fractions were pooled and dialyzed against H_2O with 2 mM DTT and lyophilized. Histones were stored at -80°C.

Purification of His_6-CFP-HP1-fusion proteins

For purification, a cell pellet corresponding to 1.5 L culture was resuspended in lysis buffer (50 mM NaP_i pH 7.9, 300 mM NaCl, 10 mM imidazole, protease inhibitor EDTA free) and lysed by three passages through the EmulsiFlex 5C homogenizer. Lysate was cleared by centrifugation at 30000 rcf, 4°C for 45min. Affinity chromatography was performed using Ni-NTA agarose beads pre-equilibrated in lysis buffer and packed in a column for gravity flow. After the lysate passed through, resin was washed with 20 mL of lysis buffer followed by 250 mL of wash buffer (50 mM NaP_i pH 7.9, 1 M NaCl, 30 mM imidazole). The CFP proteins were eluted in 4 mL elution buffer (50 mM NaP_i pH 7.9, 300 mM NaCl, 300 mM imidazole) and immediately dialyzed against 20 mM $N(EtOH)_3$ 7.5, 300 mM NaCl, 0.1 mM EDTA. Proteins were concentrated to 5-10 mg/mL with Amicon centrifugal filter with a MWCO of 30 kDa and used immediately for the CFP-HP1 binding assay with nucleosome core particle immobilized in 96-well plate or stored at 4°C.

Purification of His_6-yGCN5 and His_6-Aurora B

For purification of His_6-yGCN5 and His_6-Aurora B, cells were resuspended in lysis buffer (50 mM NaP_i pH 8.0, 10 mM imidazole, 300 mM NaCl, 2 mM β-mercaptoethanol) and lysed by three passages through the EmulsiFlex C5 homogenizer. Lysate was cleared by centrifugation at 30000 rcf at 4°C for 45 min. 50 mL lysate was incubated with in lysis buffer pre-equilibrated Ni-NTA agarose slurry for 1 h at 4°C. Ni-NTA resin was allowed to settle in a column and washed with 20 mL lysis buffer and 100 mL wash buffer (50 mM NaP_i pH 8.0, 10 mM imidazole, 500 mM NaCl, 2 mM β-mercaptoethanol). His_6-tagged protein was eluted with 50 mM NaP_i pH 8.0, 300 mM NaCl, 5 % glycerol, 2 mM β-mercaptoethanol, 300 mM imidazole. Eluate was concentrated and diluted using 3x GCN5 buffer (30 mM TRIS-HCl pH 8.0, 30 % glycerol 0.3 mM EDTA, 15 mM β-mercaptoethanol) to 40 μM, aliquoted, then they were flash frozen and stored at -80°C.

2.3.4 Assembly of histone octamers

According to the established protocol[129], lyophilized histones were dissolved in unfolding buffer (20 mM TRIS-HCl pH 7.5, 7 M guanidine hydrochloride, 10 mM DTT) to 2 mg/mL. Concentration of histones were determined by measuring the absorbance at 276 nm using extinction coefficient and molecular weight listed in table 2.16. Histones were combined equimolar and diluted using unfolding buffer to a final protein concentration of 1 mg/mL. Histone octamers were dialyzed against RB high (10 mM TRIS-HCl pH 7.5, 2 M NaCl, 1 mM EDTA, 2 mM DTT). Any precipitate was removed by centrifugation at 3220 rcf, 4°C for 10 min. In preparation for size exclusion chromatography, histone octamers were concentrated using Amicon Ultra-15 centrifugal filter with MWCO 30 kDa. Precipitate was removed by centrifugation at 10000 rcf, at 4°C for 10 min. Histone octamers were purified using either Superdex 200 10/300 GL or HiLoad Superdex 200 16/600 PG depending on the input volume. Elution fractions were analyzed by SDS PAGE (chapter 2.3.1). Those fractions containing histone octamer showing an equal amount of all four histones were pooled and stored in 50 % glycerol at -20°C. IntC-H2A containing octamers were directly used for nucleosome core particle reconstitution.

2.3.5 Reconstitution of ligation-ready nucleosome core particles

For the reconstitution of NCP the standard protocol was followed[129]. In general, the concentration of histone octamer was determined by measuring the absorbance at 276 nm and assessing the concentration, using an extinction coefficient calculated by summation of the single extinction coefficients of each histone (table 2.16) as it has been suggested by Dyer *et al.*[129]. For NCP reconstitution, histone octamers and DNA were set up in RB high (10 mM TRIS-HCl pH 7.5, 2 M NaCl, 1 mM EDTA, 2 mM DTT). For small scale titration series, 0.9-1.2 eq. octamer was mixed with 1.0 eq. DNA in RB high (small scale: 1.0 eq. = 140 pmol, 3-5 μM, large scale: 1.0 eq. $>$ 500 pmol, 3 μM). Prior to the addition of histone octamer, the DNA was adjusted with 5 M NaCl to 2 M NaCl. Using a peristaltic pump a gradient to RB low (10 mM TRIS-HCl pH 7.5, 25 mM NaCl, 1 mM EDTA, 2 mM DTT) was applied by dialysis at 4°C over 24 h (small scale) or 36 h (large scale). Quality of NCP reconstitution was analyzed by agarose gel electrophoresis (chapter 2.2.3).

2.3.6 Immobilization of nucleosome core particles in 96-well plate

For eCFP-HP1 binding-and enzymatic activity assay on immobilized H3-NCP library in 96-well format, ligation-ready H3Δ-NCP were immobilized on 96-well black, STA coated 96-well plates (BA-plates, 100 μL STA coating volume, high binding capacity: 125 pmol/well) or 96-well, white Flash plates (200 μL STA coating volume, binding capacity $\sim$40 pmol/well). STA coated 96-well plates were prepared for NCP immobilization by washing 3x 200 μL with RB low (10 mM TRIS-HCl pH 7.5, 25 mM NaCl, 1 mM EDTA, 2 mM DTT). NCP were immobilized by adding 50 μL per well (BA-plates) or 100 μL (Flash plates) of H3Δ-NCP (4 μM) and incubation for 20 h at RT. Unbound NCPs were removed and stored at 4° and reused for NCP coating of more plates. Wells containing immobilized NCP were washed 3x 200 μL BA-buffer (20 mM $N(EtOH)_3$ pH 7.5, 300 mM NaCl, 5 % [v/v] glycerol, 0.1 mM EDTA) and stored in 200 μL BA-buffer at 4°C.

2.3.7 Ligation of histone H3 tail to H3Δ-NCP using Sortase A

Synthesis of histone tails carrying PTMs listed in table 2.17 and their Sortase A mediated ligation to immobilized H3-Δ-NCP in 96-well BA- and Flash plate was performed by Diego Aparicio Pelaz (Eberhard Karls Universität Tübingen, Tübingen).

Table 2.17: Library of histone H3 modifications used for binding and activity assays and H2A modifications

# (k)	Histone H3 modifications	# (k)	Histone H3 modifications
1	H3K4me2	19	H3K9me2K27me2
2	H3K4me2 K9me2	20	H3K9me2S28ph
3	H3K4me2S10ph	21	H3K9me2S10phK27me2
4	H3K4me2K27me2	22	H3K9me2S10phS28ph
5	H3K4me2S28ph	23	H3K9me2K27me2S28ph
6	H3K4me2K9me2S10ph	24	H3K9me2S10phK27me2S28ph
7	H3K4me2K9me2K27me2	25	H3S10ph
8	H3K4me2K9me2S28ph	26	H3S10phK27me2
9	H3K4me2S10phK27me2	27	H3S10phS28ph
10	H3K4me2S10phS28ph	28	H3S10phK27me2S28ph
11	H3K4me2K27me2S28ph	29	H3K27me2
12	H3K4me2K9me2S10phK27me2	30	H3K27me2S28ph
13	H3K4me2K9me2S10phS28ph	31	H3S28ph
14	H3K4me2K9me2K27me2S28ph	32	unmodified
15	H3K4me2S10phK27me2S28ph	33	H3Δ1-32
16	H3K4me2K9me2S10phK27me2S28ph	34	H3K4ac

Table 2.17 – continued from previous page

#(k)	Histone H3 modifications	#(k)	Histone H3 modifications
17	H3K9me2	35	H3K27ac
18	H3K9me2S10ph	36	H3K9ac
#(k)	**Histone H2A modifications**	**#(k)**	**Histone H2A modifications**
A	H2AK5ac	E	H2AR3me2a
B	H2AK5acR3me2a	F	H2AS1ph
C	H2AS1phK5ac	G	H2AS1phR3me2a
D	H2Aunmodified	H	H2AS1phR3me2aK5ac

2.3.8 Ligation of histone H2A tail to IntC-H2A-NCP using protein *trans*-splicing

Ligation conditions were set up on the base of Ludwig *et al.*[97]. Accordingly, IntC-H2A NCP were dialyzed against AB25 (50 mM TRIS-HCl pH 7.0, 25 mM NaCl, 1 mM EDTA, 2 mM DTT, 10 % glycerol). 100 μL IntC-H2A-NCP (181 pmol, stock 1.8 μM) were adjusted to 300 mM NaCl (5.83 μL, stock 5 M) and 10 eq. of unmodified IntC-H2A$_{1-18}$ (5.42 μL, 1.81 nmol, stock 334 μM) in a final volume of 111.24 μL and incubated for 4 h at 25°C. Further optimization was done by Diego Aparicio Pelaz (Eberhard Karls Universität Tübingen) with the final conditions: protein *trans*-splicing was performed in solution in total volume of 650 μL per modification with 325 μL IntC-H2A-NCP (2.74 nmol, stock 8.45 μM) and 58.5 μL H2A-peptide (58.5 nmol, stock 1 mM) incubating for 72 h at RT.

2.4 Biochemical assays

2.4.1 Peptide pull-down – standard protocol

In order to check whether CFP-derivatives HP1 conjugates distinguish between histone H3 tail unmodified (pH3um) and methylated on lysine 9 (pH3K9me3), peptide pull-down was performed. First, 40 μL of streptavidin coated beads were equilibrated in PBS buffer (137 mM NaCl, 2.7 mM KCl, 4.3 mM Na_2HPO_4, 1.4 mM KH_2PO_4, pH 7.3) by washing 3 x 80 μL PBS. The peptide of interest was bound to the beads by incubation of 10 μg peptide in 80 μL total volume PBS and rotation for 3 h at RT. Beads were washed 3 x 80 μL PBS. 5 μg His$_6$-

CFP-HP1 fusion protein (95 pmol) in 500 μL pull-down buffer PD-300 (20 mM HEPES pH 7.9, 300 mM NaCl, 0.2 % Triton X-100, 20 % glycerol) was incubated for 4 h or ON with the immobilized peptides on the beads, rotating at 4°C. Beads were washed 6 x 500 μL for 5 min with PD-300. For analysis, peptide bound proteins were eluted by adding 20 μL of 2 x SDS buffer and boiling for 5 min at 95°C. Proteins bound to the according peptide was detected by standard SDS-PAGE and western blot analysis using antibody against GFP that also recognizes CFP derivatives.

2.4.2 Peptide pull-down – optimized protocol

Peptides were immobilized on streptavidin coated magnetic beads as described above (chapter 2.4.1). 5 μg His_6-CFP-HP1 fusion protein (95 pmol) in 500 μL pull-down buffer PD_{opt}-300 (20 mM $N(EtOH)_3$ pH 7.5, 300 mM NaCl, 0.1 % [v/v] Triton X-100, 0,1 mM EDTA, 15 % [v/v] glycerol, 1 mg/mL BSA) was incubated for time frames as indicated (1.5, 4 h or ON) with peptide-bound beads, rotating at 4°C. Beads were washed 6 x 500 μL with PD_{opt}-300 (-BSA) for 5 min. For analysis, peptide bound proteins were eluted by adding 20 μL of 2 x SDS buffer and boiling for 5 min at 95°C. Proteins bound to the according peptides were detected by standard SDS-PAGE and western blot analysis using antibody against GFP that also recognizes CFP derivatives.

2.4.3 Binding assay – 96-well format

Streptavidin coated 96-well plates with a coating volume of 100 μL and high binding capacity of 125 pmol/well were used for all fluorescence based binding assays. They were coated with 50 μL of ligation-ready NCPs as described in chapter 2.3.6.

Proof of principle experiment

In order to check whether the principle experimental design was functional, binding of eCFP-labeled HP1 to immobilized and H3 modified NCP was observed by detection of in-well fluorescence of eCFP-HP1. Herefore, eCFP-HP1 protein was thawed and dialyzed into 10 mM $N(EtOH)_3$ pH 7.5, 150 mM NaCl. Subsequently diluted 1:1 with binding buffer (10 mM

$N(EtOH)_3$, 150 mM NaCl, 0.2 % [v/v] Triton X-100, 10 % [v/v] glycerol, 0.2 mM EDTA) to a final concentration of 10 μM. Wells were washed 3 x 100 μL binding buffer (10 mM $N(EtOH)_3$, 150 mM NaCl, 0.1 % [v/v] Triton X-100, 5 % [v/v] glycerol, 0.1 mM EDTA). 50 μL of eCFP-HP1 (10 μM) was added into each well and incubated ON at 4°C, rocking. Unbound proteins were removed and wells were washed 4 x with 50 μL binding buffer except for the third washing step (100 μL). Measurement of eCFP and Cy5-fluorescence took place after each washing step with the settings listed in table 2.18.

Table 2.18: Measurement parameters using GENios plate reader

Parameter	CFP proteins	Cy5
Excitation wavelength	450 nm	612 nm
Emission wavelength	520 nm	670 nm
Gain (optimal)	66	66
Integration time	40 μs	40 μs

Conditions for optimization of incubation time and wash steps

In order to check the impact of incubation time and wash steps on the signal intensities, 17.5 μM eCFP-HP1 in BB-H (20 mM HEPES, 150 mM NaCl, 0.1 % [v/v] Triton X-100, 5 % [v/v] glycerol, 0.1 mM EDTA) was incubated in a total volume of 50 μL/well with immobilized H3um-NCP and H3K9me2-NCP for 5, 30, 60 and 180 min at 4°C, rocking. After indicated incubation time, wells were washed 3 x 100 μL/well for 5 min with WB-H (20 mM HEPES, 300 mM NaCl, 0.1 % [v/v] Triton X-100, 5 % [v/v] glycerol, 0.1 mM EDTA) at 4°C, rocking. Subsequently, 50 μL PBS (137 mM NaCl, 2.7 mM KCl, 4.3 mM Na_2HPO_4, 1.4 mM KH_2PO_4, pH 7.3) were added for the first fluorescence measurement after an incubation time of 180 min (measurement #1). The plate was incubated over night at 4°C and reread (measurement #2). 50 μL/well PBS were added and fluorescence measurement was performed (measurement #3). Subsequently, wells were washed 3 x 100 μL/well WB-H for 5 min at 4°C and measured in 50 μL/PBS (measurement #4). This last wash cycle was repeated once more and fluorescence data were obtained (measurement #5). Fluorescence was measured with the settings listed in table 2.19. The plate reader was changed because the infinite M1000Pro selects excitation wavelength by an monochromator and not by filters as it is in the GENios plate reader. This allowed an excitation of the fluorophore within a range of $\pm$ 5 nm.

Table 2.19: 1^{st} settings using infinite M1000Pro plate reader

Parameter	CFP proteins	Cy5
Excitation wavelength	434 nm	649 nm
Emission wavelength	477 nm	670 nm
Excitation bandwidth	5 nm	5 nm
Emission bandwidth	5 nm	5 nm
Gain optimal (100 %)	variable	variable
Number of flashes	50	50
Integration time	20 μs	20 μs
Z-position (standard)	2000 μm	20000 μm

Conditions for 1^{st} eCFP-HP1 binding assay on H3-NCP library

The first experiment on one whole library (modification #1-33, table 2.17) was performed with eCFP-HP1 from a stock of 70 μM adjusted with 2 x binding buffer (2 x BB-H: 40 mM HEPES pH 7.5, 300 mM NaCl, 0.2 % [v/v] Triton X-100, 10 % [v/v] glycerol and 0.2 mM EDTA) to a final concentration of 17.5 μM eCFP-HP1 in 1 x BB-H. Proteins were incubated over night at 4°C, rocking. eCFP-HP1 load per well was measured, unbound proteins were removed and wells were washed 3 x 200 μL WB-H300 (10 mM HEPES pH 7.5, 300 mM NaCl, 0.1 % [v/v] Triton X-100, 5 % [v/v] glycerol and 0.1 mM EDTA). Bound eCFP-HP1 and immobilized NCP were detected in WB-H300 using the settings listed in table 2.19.

Conditions for 2^{nd} eCFP-HP1 binding assay on three H3-NCP libraries

In contrast to the afore mentioned HP1-binding assay, assay conditions were altered in several points: H3-NCP libraries were pre-blocked with BSA and DNA, eCFP-HP1 incubation time with the library was reduced and fluorescence was detected in PBS. In detail, three libraries were washed 3 x 100 μL BB-H (10 mM HEPES pH 7.5, 150 mM NaCl, 0.1 % [v/v] Triton X-100, 5 % [v/v] glycerol and 0.1 mM EDTA) and blocked with blocking buffer (1.0 mg/mL BSA, 0.1 mg/mL ssDNA, 1 x BB-H) for at least 15 min at 4°C, rocking. Pre-blocked libraries were incubated with 50 μL eCFP-HP1 (30 μM) protein adjusted with 2 x BB-H to final 30 μM in 1 x BB-H for 90 min at 4°C, rocking. Unbound protein was removed and wells were washed 3 x 100 μL WB-H300 (10 mM HEPES pH 7.5, 300 mM NaCl, 0.1 % [v/v] Triton X-100, 5 % [v/v] glycerol and 0.1 mM EDTA) for 5 min at 4°C. Libraries were measured in 1 x PBS (137 mM

NaCl, 2.7 mM KCl, 4.3 mM Na_2HPO_4, 1.4 mM KH_2PO_4, pH 7.3) using the settings listed in table 2.20.

Release of bound material into solution using restriction enzyme *Eco*RI

In order to see whether the release of NCP into solution would have an impact on the signal intensity of Cy5 and eCFP, one library was washed 3 x 100 μL BB-H (10 mM HEPES pH 7.5, 150 mM NaCl, 0.1 % [v/v] Triton X-100, 5 % [v/v] glycerol and 0.1 mM EDTA) and blocked with blocking buffer (1.0 mg/mL BSA, 0.1 mg/mL ssDNA, 1 x BB-H) for at least 15 min at 4°C, rocking. The pre-blocked library was incubated with 60 μM eCFP-HP1 and washed 3 x 100 μL with WB-H100 (10 mM HEPES pH 7.5, 100 mM NaCl, 0.1 % Triton X-100, 5 % [v/v] glycerol and 0.1 mM EDTA). The libraries were measured in 60 μL *Eco*RI buffer (50 mM TRIS-HCl pH 7.5, 10 mM $MgCl_2$, 50 mM NaCl) then 10 μL per well of *Eco*RI (1 U/ μL in *Eco*RI buffer) was added and incubated at 37°C. After 5 min the first measurement was taken and incubation at 37°C was continued in the plate reader. Every 5 min for 1 h, fluorescence of eCFP and Cy5 was measured. An 1:1 dilution series of eCFP and Cy5 in *Eco*RI buffer for signal calibration was placed on the plate ranging from 500 pmol/well to 4 pmol/well for eCFP and 100 pmol/well to 1 pmol/well for Cy5 fluorophore.

Final eCFP-HP1 binding assay conditions

Optimized eCFP-HP1 binding assay conditions were developed and used for eCFP-, mCFP- and Cerulean-HP1 binding. In detail, on BA-plates immobilized H3 modified-NCP were washed 3x200 μL binding buffer PD_{opt} 300 (20 mM $N(EtOH)_3$ pH 7.5, 300 mM NaCl, 0.1 [v/v] Triton X-100, 15 % [v/v] glycerol, 0.1 mM EDTA). The wells and immobilized NCP were pre-blocked for 30 min at 4°C with 100 μL blocking buffer (1.0 mg/mL BSA, 0.1 mg/mL ssDNA, 1 x PD_{opt} 300). NCP-coated wells were loaded with 50 μL/well binding mix (33 μM CFP-HP1 protein, 1.0 mg/mL BSA, 0.1 mg/mL ssDNA in 1 x PD_{opt} 300) and incubated for 90 min at 4°C, slightly shaking. After incubation, the binding mix was removed, wells were briefly washed with 200 μL wash buffer (20 mM $N(EtOH)_3$ pH 7.5, 150 mM NaCl, 0.1 [v/v] Triton X-100, 15 % [v/v] glycerol, 0.1 mM EDTA) and placed in 50 μL measuring buffer (20 mM $N(EtOH)_3$ pH 7.5, 150 mM NaCl, 15 % [v/v] glycerol, 0.1 mM EDTA). An 1:1 dilution series in measuring buffer for CFP and Cy5 fluorophores was prepared from 50.0 to 0.39 pmol Cy5

and 80.0 to 0.62 pmol CFP-HP1 and placed into the plate. The plates were let to adapt to measuring temperature (20°C) and measured in triplicates with 1 min interval between one reading of the plate using the plate reader settings shown in table 2.20.

Table 2.20: 2^{nd} settings using infinite M1000Pro plate reader

Parameter	CFP proteins	Cy5
Excitation wavelength	434 nm	649 nm
Emission wavelength	477 nm	670 nm
Excitation bandwidth	5 nm	5 nm
Emission bandwidth	5 nm	5 nm
Gain	107	107
Number of flashes	50	50
Integration time	20 μs	20 μs
Z-position (Manual)	17687 μm	17687 μm

2.4.4 Data analysis for plates with reference wells for fluorophores

Conversion of raw fluorescence data [a.u.] into [pmol]

Well A_k with the modification k = 1 to 36 (see table 2.17, page 37) was sequentially measured for eCFP-HP1 and Cy5-NCP fluorescence. The fluorescence of eCFP-HP1 was measured in a.u. and the whole plate was measured three times (*n*=1, ..., 3) with an interval of one minute between each plate measurement. Fluorescence data of the dilution series of eCFP or Cy5 reference wells were plotted against the concentration. A linear regression was performed ($R^2 > 0.95$) resulting in a linear calibration curve with $c_n = f(x_n) = ax_n + b$ for eCFP-HP1 and for Cy5-NCP $d_n = f(y_n) = ay_n + b$ for the transformation of the units [a.u.] into [pmol].

Error propagation of independent fluorescence detection of eCFP and Cy5

Before starting with the data analysis for plates containing reference wells for eCFP and Cy5-fluorescence, the error resulting from the independent measurement of Cy5 and eCFP fluorescence and its propagation to the final ratio of eCFP-HP1/Cy5-NCP was determined. To this end, the standard error $\bar{s}$ was determined on base of three technical repeats for each modification. For eCFP, $\bar{s}_{\bar{x}} = \frac{\sigma_{\bar{x}}}{\sqrt{n}}$ and Cy5, $\bar{s}_{\bar{y}} = \frac{\sigma_{\bar{y}}}{\sqrt{n}}$ with σ being the standard deviation

of the technical replicates n in the eCFP (x) or Cy5 (y) channel. This led to the following description of the measurement in each well for each modification k: $X_k = \bar{x}_k \pm \bar{s}_{\bar{x}}$ with the mean $\bar{x} = \frac{1}{n} \cdot \sum_{i=1}^{n} x_{ki}$. The same was applied for Cy5: $Y_k = \bar{y}_k \pm \bar{s}_{\bar{y}}$ with $\bar{y} = \frac{1}{n} \cdot \sum_{i=1}^{n} y_{ki}$.
The recruitment of eCFP-HP1 to NCP depended on how many NCP molecules were present in the well: $Z_k = \bar{z}_k \pm \Delta z_k$ with $\bar{z}_k = \frac{\bar{x}_k}{\bar{y}_k}$ and $\Delta z_k = \left|\frac{\bar{x}}{\bar{y}}\right| \cdot \sqrt{\left(\frac{\bar{s}_{\bar{x}}}{\bar{x}}\right)^2 + \left(\frac{\bar{s}_{\bar{y}}}{\bar{y}}\right)^2}$. The absolute Δz_k or relative errors $\left|\frac{\Delta z_k}{\bar{z}_k}\right|$ were propagated using the Gaussian relation for propagating the standard error from both sources of uncertainty: the error introduced by the eCFP and the Cy5 measurement[130]. From the experiment described in figure 3.15, the mean of the relative error over one whole library was for replicate #1, #2, and #3 3.24 %, 3.95 % and 1.76 %, respectively. As the technical error was < 5 % over the whole library, the contribution of the technical error to the overall uncertainty was minor. Therefore it was neglected in further considerations.

Data analysis and normalization

Raw fluorescence data was transformed from [a.u.] into [pmol] as described above. The eCFP signal was normalized to the Cy5-NCP fluorescence signal for each well. The eCFP-HP1 recruitment to Cy5-NCP with the modification k was plotted as the mean $\bar{z}_k^l$ with $\pm$ the standard deviation as error bar ($\pm\sigma_k^l = \sqrt{\frac{1}{n}\sum_{l=1}^{n}\left(\frac{\sigma z_k^l}{\bar{z}_k^l}\right)^2}$) for experiments performed in replicates l > 2.
For direct comparison of data sets from different plates, data of each modification k with k = 1, ..., 36 was normalized to one modification $\bar{z}_j^l$ (e.g. H3Δ) within one library l:$Z_{norm} = \frac{\bar{z}_k^l}{\bar{z}_j^l}$.

2.4.5 Data analysis for plates without reference wells for fluorophores

Early measurements were taken without reference wells for fluorescence calibration on the plate with automatically or manually entered gain settings. For data processing, background values (buffer only, N) were subtracted from signal and divided by the gain used by the plate reader. This was performed for eCFP-HP1 $X_k = \frac{S_k - N}{Gain}$ and Cy5-NCP $Y_k = \frac{S_k - N}{Gain}$. Recruitment of HP1 per NCP was calculated with $Z_k = \frac{x_k}{y_k}$ and only the error based on the standard deviation between l wells of the same modification was plotted as error bar.

2.4.6 Activity assay – 96-well format

For all radioactivity based activity assays, STA coated Flash plates were used with a STA-coating volume of 200 μL, biotin binding capacity $\sim$40 pmol/well. Flash plates were coated as described in chapter 2.3.6 with 100 μL NCPs if not stated otherwise.

HAT assay

For optimization experiments 50-200 μL/well NCPs containing WT histones were immobilized on STA-coated 96-well Flash plate and washed 3 x with 200 μL HAT assay buffer (50 mM TRIS-HCl pH 8.0, 50 mM NaCl, 10 % [v/v] glycerol, 0.1 mM EDTA, 1 mM DTT and 10 mM n-butyrate). 50-200 μL/well reaction mix (2.4 μM yGCN5, 0.08 μCi/well [acetyl-1-14C]-acetyl coenzyme A in HAT assay buffer) was added to the well, spun for 1 min, 3220 rcf at 4°C and incubated for 2 h at 30°C, slightly shaking (hybridization oven). After removal of the reaction mix, wells were washed 3 x 200 μL HAT wash buffer (50 mM TRIS-HCl pH 8.0, 300 mM NaCl, 10 % [v/v] glycerol, 1 % [w/v] CHAPS 0.1 mM EDTA) and incorporated radioisotopes were detected in 100 μL HAT wash buffer for 120 sec/well using the standard settings for 14C-detection (low limit 50 and high limit 900, Chameleon V plate reader).
For the initial experiment shown in figure 3.20 (B), 200 μL reaction mix (1.2 μM GCN5, 0.02 μCi 14C-AcCoA in 1 x HAT buffer) were incubated for 45 min at 30°C and washed 4 x 700 μL HAT wash buffer, last wash over night.

Final conditions: H3Δ-NCPs were immobilized with 100 μL coating volume on 96-well plates and two libraries of histone H3 modifications described in table 2.17 were ligated in a random pattern on the plate using Sortase A (ligation was performed by Diego Aparicio Pelaz, Eberhard Karls Universität Tübingen, Tübingen). The HAT assay with GCN5 was performed in 100 μL reaction mix per well (2.4 μM yGCN5, 0.08 μCi/well [acetyl-1-14C]-acetyl coenzyme A in HAT buffer), washed with 3 x 200 μL HAT wash buffer (50 mM TRIS-HCl pH 8.0, 300 mM NaCl, 10 % [v/v] glycerol, 1 % [w/v] CHAPS, 0.1 mM EDTA) and counted in 100 μL HAT wash buffer for 120 sec/ well. Fluorescence of Cy5-NCP was measured with the same device using a manual gain of 20.

Kinase assay

Similar to the HAT assay, the kinase assay with Aurora B was performed using described buffer conditions[131]. Wells were washed 3 x 200 μL with kinase buffer (5 mM MOPS pH 7.2, 1 mM EGTA, 0.4 mM EDTA, 5 mM $MgCl_2$). 100 μL of the reaction mix (40 nM Aurora B, 20 nM [γ 32P] ATP, 40 nM ATP, 2.5 mM β-glycerophosphat, 50 μM DTT) were added to each well and incubated for indicated time points (maximal 120 min) at 30°C, slightly shaking (hybridization oven). After removal of the reaction mix, wells were washed with 200 μL wash buffer (5 mM MOPS pH 7.2, 1 mM EGTA, 0.4 mM EDTA, 1 % CHAPS, 300 mM NaCl). Wells were counted for 3 x 10 sec in 100 μL kinase buffer using the plate reader Chameleon V and the standard settings for 32P (low limit: 10 and high limit 1023). Fluorescence of Cy5-NCP was measured with the same device using a manual gain of 20.

Data analysis of radioactive HAT-, and kinase assays

Cy5-NCP fluorescence was converted from [a.u.] to [pmol] as described in chapter 2.4.4 by means of a dilution series of Cy5 calibration wells within the plate. Fluorescence intensity were plotted against the concentration and a linear regression was performed. Radioactivity was measured for 120 seconds (32P for 3 x 10 sec) in CPM and corrected for the background, that was empty wells incubated with reaction mix and treated exactly as the sample wells were treated. The division of background corrected counts by Cy5-NCP coverage in [pmol] resulted in an activity signal per NCP [CPM/pmol] for each well and modification. Error bars were plotted as the standard deviation of at least 3 different wells containing the same modification.

Outliers were identified by determining the inter quartile range (IQR: Q_3 - Q_1) of the whole data set (with replicates $l > 4$) falling either below the inner lower (IQR - 1.5·Q_1) or above the inner upper limit (IQR - 1.5·Q_3). In addition, values were not taken for analysis, when no NCP signal was obtained for a specific modification.

Significance was tested by using a two sample, heteroscedastic, two sided t-test.

3 Results

3.1 Building block for reconstitution of ligation-ready NCPs

For the development of immobilized ligation-ready nucleosomes, we used recombinant *Xenopus laevis* histones. In general, histones are quite conserved among species. Histones from *X. laevis* share high sequence identity with human histones (H2A: 94 %, H2B: 95 % H3: 99 %, H4: 100%) and are well characterized[3;128]. For the stable and uniform assembly of chromatin, the artificial '601 Widom' positioning DNA sequence was used[122;132]. A minimum of 147 base pairs of the '601 Widom' sequence is needed to wrap around the histone octamer to assemble the nucleosome core particle NCP (from now on referred to as '147'-positioning sequence).

3.1.1 Biotin- and Cy5-labeled '147'-DNA template

For the immobilization of NCPs in 96-well plates, we wanted a site-directed, irreversible linkage between the plate and NCPs under mild reaction conditions. Such a linkage is provided by the affine interaction between streptavidin and biotin[133]. Since streptavidin coated plates were commercially available, biotin was introduced to the 5' end of the '147'-positioning sequence using a biotinylated primer. For the purpose of normalization and determination of NCP coating within each well, the 3' end of the '147'-positioning sequence was labeled with a Cy5 fluorophore using a Cy5-labeled primer. To allow for flexible usage of the generated modified NCP, e.g. for analytics of the NCP complex outside the 96-well-plate, three different DNA recognition sequences for restriction enzymes (*Hin*dIII, *Eco*RI and *Eco*RV) were inserted between the biotin tag and the '147'-positioning sequence (see figure 3.1 (A)). In the following, the whole modified construct will be referred to as '147'-DNA, since this is

the length of the positioning sequence. PCR amplified '147'-DNA constructs were purified by PEG precipitation. This way, surplus primer and polymerase were efficiently removed in one purification step. The efficiency of the PCR reaction was observed by detection of Cy5-fluorescence of the unprocessed PCR product revealing '147' product and surplus primer (see figure 3.1(B)). This protocol yielded about 200 μg DNA per plate.

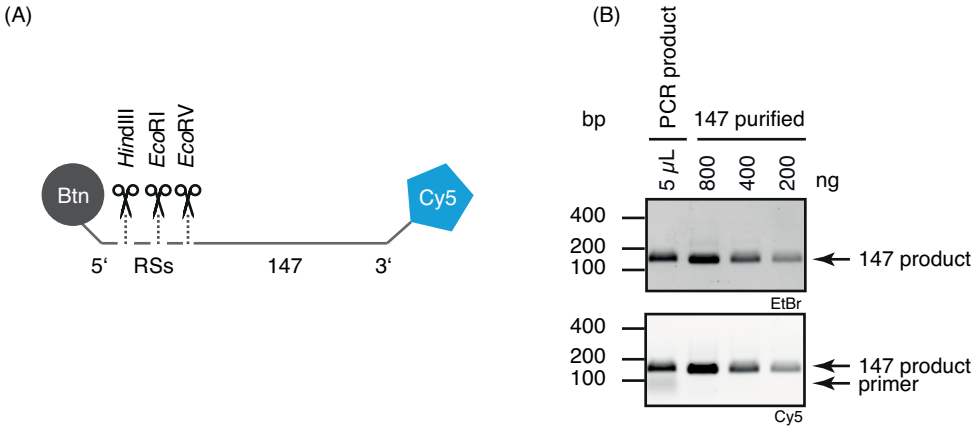

Figure 3.1: Biotin- and Cy5-labeled '147'-DNA
(A) Schematic representation of '147'-DNA 5' labeled with biotin, followed by three restriction sites (RSs) for restriction enzymes *Hin*dIII, *Eco*RI and *Eco*RV and 3' labeled with Cy5 dye. (B) Agarose gel of purified, EtBr stained '147'-DNA, observed under UV shows the quality of the PCR reaction. Detection of Cy5-fluorescence revealed the efficiency of PCR reaction by the amount of unused primer during PCR reaction.

3.1.2 Assembly of ligation-ready histone octamers

For the introduction of post-translational modified histone tails to the corresponding histone (H2A or H3), we wanted to perform histone type-specific ligation in the context of NCP. Therefore, histones were modified in a way that allows for site-specific ligation. To this end, histone H2A was modified for ligation using protein *trans*-splicing. Whereas, H3 was modified to allow for Sortase A mediated ligation. This meant generating an IntC-SIE-H2AΔ1-18 and a truncated H3Δ1-32 fusion construct for recombinant expression in bacteria. The native, intein flanking amino acid sequence 'SIE' between IntC and H2A enhances the efficiency of ligation[96]. Such recombinant modified and wild type histones were assembled to histone octamers[129]. In agreement with the literature[129], we observed three major protein fractions for a typical purification by size exclusion chromatography of assembled octamers. At first,

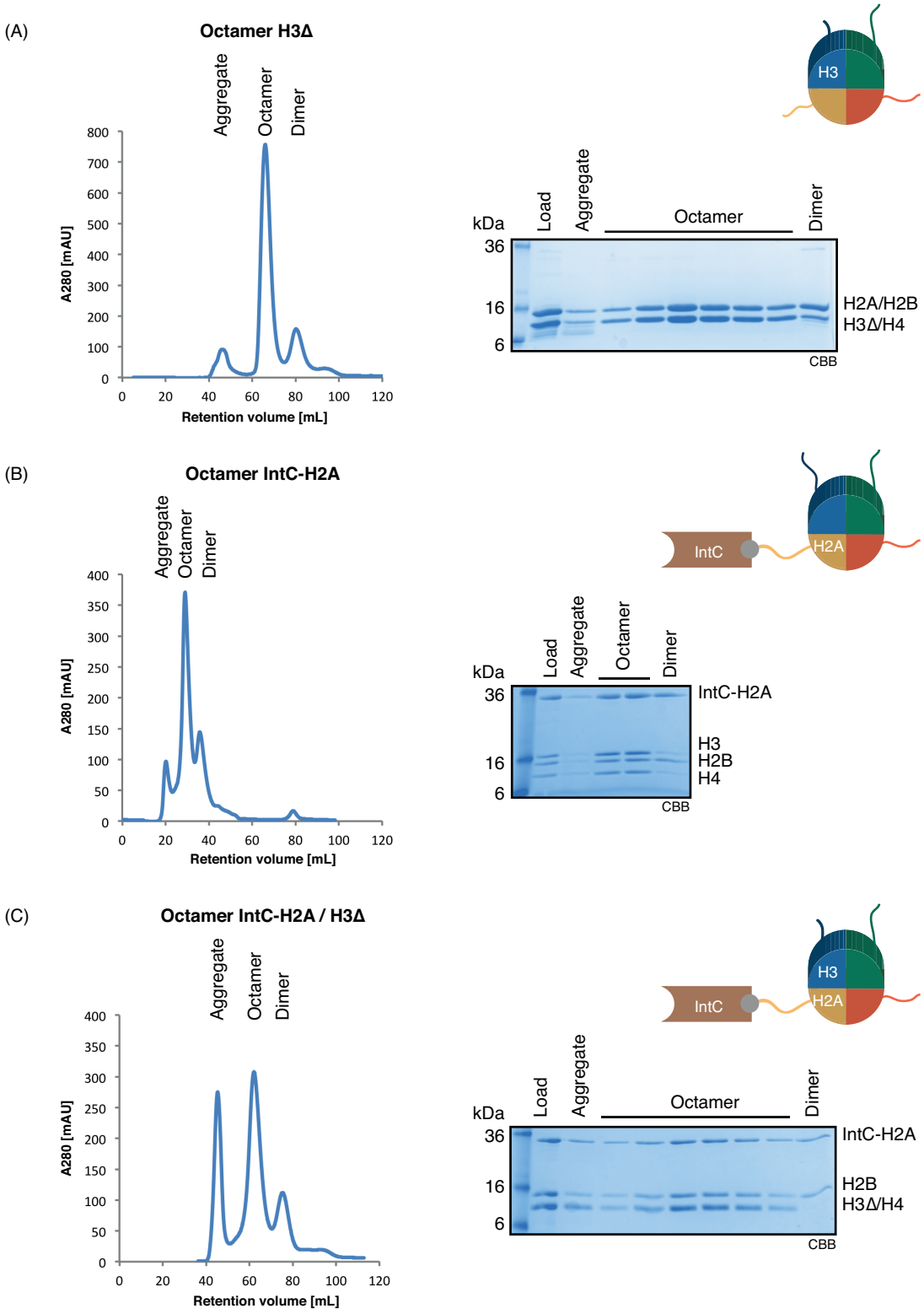

Figure 3.2: Quality of the assembly of mono and double modified histone octamer
Elution profile of size exclusion chromatography using HiLoad Superdex200 16/60 PG column for the purification of *in vitro* assembled histone octamer H3Δ (A), IntC-H2A (B) and double modified IntC-H2A/H3Δ (C). Analysis of aggregate-, octamer-, and dimer-fractions using SDS-PAGE and subsequent CBB staining.

close to the void volume of the size exclusion column eluted aggregated material. Secondly and thirdly eluted the octamer and dimer fractions, which had a good peak separation. The assembly of mono-modified histone octamer with H3Δ1-32 displayed the best ratio between octamer, aggregate and dimer fraction (figure 3.2 (A)). Whereas, histone octamers containing IntC-H2A assembled less efficient (figure 3.2 (B)). During the assembly of octamers containing both IntC-H2A and H3Δ1-32, a significant amount formed aggregates (figure 3.2 (C)). Nevertheless, octamer fractions contained equal amounts of all four histone types assessed by CBB stained polyacrylamide gels (figure 3.2) were used for nucleosome reconstitution.

3.1.3 Reconstitution of ligation-ready NCPs

NCP were reconstituted from histone octamer and '147'-DNA by dialyzing both components together from high salt to low salt conditions by applying a salt gradient over 36 h as described by Luger *et al.* Before each large-scale reconstitution (1.0 eq $>$ 500 pmol), in a small-scale set up (1.0 eq $\approx$150 pmol) ratios were tested between DNA and octamer in a range of 0.9-1.2 eq octamer to 1.0 eq '147'-DNA. The NCP reconstitution was analyzed by native agarose gel electrophoresis. It showed the efficiency of NCP formation by the amount of free DNA, which migrated faster than the NCP. For the reconstitution of H3Δ-NCP, typically an octamer:DNA ratio of 1.0 -1.1 was sufficient for consumption of all free DNA. In contrast, during the reconstitution of NCPs with IntC-H2A containing octamers, aggregation of the complex was observed concomitantly with the consumption of free DNA. Thus, the octamer:DNA ratio was chosen to keep precipitation at a moderate level, resulting in small amount of free DNA after the reconstitution of NCPs (figure 3.3). IntC-H2A containing NCPs were transferred into the P*t*S-ligation buffer containing low salt for further immobilization. Whereas, H3Δ-NCPs were stable in reconstitution buffer.

3.2 Ligation in context of NCP

We wished to ligate post-translational modified H2A and H3 histone tails synthesized by SPPS to the corresponding histone type in the context of the nucleosome core particle. For this, SrtA mediated ligation was chosen for addressing histone H3 and P*t*S for histone H2A.

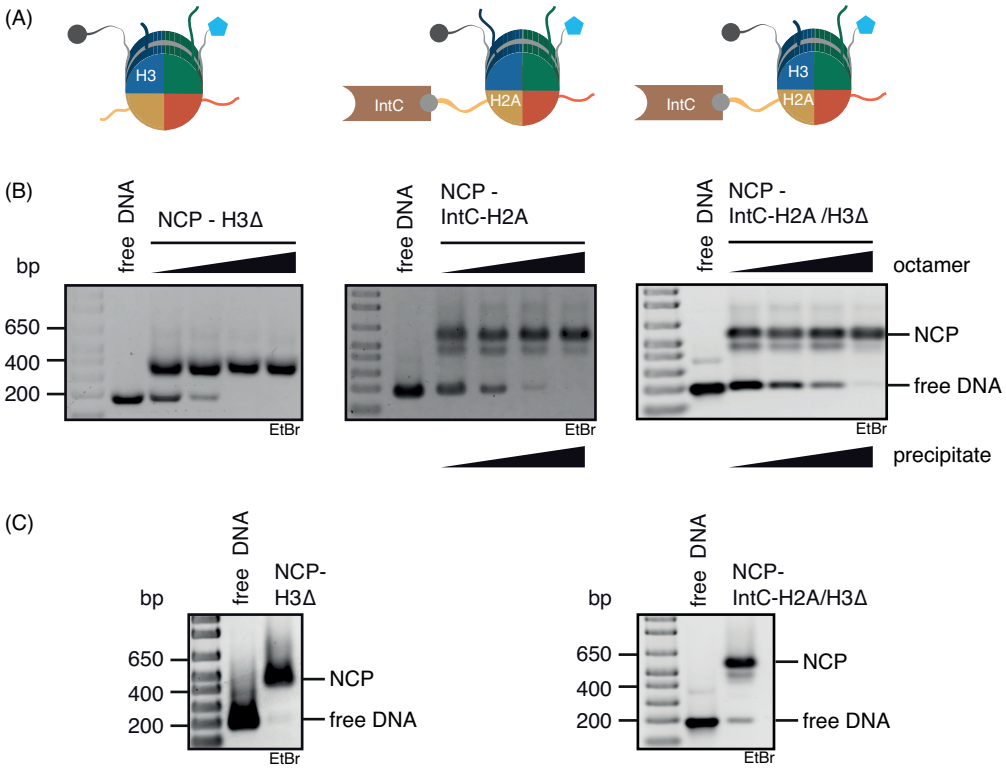

Figure 3.3: Analysis of reconstituted single and double modified NCPs
(A) Schematic representation of reconstituted NCP with corresponding modified histones. (B) EtBr stained native agarose gel of small-scale titration series to determine the ratio between octamer and '147'-DNA for large-scale reconstitution. (C) Analysis of large-scale reconstitution of mono (H3Δ) and double (IntC-H2A/H3Δ) modified NCPs by EtBr stained native agarose gel electrophoresis.

3.2.1 Histone H3: Sortase A mediated ligation

Sortase A mediated ligation was chosen to target histone H3, because the recognition sequence of SrtA is present in the native sequence of H3. However, the very promising SrtA mutant F40 accepting the amino acid sequence APXTG as substrate which is truly native in H3 (H329-32: APAT) was not efficient enough to mediate ligation between histone tail and H3 in the context of NCP for all histone tail modifications. Nevertheless, the original SrtA recognizing LPXTG motif was more efficient for H3Δ-NCP ligation with modified H3-tail-peptides resulting in H3A29L ligation product. To this end, 32 H3 tail peptides carrying di-methylation on H3K4, H3K9, H3K27 and phosphorylation on H3S10 and H3S28 were synthesized in all combinations ranging from single-modified to pentupel-modified H3 tail peptides. Ligation was performed by SrtA with immobilized H3Δ-NCP in a 96-well plate. This way, each well contained NCPs carrying a specific type of histone tail modifications. In figure 3.4 the conversion of H3Δ-NCP to full-length H3-NCP (H3$_{FL}$-NCP) is shown by western blot analysis for all 32 modifications. The yield for each modification was determined by quantification of western blot analysis with n= 3-5 reactions/modification and plotted with the standard deviation as error bars in figure 3.4 (C). Synthesis of H3-peptides, SrtA reaction and analysis was performed by D. Aparicio Pelaz (Eberhard Karls Universität, Tübingen). Thus, we were able to ligate H3 histone tails of 32 different PTM patterns with immobilized H3Δ-NCP using SrtA with an over all yield of 83$\pm$3 %. This meant, on average 17 % of non-ligated H3Δ-NCP material was present within each H3-NCP library. In order to evaluate the impact of non-ligated H3Δ material within each experiment an H3Δ-NCP control was included into the library.

3.2.2 Histone H2A: protein *trans*-splicing

In order to address H2A histone type specific, P*t*S was chosen. Here, the C-terminal part of the evolved M86 split-intein (IntC) was genetically fused to the globular domain of H2A. The H2A tail amino acids 1-18 and IntN (11 aa) were synthesized by SPPS. Firstly, we were interested whether protein *trans*-splicing worked in the context of NCP and whether this complex remained stable throughout the ligation procedure. To test this, a short peptide sequence (KKESG) was labeled N-terminal with FAM and linked C-terminal to IntN. Protein *trans*-splicing was allowed to proceed over 24 h (figure 3.5). The SDS-PAGE fluorescence

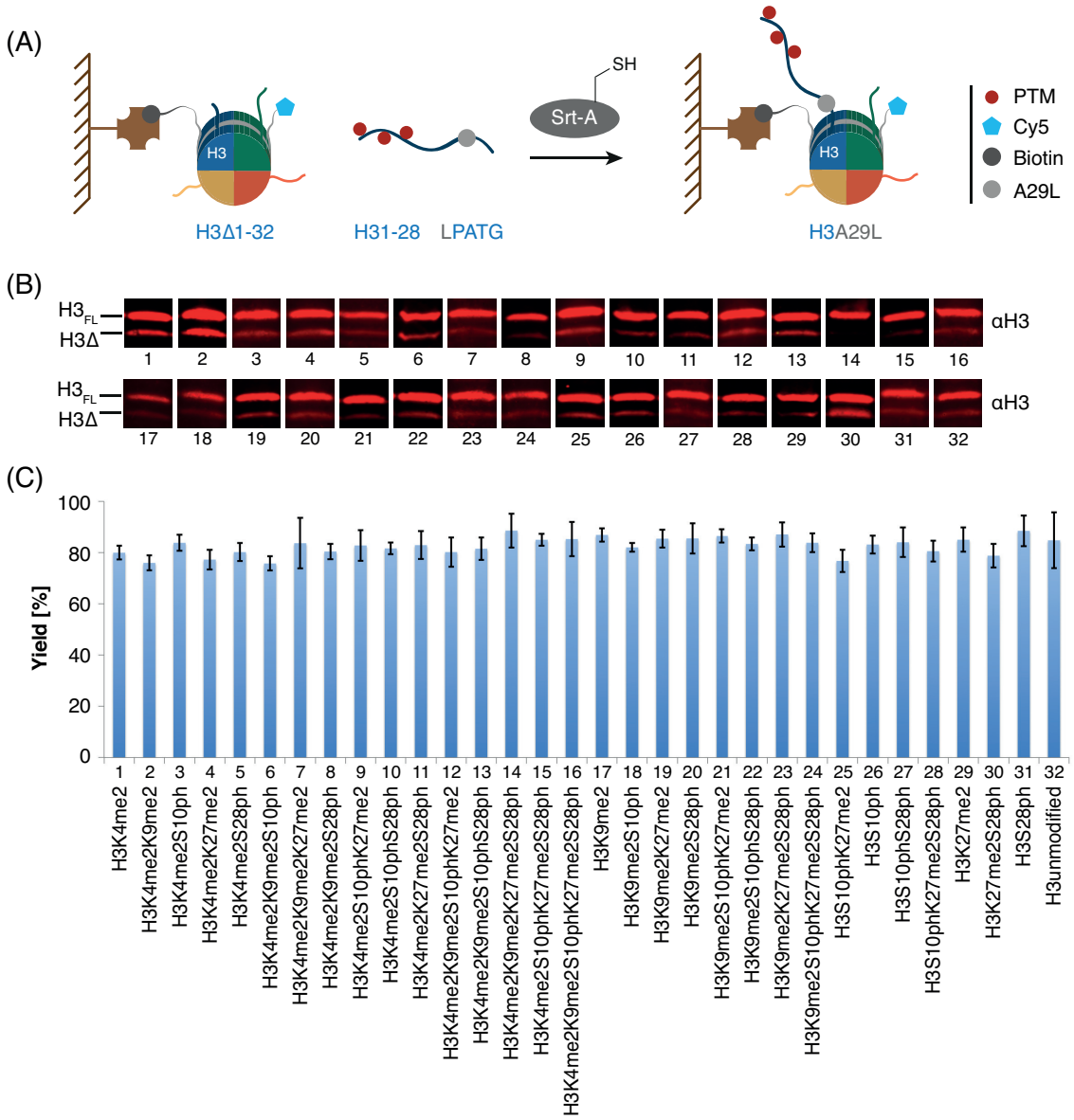

Figure 3.4: Sortase A mediated ligation of H3-NCP library performed on average with a yield of 83 $\pm$ 3 %

Western blot analysis of SrtA mediated ligation of H3 peptide library member 1-32 was performed by D. Aparicio Pelaz. (A) Schematic representation of SrtA mediated ligation in the context of immobilized ligation-ready NCP. (B) Western blot analysis of SrtA mediated ligation between 32 modified H3-peptides with H3Δ-NCP using αH3 antibody recognizing both, H3Δ and the ligation product full-length H3 (H3$_{FL}$). (C) Quantification of SrtA mediated ligation with n=3-5 reactions per modification. Standard deviation is depicted as error bars.

analysis in figure 3.5 (C) showed after 3 h reaction the formation of a FAM-labeled product. The observation of the same reaction with native agarose gel electrophoresis revealed

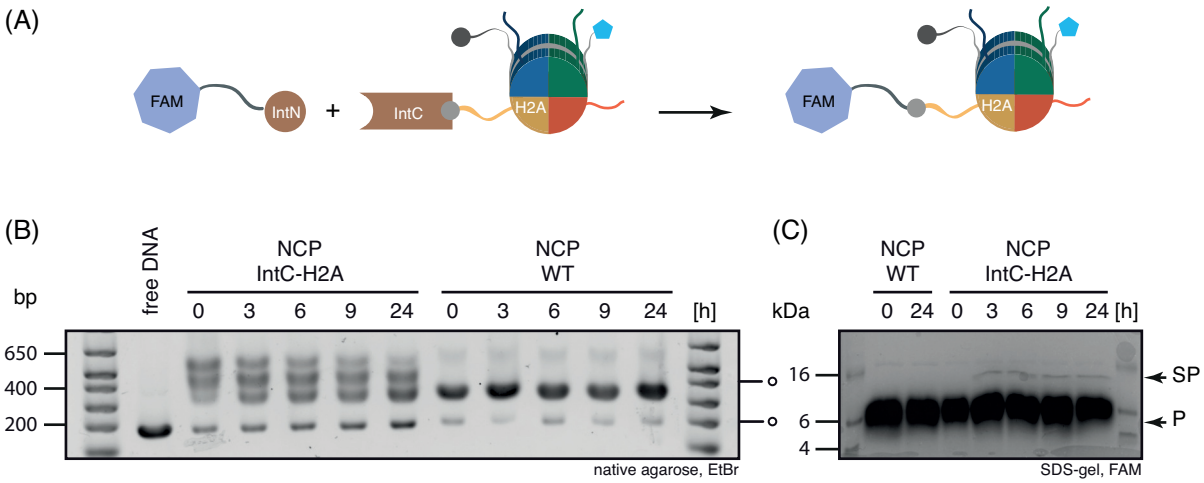

Figure 3.5: Protein *trans*-splicing in context of NCP using FAM-IntN peptide
(A) Schematic representation of protein *trans*-splicing in context of NCPs. (B) Native agarose gel observing P*t*S dependent conversion of IntC-H2A-NCP WT-like-NCP product within 24 h. (C) The polyacrylamide gel shows formation of FAM-peptide-H2A-NCP the splice product (SP) after 3 hours, P: FAM-IntN-peptide. ○: free DNA and side products originating from unsaturated NCP reconstitution.

after 3 h reaction a fast migrating complex on the same height as WT-NCP. After 24 h, IntC-H2A-NCP was almost consumed and a complex had formed that co-migrated with WT-NCP. Fluorescent splice product was only formed with IntC-modified NCPs. NCP species (labeled with ○) which migrateted between IntC-H2A-NCP and splice product originated from unsaturated NCP reconstitution. Hence, it was present already at the beginning of the splice reaction and was observed as well after NCP reconstitution (figure 3.3).

Next, we asked whether the native H2A$_{1-18}$-IntN was able to perform P*t*S in nucleosomal context. To this end, P*t*S was performed under ligation conditions with both FAM-IntN and H2A-IntN peptides over 24 h along with a control for IntC-H2A-NCP stability. It is shown in figure 3.6 (B) for FAM-IntN peptide, that most of the product had formed after 4 h of incubation and only little initial IntC-H2A-NCP complex remained. However, using native H2A-IntN peptide, complete consumption of IntC-H2A-NCP educt was observed after 4 h. All initial IntC-H2A-NCPs seemed to be converted into the faster migrating wild type like NCP complex. IntC-H2A-NCPs without the addition of IntN-peptides (mock control) were stable under

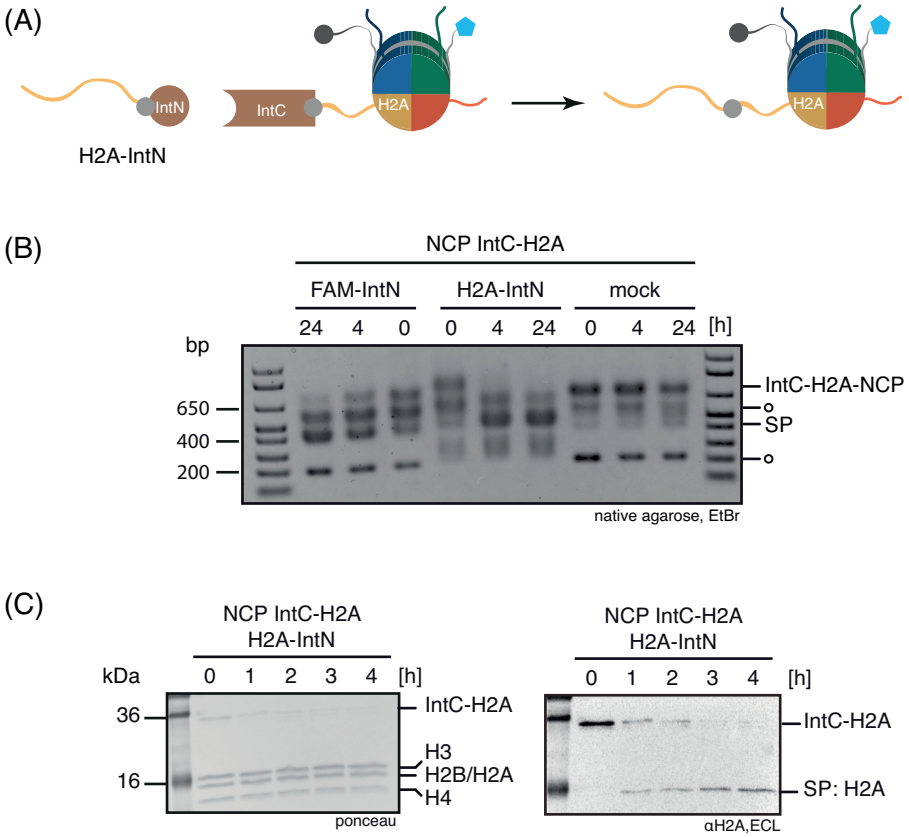

Figure 3.6: Protein *trans*-splicing in context of NCP using native H2A-IntN peptide
Protein *trans*-splicing (P*t*S) was performed in solution in context of NCP using different IntN-peptides analyzed by native agarose gel electrophoresis and western blot. (A) P*t*S in context of NCP using non-native FAM-KKESG-IntN peptide or native H2A-IntN. (B) Native agarose gel of P*t*S in context of IntC-H2A-NCP using FAM-IntN, H2A-IntN or no IntN construct (mock control) reaction was monitored by agarose gel electrophoresis. (C) P*t*S over 4 h with H2A-IntN and IntC-H2A-NCP, analyzed by ponceau staining and western blot against H2A displays decrease of IntC-H2A educt and increase of splice product.
SP: splice product, ○: free DNA and side products originating from unsaturated NCP reconstitution.

P*t*S reaction conditions over 24 h. The identity of the formed species was clarified by western blot analysis of the P*t*S reaction over 4 h. The formation of full-length histone H2A ($H2A_{FL}$) concomitant with the consumption of IntC-H2A-NCP educt was seen within 4 h of P*t*S reaction. At this stage, H2A-IntN peptides were synthesized N-terminal labeled with TAMRA

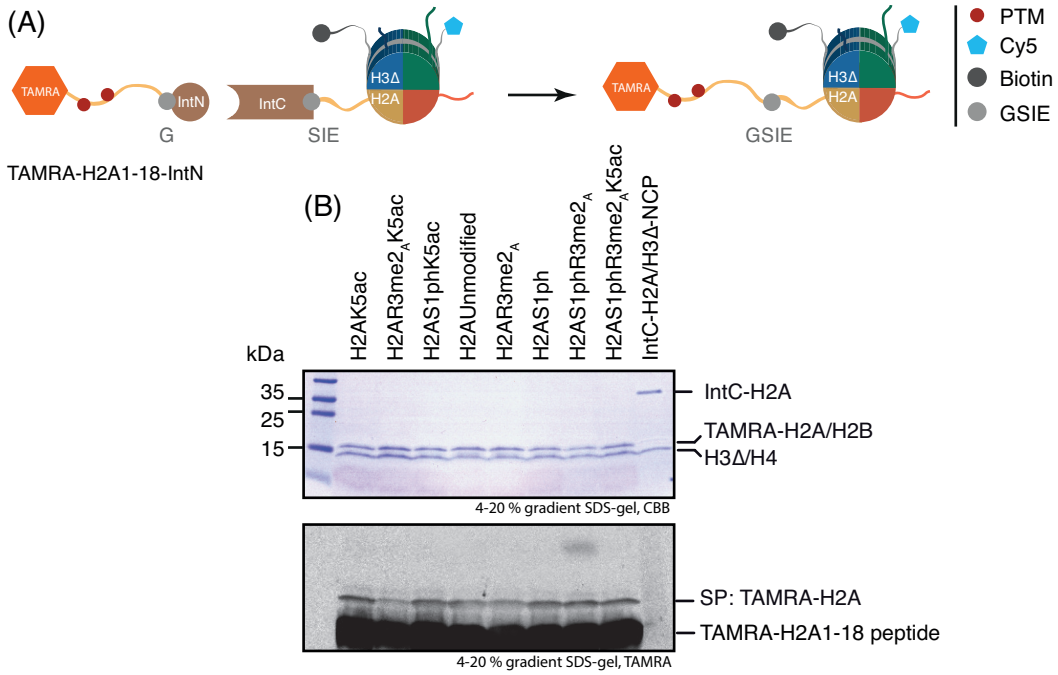

Figure 3.7: Ligation of H2A-library in context of IntC-H2A/H3Δ-NCP by P*t*S
P*t*S in the context of NCP using native TMARA-H2A-IntN peptide decorated with PTM (A). (B) Optimized P*t*S in solution with TAMRA-H2A-IntN peptides carrying PTMs and IntC-H2A/H3Δ-NCP analyzed with SDS-PAGE, detected by CBB and in-gel TAMRA fluorescence and was performed by D. Aparicio Pelaz.

and PTMs of H2A. In figure 3.7 (B) the P*t*S reaction is displayed of H2A-IntN carrying 8 different PTM patterns with double modified IntC-H2A/H3Δ-NCP over 72 h. The analysis of IntC-H2A/H3Δ-NCP conversion to modified $H2A_{FL}$/H3Δ-NCP was performed by SDS-PAGE and stained with CBB. In addition, splice product was identified by fluorescence of TAMRA-labeled $H2A_{FL}$. TAMRA-H2A-IntN peptide synthesis, the ligation of these peptides to IntC-H2A/H3Δ-NCP using P*t*S as well as the analysis of this reaction was performed by D. Aparicio Pelaz (Eberhardt Karls Universität, Tübingen).

Taken together, using SrtA mediated ligation for H3 and P*t*S for H2A we were able to generate a library with a complexity of 8 (H2A) x 32 (H3) = 256. As the ligation of H2A needed further

quantification of its efficiency, biochemical binding and activity assays were developed using the H3-NCP library.

3.3 General assay development

3.3.1 Immobilization of NCPs on 96-well plate

For convenient handling and easy separation of NCP from reactants during H3-NCP library generation and subsequently analysis, NCPs were immobilized on streptavidin-coated high binding capacity 96-well plates (BA plates) or streptavidin coated 96-well Flash plates. At first we were interested in the incubation time wich resulted in highest Cy5-fluorescence thus in highest NCP immobilization of biotin-labeled Cy5-NCPs within streptavidin coated plates. To this end, NCPs were immobilized at RT for one hour, for two hours and over night. Unbound Cy5-NCP was removed and in-well Cy5-fluorescence was observed of bound Cy5-NCP in each well (figure 3.8 (A)). ON incubation of Cy5-NCP with streptavidin coated plates yielded

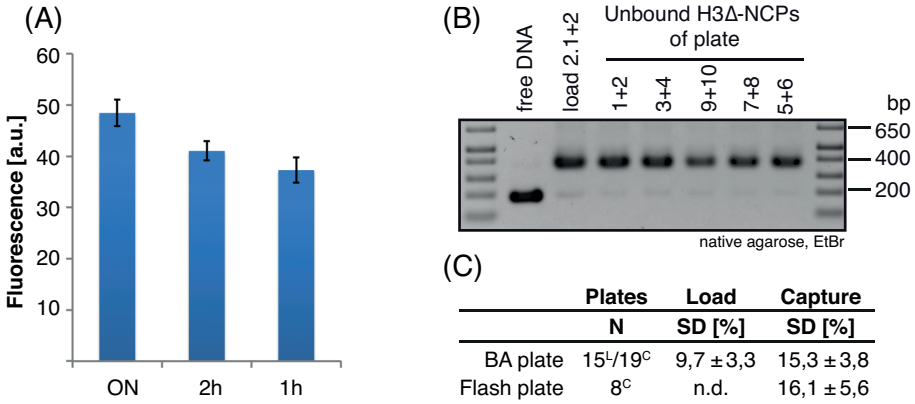

	Plates	Load	Capture
	N	SD [%]	SD [%]
BA plate	$15^{L}/19^{C}$	9,7 ± 3,3	15,3 ± 3,8
Flash plate	8^{C}	n.d.	16,1 ± 5,6

Figure 3.8: Cy5-NCP immobilization and analysis of NCP capture over 19 BA- and 8 Flash-plates
Cy5-NCP immobilization was observed in (A) by measurement of in-well Cy5-fluorescence in dependence of varying NCP incubation time: over night (ON), 2 h and 1 h. Error bars represent the standard deviation of three replicates. (B) Native agarose gel of Cy5-NCP input material before each coating cycle for 10 plates served as quality control on NCP integrity. (C) Overview of the standard deviation (SD) for load and capture of NCPs per plate for BA- and Flash-plates. The number of plates analyzed for load and capture were labeled with ^{L} and ^{C}, respectively.

most intense Cy5-fluorescence implying highest capture of NCP per well. After one and two hours of incubation 76 % and 85 % of the final NCP capture was detected, respectively. This result allowed us to choose between long and short incubation times if necessary.

In order to provide a good basis for the best signal-to-noise ratio for additional studies on immobilized and post-translational modified NCP, we chose ON incubation for coating initially 10 BA-plates with H3Δ-NCP in a coating volume of 50 μL/well. The immobilization was simultaneously performed on two plates in six coating cycles. As unbound H3-NCP was reused in each coating cycle, their integrity was analyzed by EtBr-stained native agarose gel electrophoresis (figure 3.8 (B)). We observed stable and intact H3Δ-NCP for the coating procedure for all 10 plates. This way, we assured that unbound H3Δ-NCP could be reused.

Next, we asked how NCP capture varied within one plate. To this end, the developed NCP immobilization procedure was used to coat 19 BA plates and 8 Flash plates with H3Δ-NCP. The plates were analyzed in terms of loading (15 BA-plates) and resulting capture (19 BA-plates and 8 Flash plates, see figure 3.8 (C)). Homogeneity of load and capture over one plate was reflected by the relative standard deviation of Cy5-fluorescence signal. The loading within one plate varied by 9.3 %. Whereas, the variation for captured NCPs per plate was slightly wider: BA-plates SD=15.3 % and Flash plates SD=16.1 %. So, we could assure for homogeneous capture of intact H3Δ-NCP using described immobilization protocol. However, normalization with respect to the Cy5-NCP signal of each well would gain independency of well-to-well coating variation in further experiments with immobilized NCPs.

In order to assure high NCP content in each well and low well-to-well variation, we asked how the NCP load concentration influenced the binding of NCPs to the plate (capture). In addition, we were interested in how well the Cy5-fluorescence reflected the true NCP immobilization. To address this, we used two different methods for NCP quantification: in-well Cy5-fluorescence referenced to Cy5 calibration wells on the plate (figure 3.9 (B)) and western blot analysis of immobilized NCPs quantifying H3Δ from same wells (figure 3.9 (C - E)). In order to assure western blot analysis in the linear range of detection, samples were separately analyzed that originated from wells with high concentrated NCP input (4-32 μM) and low concentrated NCP input (0.25-2 μM). As a reference for quantification of immobilized H3Δ-NCP, the 30 pmol histone H3Δ reference sample was used. Hence, the intensity of this band was

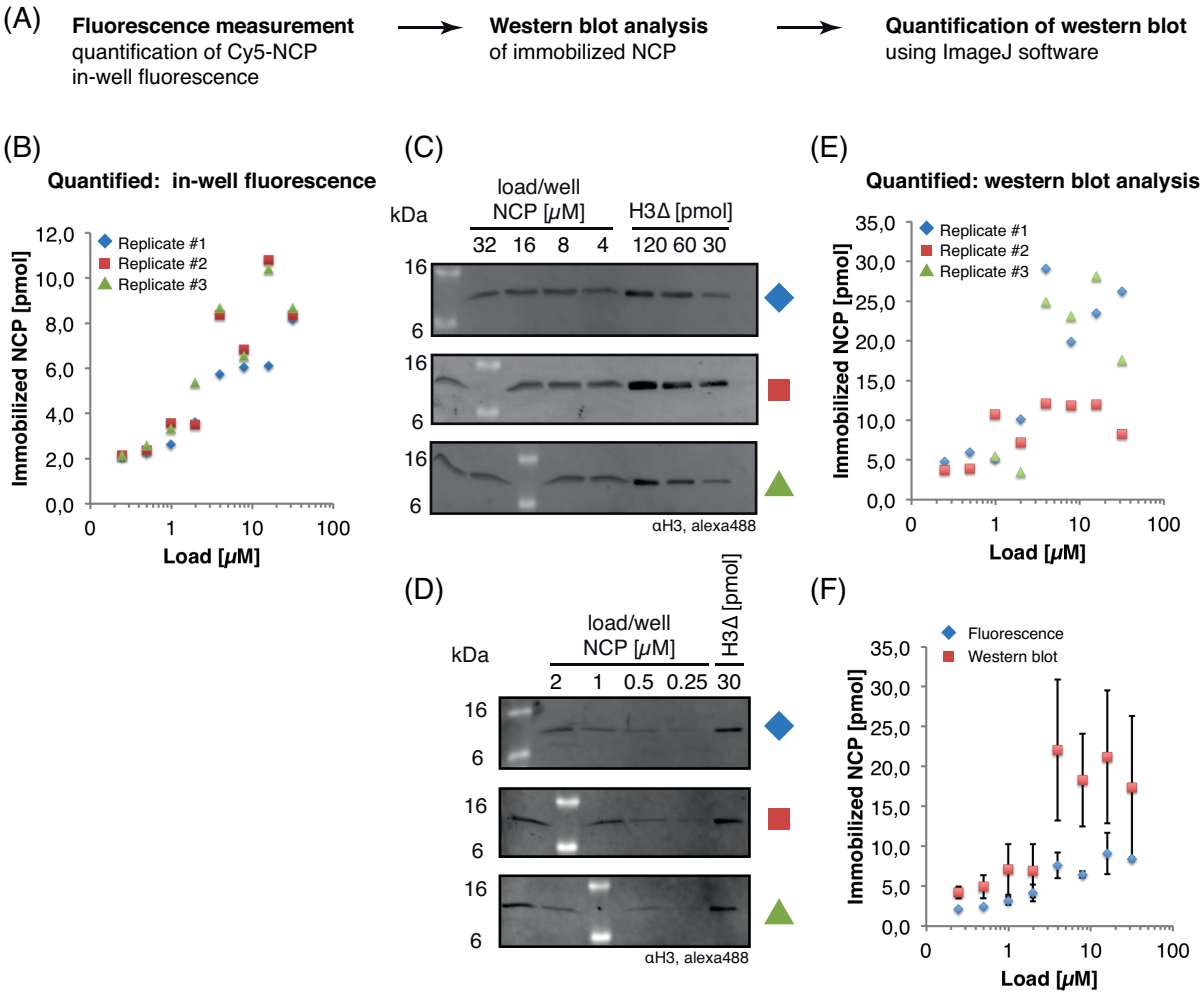

Figure 3.9: Single-well quantification of Cy5-NCP immobilization on BA-plates via in-well Cy5-fluorescence and western blot analysis

Quantification of immobilized NCP per well in dependence of Cy5-NCP input concentration (load μM) by means of Cy5-NCP in-well fluorescence and western blot analysis of immobilized NCP. (A) Flow scheme for quantification of immobilized NCP. (B) Quantification of in-well Cy5-NCP fluorescence by means of Cy5-reference wells with $R^2 = 0.99$. (C) Western blot analysis of wells with NCP load concentrations between 4-32 μM (D) Western blot analysis of wells with NCP load concentrations between 0.25-2 μM. (E) Quantification of band intensities by western blot analysis using ImageJ software and and their calibration to the band intensity of 30 pmol histone H3Δ which represents 15 pm Cy5-NCP. In (B-E) replicates are depicted: replicate #1 (blue diamond), replicate #2 (red square) and replicate #3 (green triangle). (F) Direct comparison of NCP capture quantification between in-well Cy5-fluorescence and western blot analysis. Shown is the mean of data points in (B) and (E) for fluorescence and western blot, respectively. The standard deviation is depicted as error bars for three replicates.

in the range of samples originating from high concentrated NCP input and presented in the western blot analysis of samples originating from low concentrated NCP input.

In-well fluorescence quantification revealed for low concentrated NCP load samples (0.25-2 μM) a capture of 2.0-3.5 pmol NCP per well and for high concentrated NCP load samples (4-32 μM) 6-10 pmol NCP per well (figure 3.9 (B)). The NCP quantification of wells coated with low (0.25-2 μM) and high (4-32 μM) concentrated NCP input using western blot analysis (figure 3.9 (C,D)) detected 5-10 pmol and 10-27 pmol NCP per well, respectively.
The comparison of NCP capture gained by each detection method revealed in the low concentration range (0.25-2 μM) an input dependent NCP capture. More concentrated NCP load led to saturated levels of NCP capture. Within the range of 4-32 μM NCP load, on average 8$\pm$1.5 pmol per well were quantified by in-well Cy5-fluorescence and 20$\pm$8 pmol per well by western blot analysis (figure 3.9 (F)). Between these two quantification methods we observed a 2 and 2.5 fold difference in NCP capture for NCP immobilization using low and high concentrated NCP load. Therefore, we concluded that the detection of in-well fluorescence of Cy5-NCP reflected the immobilized material. In addition, in-well fluorescence quantification seemed to be more sensitive than western blot analysis although it remained to be investigated which method revealed the true NCP capture per well. Besides, we could take from these experiments that the optimal input concentration was in the range of 4 μM. This was an excess of 1.75 over available binding sites.

For further evaluation of the observed 2-2.5 fold difference in NCP immobilization detected by Cy5-NCP in-well fluorescence quantification and western blot analysis and because of a limited sample size in the previous experiment, NCP immobilization was determined by a third method: determination of the concentration of loaded and unbound NCP by the DNA absorbance at 260 nm. The difference in load and unbound NCP sample ($\Delta A_{260} = A_{260}$(load) – A_{260}(unbound)) reflected the immobilized NCP for one coating cycle. Therefore, 34-39 wells were coated simultaneously in one NCP immobilization step as described in chapter 2.3.6. This way, in total 6 immobilization cycles were performed. An initial NCP load concentration of 3.3 μM was chosen to explore the range between the previously described low (0.25-2 μM) and high (4-32 μM) concentrated NCP load dependent immobilization procedure. As the unbound NCP of the preceding immobilization cycle was the input of the subsequent immobilization cycle, the concentration decreased over 6 cycles to 1.2 μM. The

mean of NCP immobilization per well deduced from direct in-well Cy5-fluorescence and indirect ΔA_{260} absorbance is plotted in figure 3.10 (A). It showed for Cy5-fluorescence detection

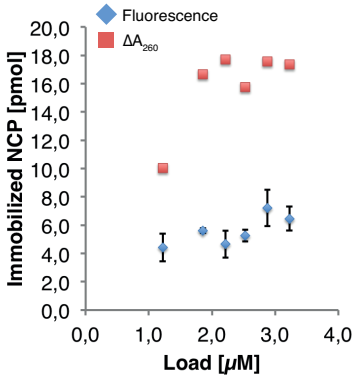

Figure 3.10: Quantification of NCP immobilization in 34-39 wells via in-well Cy5-fluorescence and ΔA_{260} absorbance
It is shown the mean immobilization degree over 34-39 wells determined by in-well Cy5-fluorescence and DNA absorbance at 260 nm: ΔA_{260}=A_{260}(load)-A_{260}(unbound) of pooled load and unbound material. Shown are 6 NCP immobilization cycles with NCP load concentrations from 3.3-1.2 μM. The standard deviation from three replicates is depicted as error bar.

only little variations of NCP capture (4.4-6.4 pmol per well). Similar low variations were observed for the indirect (ΔA_{260}) determination of NCP capture (18 pmol per well). In contrast, the capture dropped to 10 pmol NCP per well for an input concentration below 1.9 μM NCP. Using the direct and indirect quantification method, a 3 fold difference was observed between Cy5- and ΔA_{260}-quantification in the range of 3.3-1.9 μM load and a 2 fold difference for lower input concentrations. Taken together, the results of the three quantification methods in-well Cy5-fluorescence, western blot analysis and indirect determination of NCP concentration by ΔA_{260} pointed out, that the true NCP-coverage within each well was 2-3 fold higher than identified by in-well Cy5-fluorescence of captured NCP. Although shifted, in-well Cy5-fluorescence correlated with NCP capture, therefore this signal was used for normalization of NCP content per well.

3.4 Development of a binding assay with fluorescence readout

With ligation-ready NCP immobilized in 72 wells, we were able to introduce by Sortase A mediated ligation any histone H3 tail modification we had prepared by SPPS. For the assay development and characterization we chose to attach H3K9me2 and H3um peptides to immobilized ligation-ready NCP. As a binding protein we chose the well-characterized HP1β which does not bind to H3um peptides but binds to H3K9me2 peptide with a K_D of 3 μM[33]. In order to monitor for HP1 binding, eCFP was linked to HP1 (eCFP-HP1). ECFP has an excitation maximum at $\lambda = 433$ nm and emission maximum at $\lambda = 476$ nm[135], which allowed us to detect eCFP-HP1 binding modified NCP via eCFP fluorescence. Moreover, to control for NCP coverage in each well '147'-DNA was labeled with the fluorogenic probe Cy5. Cy5 has an excitation maximum at $\lambda = 649$ nm and emitts at $\lambda = 670$ nm[136].

3.4.1 Proof of principle experiment

The principle idea of the HP1 binding assay was whether we could observe via in-well fluorescence the selective binding behavior of eCFP-HP1 to H3K9me2- and H3um-NCP immobilized in 96-well plates. In order to check the feasibility of the experimental design, eCFP-HP1 was incubated on BA-plates with immobilized H3um-, H3K9me2-NCP and no NCP (mock control) over night. As we were uncertain how washing of the wells affected the eCFP-HP1 signal, eCFP- and Cy5-fluorescence was measured after each washing step (figure 3.11 (B-C)). After 5 washes, bound material was analyzed by western blot (figure 3.11 (D)). Plotting eCFP fluorescence against the wash steps for H3um, H3K9me2 and no NCP (mock control) a general drop in signal intensity was observed for all conditions. This was expected because HP1 binding is reversible. The equilibrium between bound and unbound material would adjust after every wash step. Therefore, a minimum number of washes should be applied. In this experiment at least three wash steps were necessary to remove eCFP-HP1 from wells without NCPs (mock control) (figure 3.11 (B)). In figure 3.11 (C) the eCFP-HP1 recruitment is plotted against the NCP content of each well displaying different binding intensities to H3um- and H3K9me2-NCP. This same specificity of HP1 binding was observed by western blot analysis of bound material (figure 3.11 (D)). With both detection techniques, specific recruitment of eCFP-HP1 to H3K9me2 modified NCP was observed.

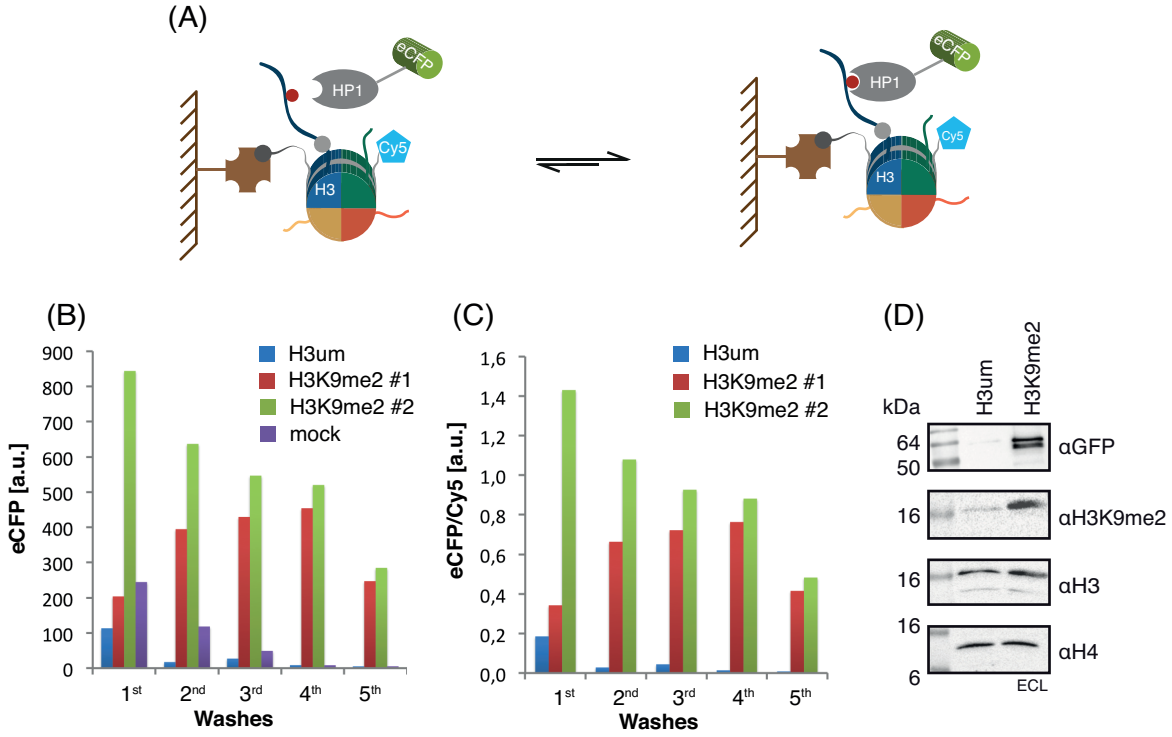

Figure 3.11: Proof of principle assay design: eCFP-HP1 recruitment by immobilized H3K9me2- and H3um-NCP observed by in-well fluorescence and western blot analysis

(A) Schematic representation of eCFP-HP1 binding to H3 modified NCP immobilized on solid support (plate). (B) Presence of eCFP-HP1 in wells containing H3um-NCP, H3K9me2-NCP and no NCP (mock control) after each wash step. (C) eCFP-HP1 fluorescence normalized to NCP content after each wash step. (D) Western blot analysis of bound eCFP-HP1 to H3um- and H3K9me2-modified NCP.

Taken together, fluorescence and western blot analysis revealed the feasibility of the principle layout of the binding assay.

3.4.2 Elucidating experimental conditions: time and washing steps

Because over night incubation might be unsuitable for proteins less stable than HP1, we were interested in the effect of incubation time on signal intensities. To this end, on the plate immobilized H3um-NCP and H3K9me2-NCP were incubated with eCFP-HP1 for 5, 30, 60 and 180 min, washed, and measured in PBS as described in detail in chapter 2.4.3 and schematically represented in figure 3.12 (A). The eCFP fluorescence after indicated wash steps for the incubation time of 180 min is plotted in figure 3.12 (B). As observed before in the proof of principle experiment, wash steps influenced the signal intensities and led to a smaller standard deviation for unspecific interactions (binding to NCP-H3um). Moreover, eCFP-HP1 signal normalized with respect to the NCP signal and plotted against the incubation time showed a discrimination between H3um and H3K9me2 already after 30 minutes (figure 3.12 (C)). In addition, peptide pull-down was performed using peptides (pH3um, pH3K9me3) bound to beads and they were incubated for 1.5 h-ON with eCFP-HP1. Under these experimental conditions discrimination between pH3um and pH3K9me3 was observed for incubation times of 1.5-4 hours. Over night incubation led to weak interaction signal of eCFP-HP1 with pH3um (figure 3.12 (D)). From these results we concluded, that long incubation times led to high eCFP-HP1 recruitment. However, recruitment to H3um was also increased. In few wells coated with H3um-NCPs, HP1 was resistant to washing (see appendix figure 5.1). These cases were identified as outliers and were removed from further analysis. In order to obtain highest signal intesities in further experiments, we chose to incubate eCFP-HP1 with immobilized NCPs over night.

3.4.3 Library design

At this stage, we started to generate the first library on BA- plates in 96-well format with only H3-NCP modifications. The library consisted of 32 different NCP species with one to five modifications on one histone H3. H3 tail peptides were synthesized for all 32 modifications. These were ligated to immobilized ligation-ready NCPs using enzymatic Sortase A mediated

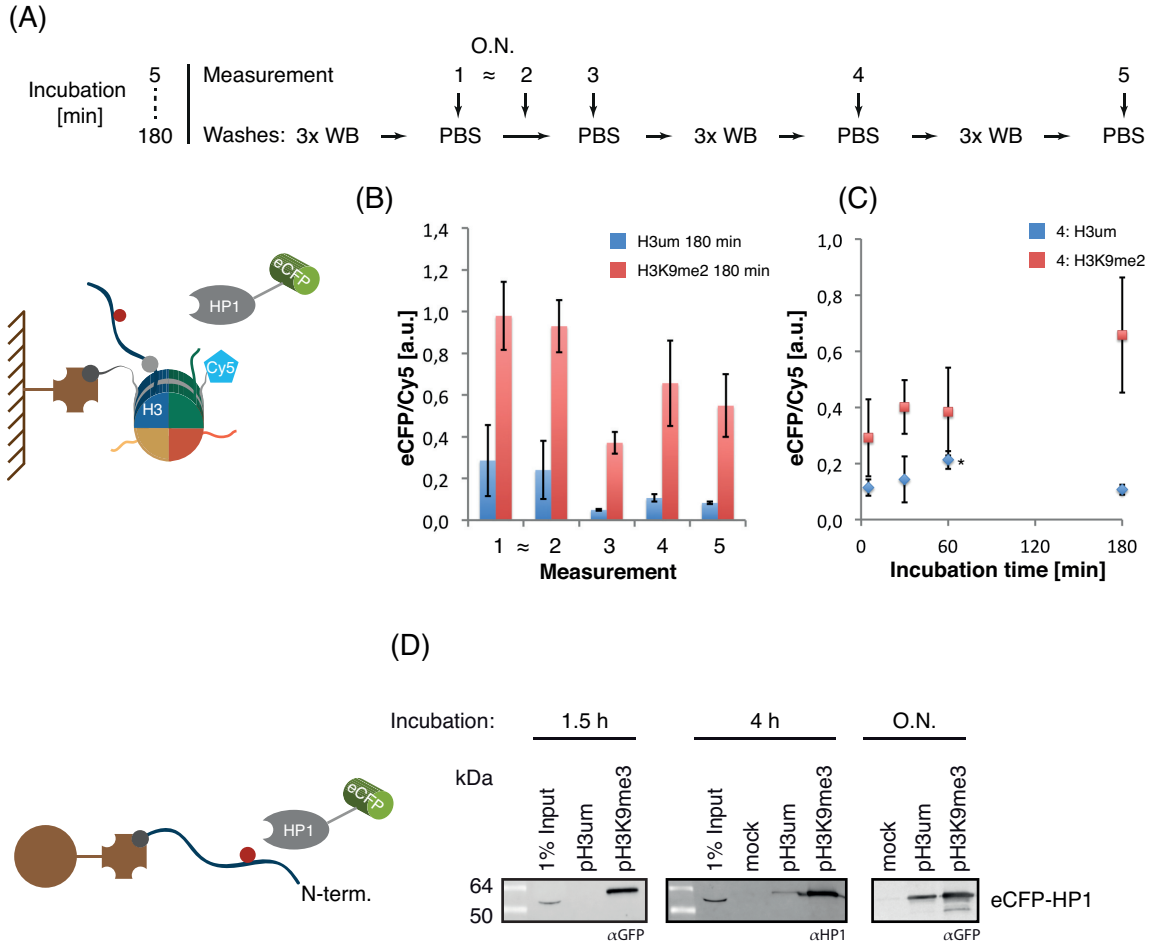

Figure 3.12: ECFP-HP1 signal intensity depended on incubation time and wash steps
(A) Schematic representation of experimental set up: eCFP-HP1 was removed after 5, 30, 60, 180 min of incubation time with n=3 wells/incubation time. Fluorescence measurement took place in PBS with wash steps in between of high salt and detergent containing buffers. (B) Influence of washes on eCFP-HP1 recruitment normalized with respect to NCP content. (C) eCFP-HP1 recruitment in dependence of incubation time after the 4^{th} measurement. ($*$) Outliers were removed on grounds of resistance to washing (see appendix figure 5.1). Standard deviation between replicates is depicted as error bar. (D) Peptide pull-down with pH3K9me3 and pH3um with eCFP-HP1 indicated incubation time. Abbreviation N-term.: N-terminus of H3 peptides WB: wash buffer.

ligation (done by D. Aparicio-Pelaz, Eberhard Karls Universität Tübingen). 2/3 of a plate were coated with NCP-H3Δ and two libraries were ligated in a random pattern, leaving one column NCP- H3Δ and three empty columns for controls and references (figure 3.13 (A)).

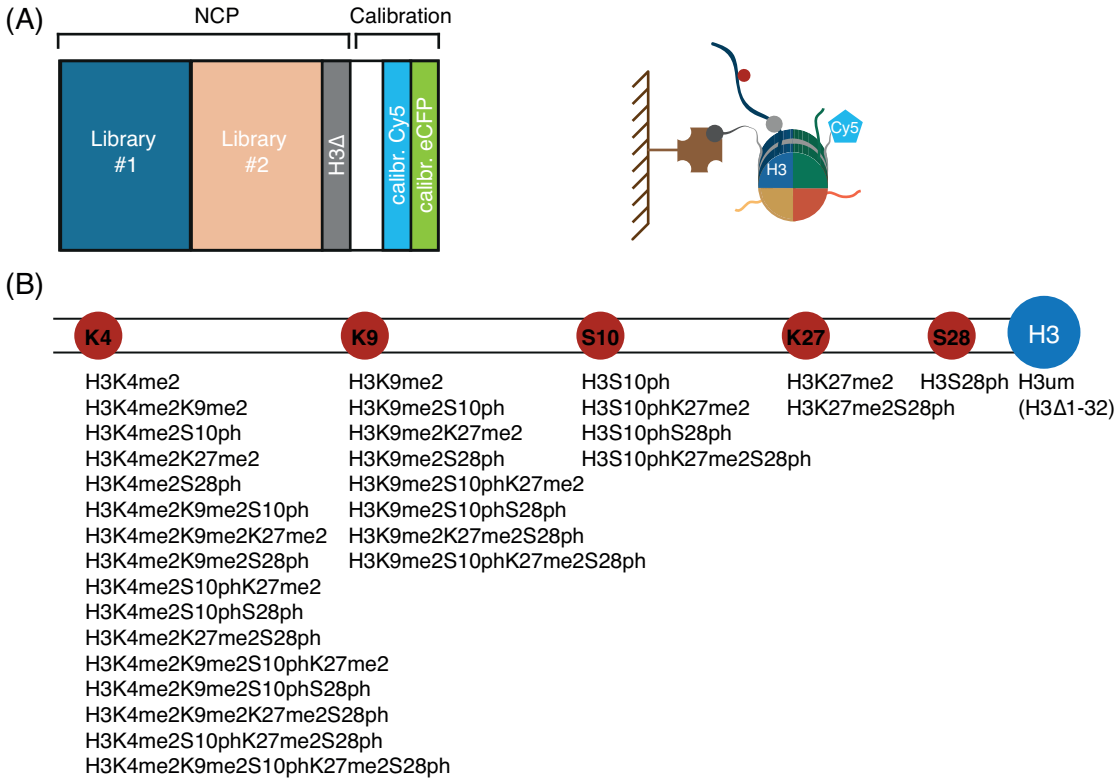

Figure 3.13: Layout of BA-plate and H3-NCP library
(A) Displays layout of BA-plate with two libraries. Modifications were placed in a random pattern within the library #1 and #2 area, 1/3 of the plate was kept for controls e.g. H3Δ-NCP-, and dye references. (B) H3-NCP modifications of library #1 and #2.

3.4.4 ECFP-HP1 binding assay on H3-NCP library

Having established the parameters for the binding assay, we were interested in how eCFP-HP1 performed on other H3-NCP modifications. In order to obtain highest signal intensities, we chose to perform the HP1 binding assay on one H3-NCP library over night (for detailed protocol chapter 2.4.3 on page 41). In figure 3.14 the relative fluorescence intensities of eCFP-HP1 to Cy5-NCP is plotted for each modification and corrected for background and gain (for detailed data analysis see chapter 2.4.5). With the assay we observed a three fold

higher binding of eCFP-HP1 to H3K9me2 than H3K9me2S10ph. As the methyl/phos-switch double modification H3K9me2S10ph is known to prevent HP1 binding to the methylated lysine[33;78], the observed difference in eCFP-HP1 binding was expected and served as an additional control to evaluate assay performance. Unspecific interactions were monitored by the H3Δ-NCP control. Suspiciously, eCFP-HP1 seemed to interact strongly with H3um-NCP.

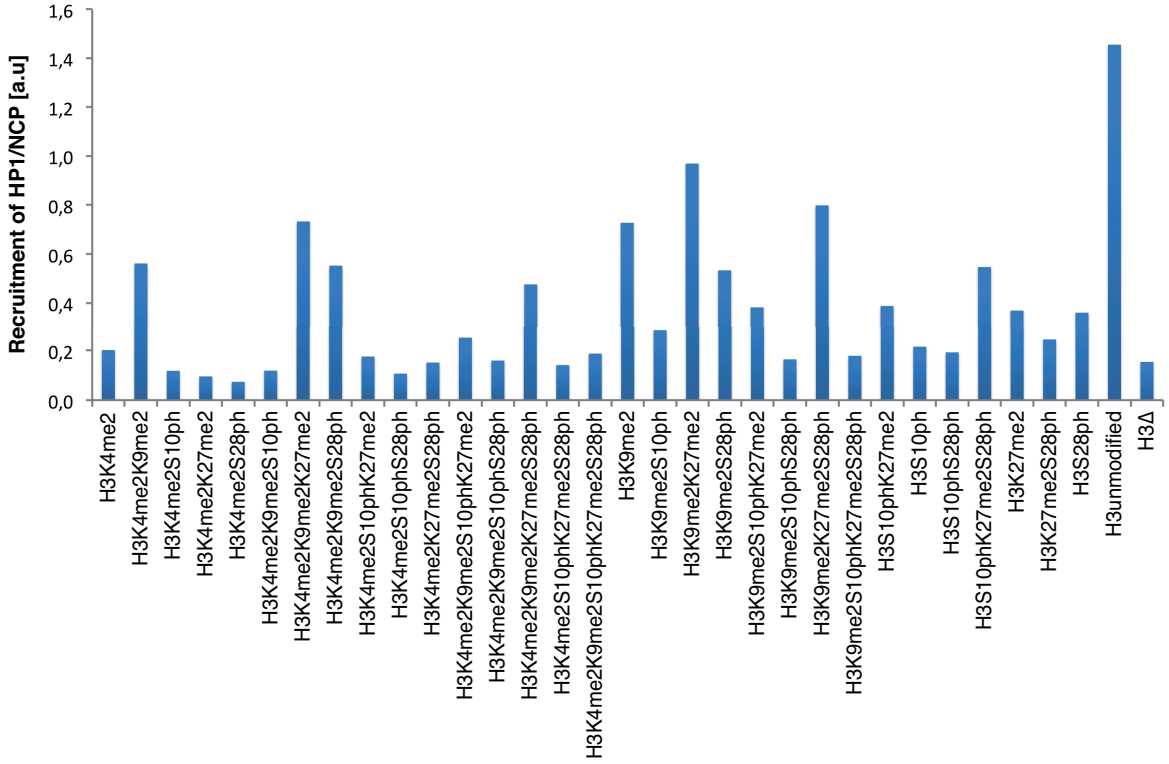

Figure 3.14: Recruitment of eCFP-HP1 to H3 modified NCP library
H3-NCP library was probed with eCFP-HP1 over night, fluorescence data for eCFP-NCP and Cy5-NCP were corrected for background and gain. ECFP-HP1 was normalized with respect to Cy5-NCP fluorescence intensities per well. [a.u.] arbitrary unit.

Thus, the question arose whether this and other prominent signals were true or false positive values. As shown before, HP1 barely interacted with H3um, this is well defined[33;77] and marked this value as false positive, therefore questioning all prominent signals.

In order to reduce false positive values, the subsequent experiments were conducted on plates where the libraries were blocked with BSA and ssDNA prior HP1 incubation. In order to calibrate eCFP and Cy5-fluorescence, reference samples for each fluorophore were introduced (for details see chapter 2.4.3). As we have determined before, washing conditions in-

fluenced strongly the signal intensity. Hence, we needed an internal reference accounting for the differences in incubation time and washing conditions between plates and experiments. H3Δ for example, seemed to be a good candidate for monitoring unspecific binding of eCFP-HP1 to the nucleosome core. Therefore, fluorescence signals above H3Δ had to be caused by specific interaction with the histone tail. The eCFP-HP1 binding assay was conducted on

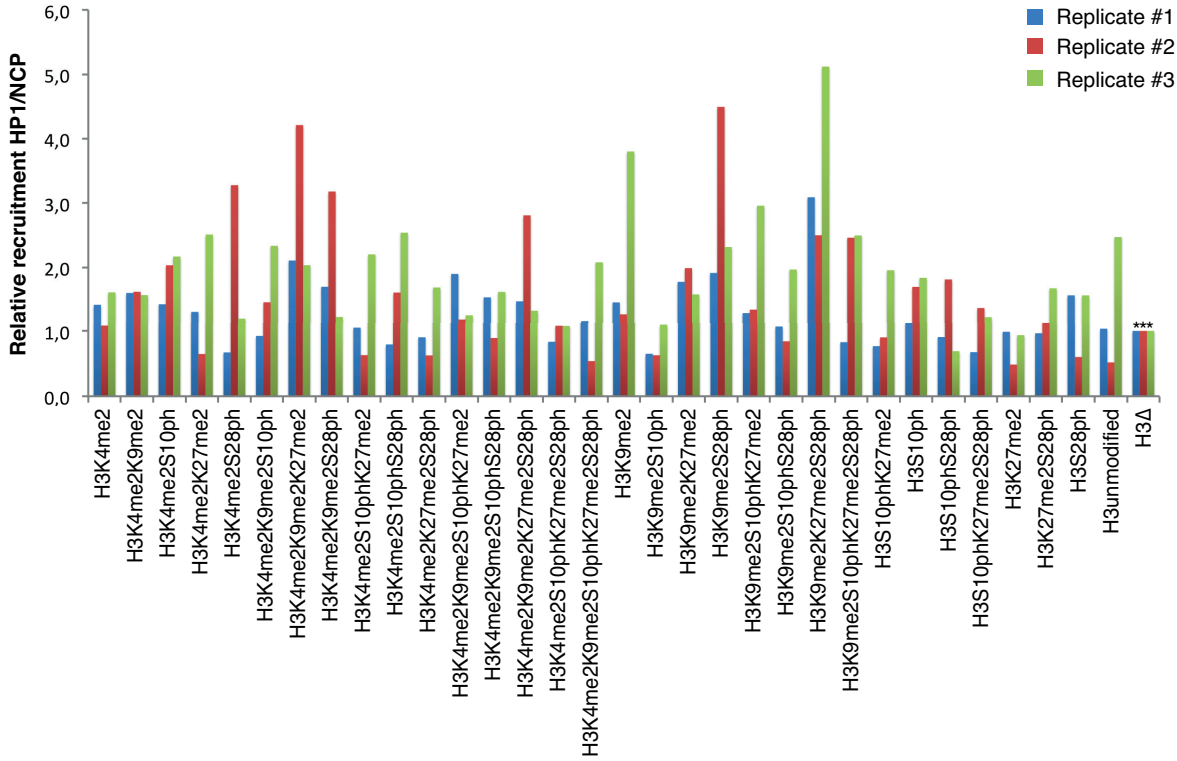

Figure 3.15: ECFP-HP1 binding assay performed on H3-NCP libraries.
ECFP-HP1 binding assay performed on pre-blocked libraries. Depicted is the recruitment of eCFP-HP1 per NCP normalized to H3Δ-NCP (∗) for each libray. Library #1(blue) and #2 (red) are located on the same and #3 (green) on a separate plate.

three libraries. Replicate #1 and #2 were conducted on libraries that shared the same plate. The recruitment of HP1 per NCP normalized with respect to H3Δ is presented in figure 3.15. Again, focusing on the HP1 discrimination of H3K9me2 over H3K9me2S10ph the difference was here 2-3:1 almost as prominent as before. Although HP1 recruitment to H3um-NCP was less intense than previously, the difference to H3K9me2 was at the best, twofold. Moreover, reproducibility of HP1 recruitment to a range of modifications was moderate. With the binding assay developed to this stage only trends of NCP-modification dependent HP1 recruitment

could be detected. With n=3 per modification it was impossible to identify false positive or negative signals.

3.4.5 Releasing NCPs into solution using the restriction enzyme *Eco*RI

Next, we were interested whether the ratios between specific and unspecific binding could be increased. Firstly, by raising the eCFP-HP1 input concentration. Secondly, by reducing the stringency of wash steps and third, by releasing bound NCPs into the solution using *Eco*RI.

*Eco*RI cuts at the enzymatic recognition site introduced between the biotin-tag and the '147'-positioning sequence. Upon addition of *Eco*RI and hereby releasing NCP and eCFP into solution, we expected a more efficient detection and thereby an enhancement of the fluorescence signal intensities. To this end, one library was probed with eCFP-HP1 using an high input concentration, incubated over night and washed with excess of less stringent (low salt) wash buffer. Recruitment of eCFP-HP1 to Cy5-NCP was detected, showing low discrimination between all modifications (figure 3.16 (A)). The release of NCPs and their binding partner eCFP-HP1 into solution had no significant impact on the recruitment ratios of eCFP-HP1 binding to H3K9me2, H3K9me2S10ph, as well as H3um.

To determine to what extend the eCFP- and Cy5-fluorescence contributed to this observation, eCFP-HP1 in pmol and Cy5-NCP in pmol were separately plotted before and after *Eco*RI treatment in figure 3.16 (B, C). For eCFP-HP1 and Cy5-NCP more molecules were available for detection after *Eco*RI treatment. While the absolute value of eCFP-HP1 binding depended on the initial detected amount before *Eco*RI treatment, we observed an increase in detected molecules per well of 10 ± 3 % upon release. In contrast, for Cy5-NCP on average 5 pmol per well after *Eco*RI treatment were detected which were not observed before *Eco*RI treatment for several modifications of H3-NCP by releasing Cy5-NCP into solution. The treatment revealed an evenly Cy5-NCP coverage for all modifications.

Taken together, we could enhance the detected fluorescence signal for eCFP-HP1 and Cy5-NCP. However, this had little effect on the relative recruitment of HP1 per NCP. Moreover, an increase in HP1 loading concentration and less stringent washes led to an increase in unspecific interaction rather than increased specific binding. The specificity in HP1 binding to H3K9me2-NCP was only 1.7 and 1.8 compared to H3K9me2S10ph- and H3um-NCP which

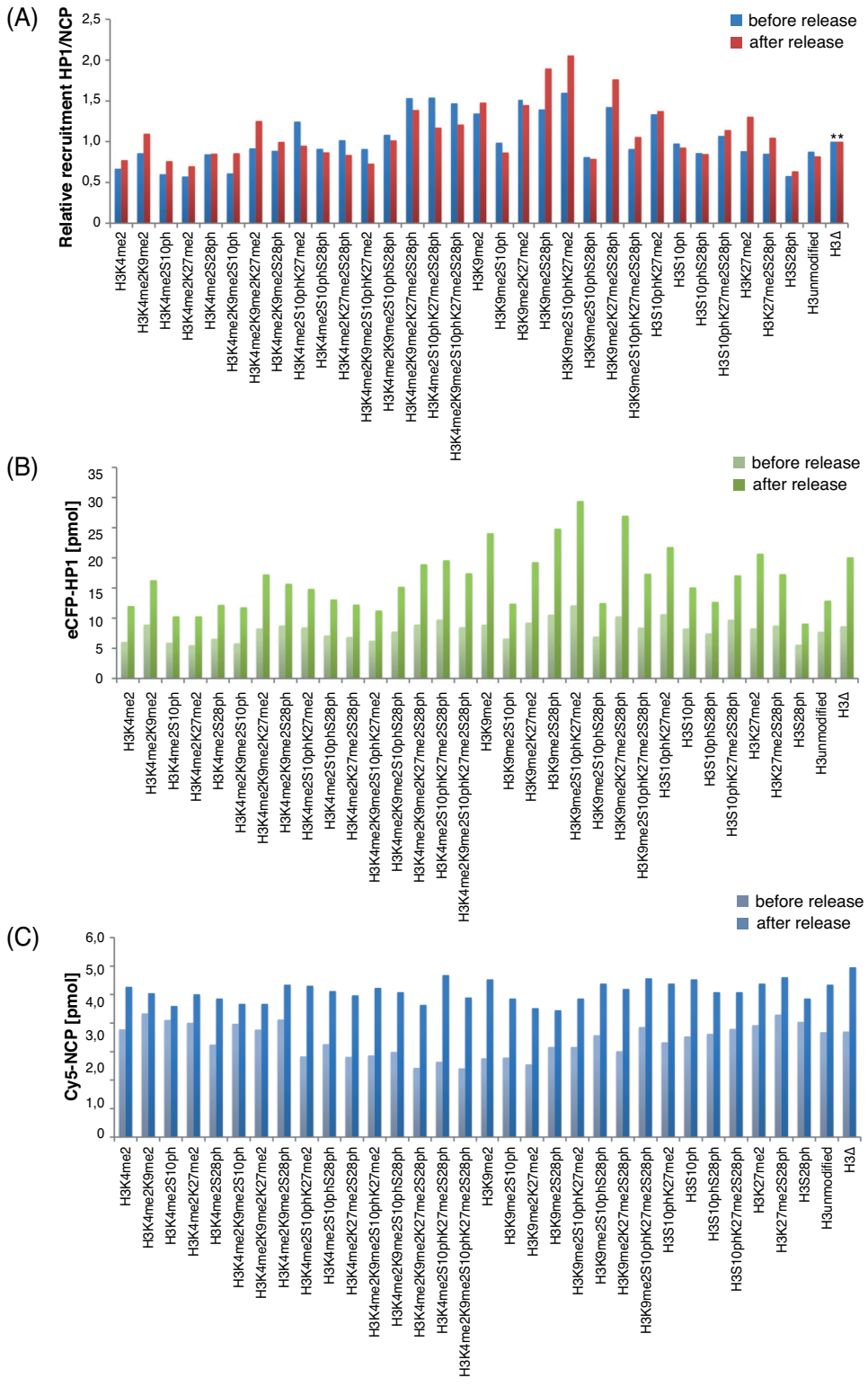

Figure 3.16: ECFP-HP1 binding assay on H3-NCP library before and after release
Binding assay performed on H3-NCP library, subsequently immobilized NCP were released using restriction enzyme *Eco*RI (A) Recruitment of HP1 per NCP normalized to H3K9me2S10 (∗) before (blue) and after (red) *Eco*RI treatment. (B) ECFP-HP1 signal before (light green) and after (dark green) *Eco*RI treatment. (C) Cy5-NCP signal before (light blue) and after (dark blue) *Eco*RI treatment.

was less than observed before. Hence, it was necessary to further optimize the experimental set up for an increased specificity of HP1 binding.

3.4.6 Optimization for better signal-to-noise ratio: experimental procedure

Although specific binding of HP1 to H3K9me2 compared to H3K9me2S10ph was observed in figure 3.15, the major concern was the high binding events of eCFP-HP1 to H3um-NCPs. To address this, peptide pull-down was chosen for optimization of buffer conditions at different stages of the experiment: peptide immobilization, protein-peptide incubation and removal of unbound protein. The buffer conditions for protein/peptide incubation and wash steps were optimized for the concentration of BSA, ssDNA, ionic strength, and glycerol content. For the

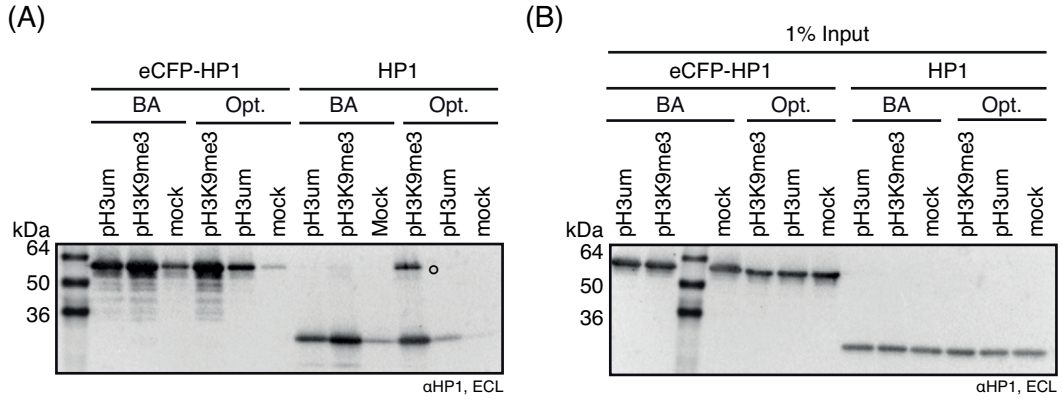

Figure 3.17: Optimization of block- and buffer-conditions during protein incubation and wash steps
Optimization was performed on histone peptide pull-down with protein incubation over night (A) Western blot analysis of peptide pull-down for eCFP-HP1 and HP1 under optimized (Opt) and in the binding assay used conditions (BA). (○) cross contamination introduced during washing. (B) Western blot analysis of 1% input of each condition shown in western blot (A).

peptide immobilization step only buffers with or without BSA were tested. The western blot analysis in figure 3.17 (A) shows a peptide pull-down experiment with conditions used in the binding assays and the optimized buffer conditions. ECFP-HP1 bound similar to pH3K9me3 in both buffer conditions. The difference was here their binding to H3um peptide (pH3um) and mock control (no peptides on the beads). However, the transfer of these conditions to the binding assay in the plate with NCPs failed. Using the optimized washing conditions led to signals close to background noise. Only the reduction in ionic strength (150 mM) in

combination with increased washing volume (4xNCP coating volume) resulted in a two fold difference in recruitment of eCFP-HP1 to H3K9me2-NCP over H3um-NCP.

3.4.7 Optimization for better signal-to-noise ratio: brighter fluorophores

In order to enhance signal-to-noise ratio, we used brighter fluorescence proteins. Derivatives of eCFP such as mCFP and Cerulean which differ relatively to eCFP only in few amino acids mCFP=eCFP/A206K and Cerulean=eCFP/S72A/Y145A/H148D[135]. mCFP is reported to have a brightness of 13 (product of extinction coefficient and quantum yield divided by 1000) whereas Cerulean's brightness is 27 which is relative to eCFP 1.2 and 2.5 fold brighter, respectively. However, the photo-stability, that is the time in seconds to reach half maximal emission intensity, is reported for mCFP with 64 sec and for Cerulean with 36 sec. Whereas the bleaching time for eCFP is reported to be 70 % of Cerulean's thus 27 sec[135;137]. Hence, it was hard to foresee whether photo-stability would overrule fluorescence intensity or vice versa. This question was addressed experimentally, eCFP-HP1, mCFP-HP1 and Cerulean-HP1 were tested using the optimized conditions. Because all CFP derivatives had similar excitation end emission spectra, experiments were performed on the same plate and measured at the same time. The eCFP and Cy5-fluorescence were converted into pmol and normalized with respect to the NCP coverage within each well. This way, the recruitment of CFP-HP1 per Cy5-NCP was obtained. In figure 3.18 is plotted the recruitment of eCFP-, mCFP- and Cerulean-HP1 which bound to H3um-, H3K9me2- and H3Δ-NCPs. The recruitment of eCFP-HP1 and mCFP-HP1 by H3K9me2 was similar with 3.5 HP1 per NCP and $\leq$ 1.5 HP1 per NCP for H3um and H3Δ. In contrast, Cerulean-HP1 bound in general less to modified and unmodified NCPs. Here, the recruitment to H3K9me2 modified NCPs was 1.5 HP1 per NCP and $<$ 0.5 HP1 per NCP for H3um-NCP and H3Δ-NCP. The western blot analysis of immobilized and bound material reflected the general observation made by fluorescence measurement.

Overall, western blot analysis revealed very similar recruitment by H3K9me2 for all three CFP derivatives. The little recruitment of Cerulean-HP1 to modified NCP observed by in-well fluorescence detection was not detected by western blot analysis. The relative CFP-HP1 recruitment to the according H3Δ ($*$) is plotted in figure 3.18 (C) for both replicates. It showed an

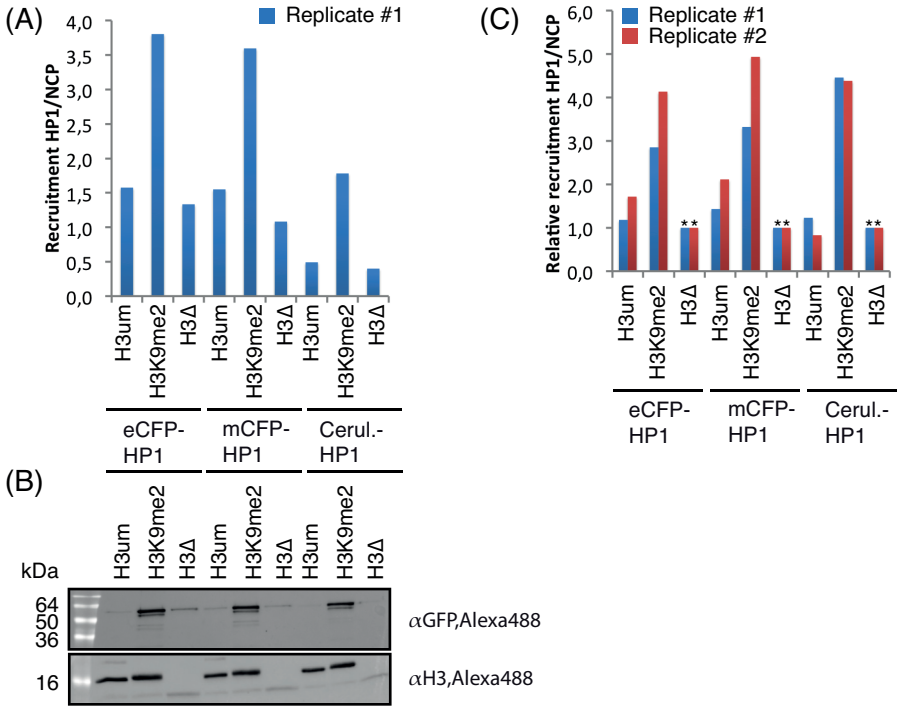

Figure 3.18: Binding assay under optimized conditions using CFP-HP1 derivatives for binding to H3K9me2 and H3um NCP

Binding assay performed in duplicates using optimized assay conditions. (A) Recruitment of HP1/ NCP for eCFP-, mCFP- and Cerulean-HP1 of replicate #1. (B) Western blot analysis of bound material for replicate #1. (C) HP1 per NCP recruitment normalized to H3Δ($*$) for both replicates.

equal 2.5 fold difference between H3um and H3K9me2 for eCFP- and mCFP-HP1 whereas the signal-to-noise ratio seemed better for Cerulean due to the low recruitment of Cerulean-HP1 by H3um-NCP. The in-well fluorescence and western blot analysis of Cerulean-HP1 did not match. This suggested quenching of the fluorophore. ECFP and mCFP had shown to be similar recruited by H3K9me2, H3um-, and H3Δ-NCP by both in-well fluorescence and western blot analysis. Therefore, both proteins were suitable for further assays. Up to this point, no gain in specific recruitment by H3K9me2 over H3um was achieved by the use of brighter CFP derivatives.

3.5 Development of an activity assay based on radioisotope labeling readout

For the activity assay, ligation-ready NCP were immobilized on streptavidin coated 96-well Flash plates. Flash plates carried a coating of a thin polysterene layer containing the scintillant. Thus, radiation from proximate radioisotopes were converted into photons which could be detected by the plate reader and no additional scintillation cocktail was necessary.

3.5.1 Library design

In order to study the influence of an additional positively charged PTM on potential GCN5 target sites and neighboring target sites of Aurora B, we expanded the H3-NCP library by three members: H3K4ac, H3K9ac and H3K27ac. Together with H3Δ, they were placed on the so far un-used NCP-H3Δ coated column (see figure 3.19). For NCP coverage determination, reference wells for Cy5 were placed. Background radioactivity was also determined using as a negative control wells without NCP-coating which were treated with the reaction mix.

3.5.2 HAT assay development using GCN5

The histone acetyltransferase GCN5 acetylates the histones H3 and H4 in non-nucleosomal context with preference for H3K4me3 modified histones[138]. GCN5 within the SAGA com-

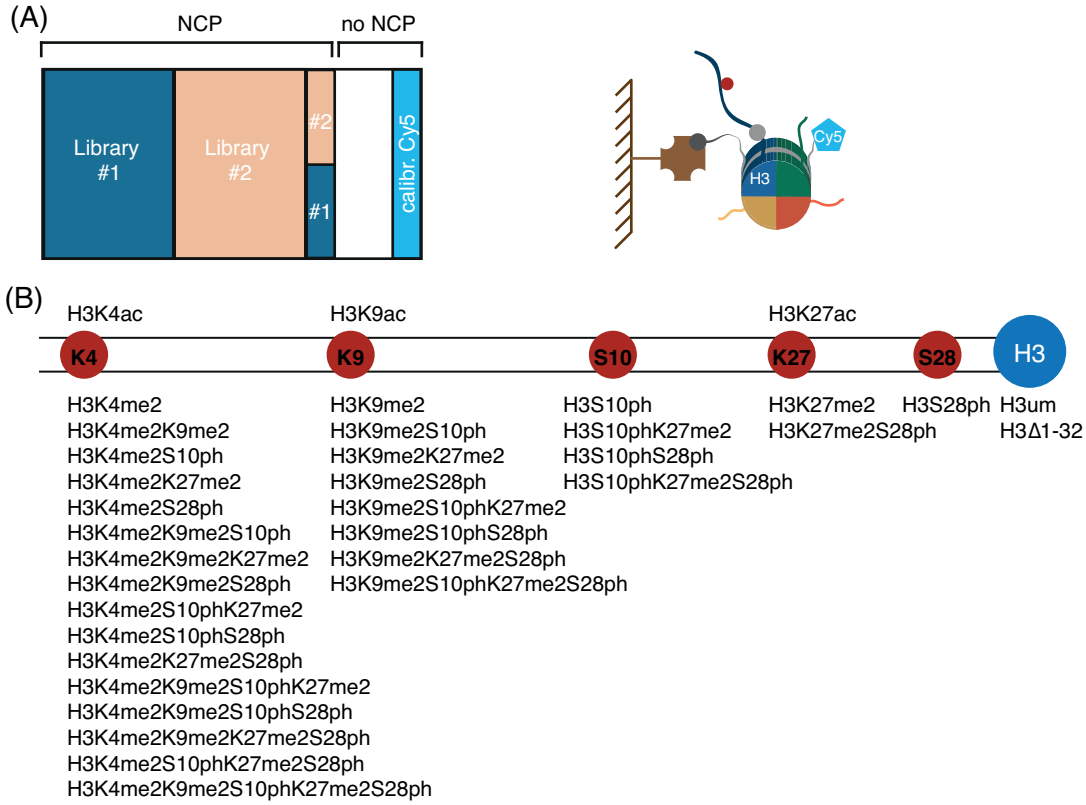

Figure 3.19: NCP-H3 library with additional acetylation on H3K4, H3K9 and H3K27
(A) 96 well plate organization of randomized Library #1 and #2, with wells for calibrating Cy5-fluorescence (calibr. Cy5). (B) PTM patterns of combinatorial NCP-H3 library with 36 members.

plex augments HAT activity and acetylates histones within the NCP[59]. In addition, recombinant GCN5 was found to acetylate nucleosomal substrates *in vitro* under certain conditions[58]. With respect to the different acetylation behavior towards histones within the NCP, we wanted to see whether the experimental set up was able to observe the incorporation of radioisotope labeled acetyl groups onto immobilized NCP by the HAT GCN5 in Flash plates (figure 3.20 (A)). To this end, NCPs containing wild type histones (WT-NCP, for octamer and NCP reconstitution see Appendix figure 5.2) were immobilized with a coating volume of 200 μL and the HAT assay was performed (figure 3.20 (B)). We observed GCN5 dependent incorporation of 14C-labeled acetyl-groups into the NCP in the absence of either GCN5 (– GNC5) or NCP substrate (BG), only little background signal was observed. Concluding, we were able to detect GCN5 dependent acetylation of WT-NCP immobilized on Flash plates.

Streptavidin coated Flash plates had a biotin binding capacity of $\approx$ 40 pmol/well with a streptavidin coating volume of 200 μL. Thus, the streptavidin coating density was lower compared to the BA-plates (biotin binding capacity: 125 pmol/well in 100μL coating volume). As the coating volume defined the amount of immobilized NCP, we were interested in how much the NCP immobilization degree would decrease by the reduction of the NCP coating surface. To this end, WT-NCP were immobilized with 50, 100 and 200 μL coating volume into 96-well Flash plates while NCP coverage was observed by in-well Cy5-fluorescence (see figure 3.20 (C)). With fluorescence readings normalized with respect to 200 μL, the fluorescence intensities of Cy5-NCP coverage within the well showed 55 and 62 % signal intensity for 50 and 100 μL Cy5-NCP coating volume. While the difference of NCP coverage for 50 and 100 μL correlated with the theoretical available surface of 50 and 100 μL, there was a loss in signal intensity of 40 % between 100 and 200 μL Cy5-NCP coating volume. Thus, the reduction of the coating volume by a factor of 0.5 and 0.25 resulted in 62 and 55 % of NCP coverage. Therefore, it seemed more efficient to use either 50 or 100μL coating volume for NCP immobilization.

The main interest however, was to find the minimal NCP coating volume where a stable and good acetylation signal could be obtained. To this end, GCN5 dependent acetylation with 14C-labeled AcCoA was performed on WT-NCP in 50, 100 and 200 μL reaction volume (figure 3.20 (D)). Signal intensities were corrected for background and counts were normalized with respect to the acetylation counts in 200 μL reaction volume. The observed NCP acety-

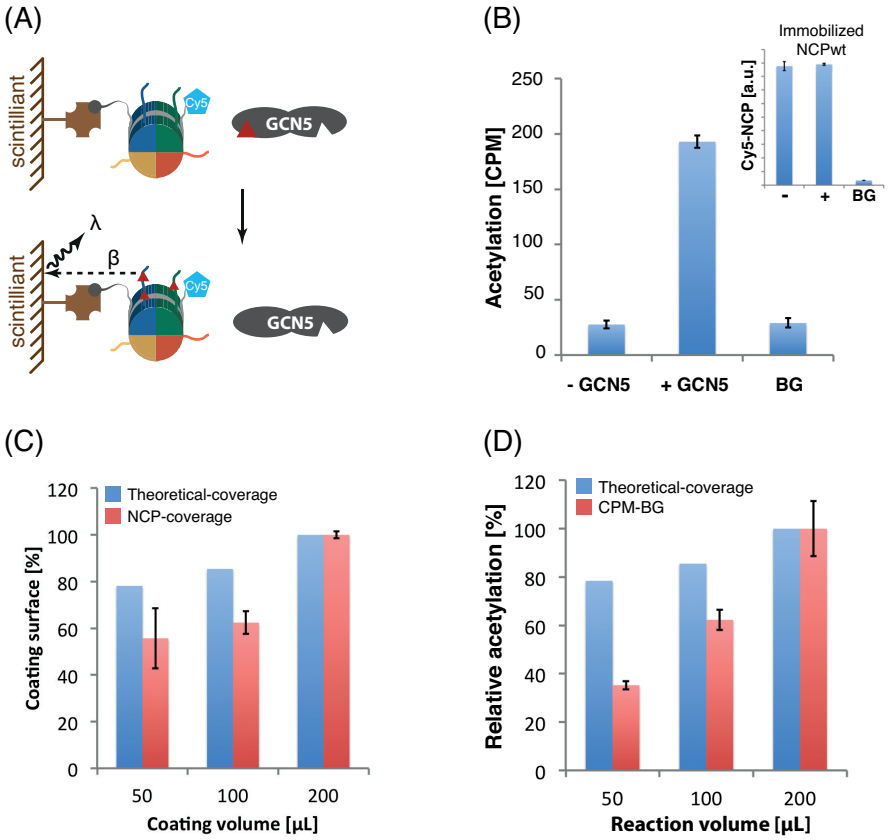

Figure 3.20: The acetylation of immobilized WT-NCP by GCN5 was observed using Flash plates

(A) Schematic representation of HAT assay with NCP immobilized on Flash plates, which have the scintillant incorporated into the well. Scintillant converted energy of β-particle emitted by incorporated isotope (14C) into photons (λ) which were detected. (B) Acetylation of immobilized WT-NCP in the presence (+) or absence (-) of GCN5 with NCP-coverage shown in the inset. BG: + GCN5 in empty wells. (C) Comparison of theoretical available coating surface in 50, 100, and 200 μL coating volume (blue) and effectively covered surface by NCP relative to 200 μL coverage. Values are plotted as mean $\pm$ s.d. of 3 replicates. (D) background corrected CPM of acetylated NCPs in 50, 100, and 200 μL reaction volume relative to acetylation in 200 μL. Values are plotted as mean $\pm$ s.d. of 3 replicates.

lation in correlation with the reaction volume displayed a linear behavior. This was contrary the expectation, that would suggest a correlation between NCP coverage and acetylation signal. Nevertheless, for 100 μL both NCP coverage and NCP acetylation displayed 60 % signal intensity relative to 200 μL reaction per coating volume. Whereas the acetylation signal observed within 50 μL coating surface did not correlate with NCP-coverage. 100 μL NCP or larger NCP coating and GCN5 reaction volume led to good correlation of NCP coverage and detected acetylation degree. Thus it was chosen to work with an NCP coating volume per GCN5 reaction volume of 100 μL.

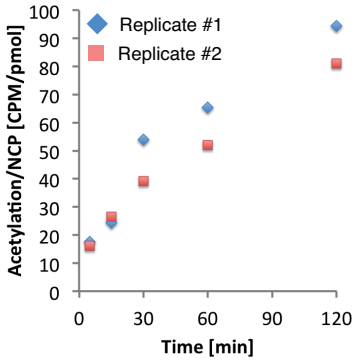

Figure 3.21: Acetylation of WT-NCP by GCN5 over 2 hours time course
Two replicates of HAT assay on immobilized WT-NCP by GCN5 over 120 minutes. Raw data was corrected for background and normalized to NCP coverage.

Next, we were interested in the time dependent acetylation of immobilized NCP by GCN5. To this end, the GCN5 reaction mix was incubated with immobilized WT-NCP and was removed from the plate at indicated time points. Wells were washed and the 14C incorporation and Cy5-NCP coverage was detected. In figure 3.21 the acetylation degree per NCP is plotted in dependence of incubation time. Acetylation of NCPs by GCN5 displayed a linear correlation over 120 min. Thus, enzymatic acetylation of WT-NCP by GCN5 had not reached saturation. As the acetylation degree of WT-NCP progressed the most within the observed time frame at 120 min without saturation, the HAT assays on the H3-NCP libraries were incubated for 120 min. This way we reasoned, we would obtain the largest range for the observation of GCN5 activity in dependence of the pre-modification of H3-NCP.

3.5.3 HAT assay performed on H3-NCP library

Having established the parameters for the GCN5 HAT assay on WT-NCP, we were interested in how the *de novo* acetylation rate by GCN5 depended on pre-modified H3-NCP. To this end, H3-NCP libraries were incubated for 120 minutes with GCN5 and 14C-labeled AcCoA. *De novo* acetylation of pre-modified H3-NCP was corrected for background, normalized with respect to both Cy5-NCP content and the *de novo* acetylation degree of H3um-NCP for each modification. This is plotted in figure 3.22. Noticeably, we observed enhanced GCN5

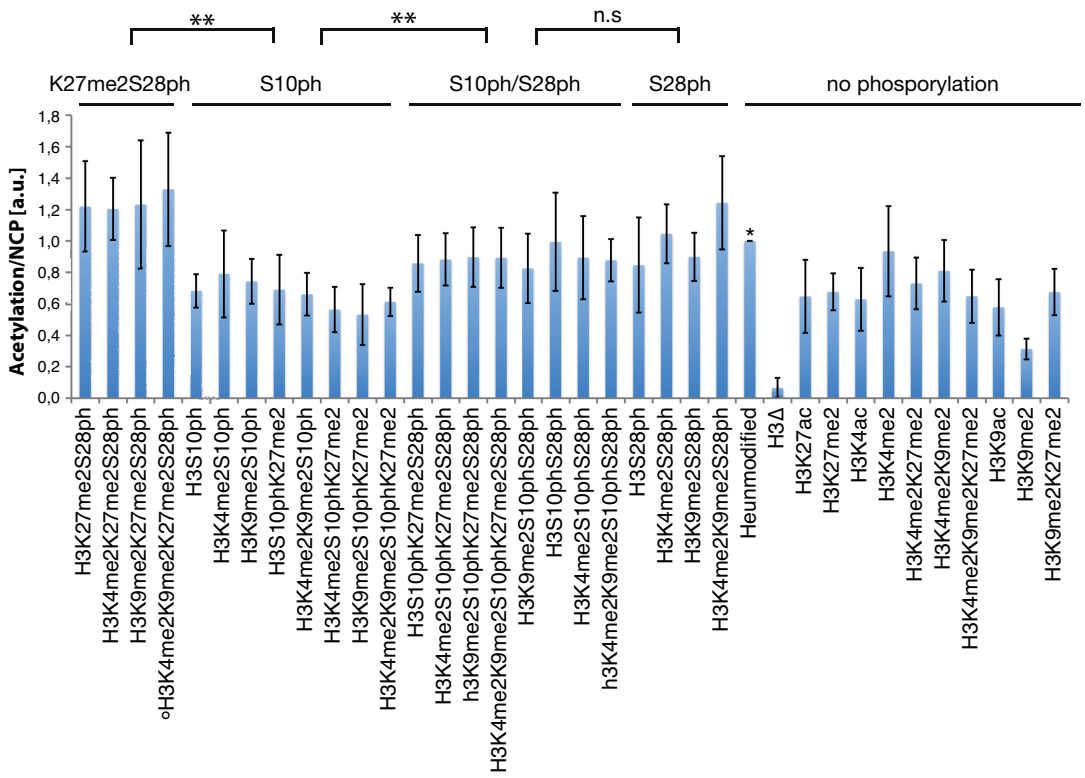

Figure 3.22: GCN5 HAT assay on H3 modified NCP library
Flash plate HAT assay on H3-NCP library incubated with GCN5 for 120 min. Raw data was corrected for background, normalized to NCP content and acetylation degree of H3um-NCP ($*$), plotted as mean $\pm$ s.d. for 7, 6 ($\circ$) replicates. Arbitrary units [a.u.], ($**$) significant $p < 0.05$, n.s. not significant.

acetylation rate for NCPs that contained H3K27me2S28ph compared to PTM patterns which contained H3S10ph. The presence of both, H3S10ph and H3S28ph displayed an acetylation degree similar to H3um. Whether H3K4 and H3K27 were acetylated or di-methylated had no impact on the acetylation rate of GCN5. In contrast, H3K9me2 strongly decreased the GCN5

acetylation rate compared to the pre-actylated (H3K9ac) version. Importantly, we observed for NCPs that carried a truncated histone H3 (H3Δ) no acetylation of these NCPs.
Taken together, this data present the successful development of an activity assay for screening the impact of pre-set histone PTMs on the acetylation rate of GCN5 using Flash plates and radioisotope readout of incorporated 14C-labeled acetyl groups. We found evidence for a new GCN5 acceleration mark H3K27me2S28ph. In comparison, H3S10ph seemed to slow down GCN5. As a single mark, H3K9me2 had a severe impact on slowing down GCN5 acetylation on these NCPs.

3.5.4 Kinase assay with Aurora B

Kinases play a crucial role in regulating cellular processes by phosphorylation[66]. Thus, having established the activity assay for the HAT GCN5 we were interested in applying the experimental design for studying kinase activity in dependence of pre-modified NCP (see figure 3.23 (A)). Here, the well characterized kinase Aurora B was chosen that is known to phosphorylate H3 on S10 and S28 during mitosis[70;139]. In a preliminary experiment, kinase

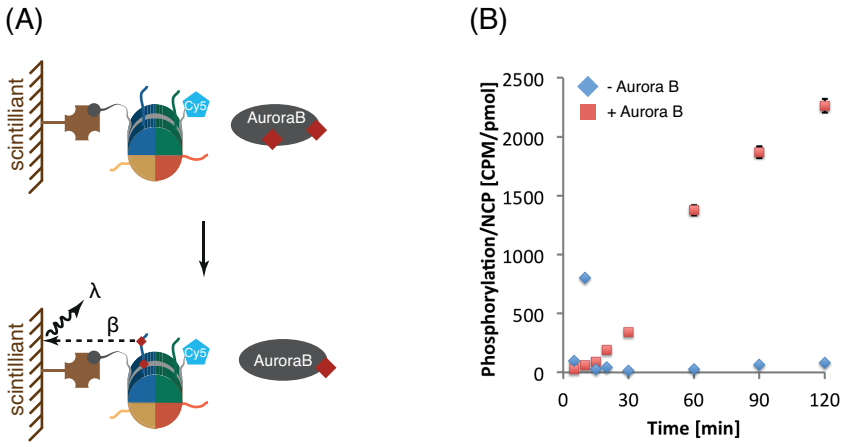

Figure 3.23: Activity assay with Aurora B on WT-NCP over 2 hours
(A) Schematic representation of kinase assay: immobilized WT-NCP were phosphorylated by auto activated Aurora B and readout of incorporated radioisotope-labeled phosphorylation marks. Scintillant converted energy of β particle into photons (λ) which were detected. (B) Kinase assay performed on WT-NCP immobilized on Flash plates for + Aurora B (red) values are plotted as mean $\pm$ s.d. of 3 replicates and - Aurora B (blue) one replicate using γ-^{32}P-ATP and WT-NCP as substrate. Raw data were corrected for background and normalized to NCP content per well.

assay conditions were tested with WT-NCP immobilized on Flash plates over an 120 min time course. In figure 3.23 (B) the phosphorylation by Aurora B per WT-NCP is plotted against the incubation time in the presence or absence of Aurora B. Within the observed time frame of 120 minutes, phosphorylation by Aurora B correlated linear with the incubation time. Importantly, no saturation of the system was observed. In the absence of Aurora B, as expected, no phosphorylation was detected except for an outlier at early time points. Thus, we decided on a 120 minutes reaction time for the enzymatic phosphorylation of the H3-NCP library by Aurora B. Having established the parameter for the kinase assay, H3-NCP libraries were

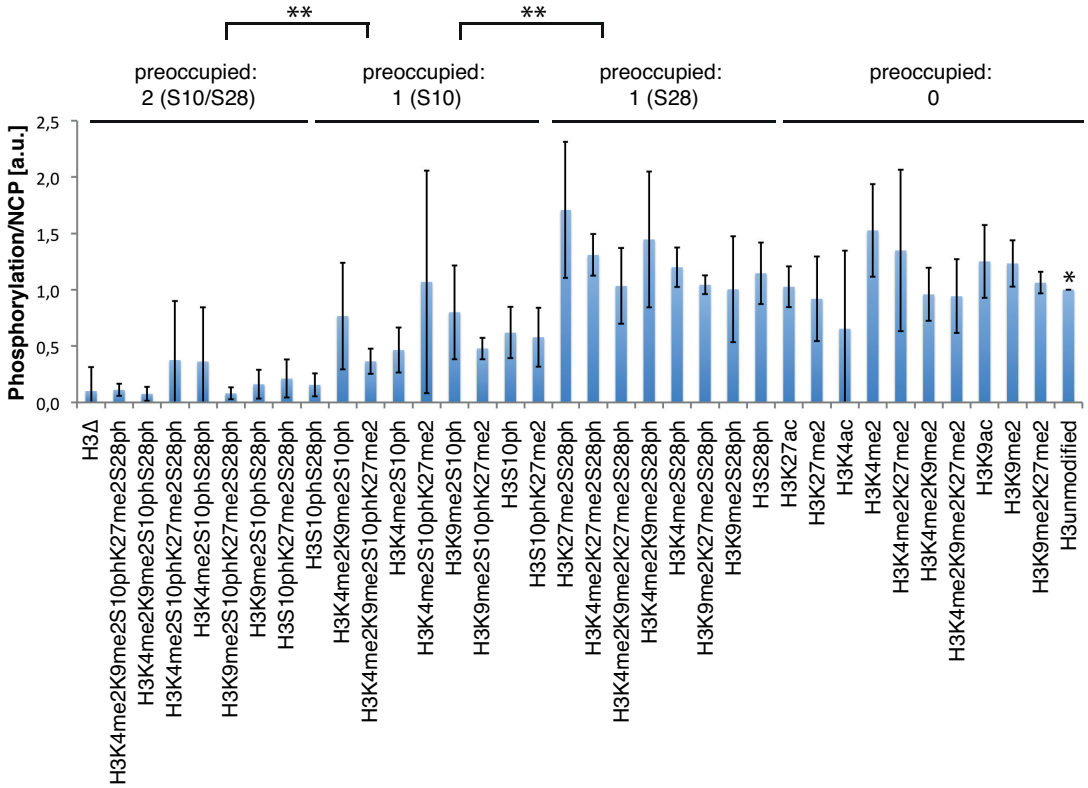

Figure 3.24: Aurora B kinase assay on H3-NCP library
Aurora B kinase assay performed on H3-NCP library over two hours with readout of incorporated 32P by Aurora B. Grouped according pre-modified (preoccupied) of serine phosphorylation sites. Raw data were corrected for background, normalized to NCP-content and H3um-NCP, set as 1, and marked with $(*)$. Data points are plotted as mean $\pm$ s.d. of 4 replicates.
$(**)$ significant $p < 0.05$, n.s. not significant.

tested for modification-dependent phosphorylation by Aurora B. Two libraries on each plate were incubated for two hours with kinase reaction mix containing Aurora B and γ-32P-ATP. The mean of incorporated 32P per NCP normalized to the phosphorylation degree of H3um-

NCP for each library is plotted in figure 3.24. The assay showed the substrate specificity of Aurora B, which phosphorylated H3S10 and H3S28. No further phosphorylation of NCP was observed for NCPs that were pre-phosphorylated on these sites. As in the preliminary experiment, we observed here as well several outliers that in part were statistically identified and removed. In addition, we detected library-to-library variations due to plate-to-plate variations and positioning within the plate[140]. Taking a close look on NCPs which were pre-phosphorylated on both sites (H3S10/S28), on one site (H3S10) and both available phosphorylation sites on H3 (0) the signal intensities for *de novo* phosphorylation were in line with available phosphorylation sites. Thus, it remained open what caused the different phosphorylation intensities between NCPs pre-phosphorylated on H3S10 or H3S28. As expected, neither H3Δ-NCPs nor doubly pre-phosphorylated NCPs were a substrate for Aurora B.
These data clearly demonstrated the successful development of an activity assay for analyzing the H3-NCP pre-modification dependent activity of Aurora B.

4 Discussion

The histone code hypothesis states that certain patterns of PTMs on the histone tails lead to a specific biological outcome[49;79]. Since the formulation of this hypothesis, it is important to decipher this code and to gain insight into the cross-talk between histone modifications within chromatin. In order to provide a platform for the systematic study of histone PTMs in the context of NCPs we designed a ligation-ready NCP, that allowed ligation of modified histone tails to H3 and H2A using Sortase A and protein *trans*-splicing, respectively. In addition, we developed an *in vitro* biochemical binding assay with fluorescence readout for studying the impact of post-translational modified H3-NCP on the interaction with the well-characterized HP1. The H3 histones within the NCPs were modified with one to five PTMs per histone tail in all possible combinations. Moreover, we developed proximity-based radioactive, enzymatic assays for studying the impact of 36 differently pre-modified H3-NCPs on the activity of the histone acetyltransferase GCN5 and the kinase Aurora B.

4.1 Assay performance

4.1.1 Consequences of ligation in nucleosomal context for biochemical assays

In this study we used a H3-NCP library of 36 members, that was generated by enzymatic ligation of modified histone tails. The overall ligation efficiency for in 96-well plates immobilized H3Δ-NCP was 83 ± 3 % (figure 3.4). Thus, on average 17 % remained as H3Δ-NCP for each modification. Consequently, we included the truncated, non-ligated, ligation-ready NCP (H3Δ-NCP) as a separate modification into the H3-NCP library to observe its performance within the assays. For binding assays, this served as a good control for unspecific bind-

ing. For the enzymatic activity assays, it was demonstrated that the non-ligated H3Δ-NCP had no impact on the enzymatic activity. H3Δ-NCP was found to be no substrate for both enzymes (Aurora B and GCN5). The incomplete ligation had only an impact on the quantification of immobilized H3-NCP. Hence, the actual degree of modified, full-length H3-NCP within each well was on average 17 % lower than determined by in-well Cy5-NCP fluorescence. We normalized the data with respect to the Cy5-NCP signal representing both H3Δ and H3-modified-NCP content in each well for the following reason: the assay reported protein binding or enzymatic activity on all H3-NCP modifications at the same time. Hence, we were interested in their relative instead of absolute impact on binding or enzymatic activity. To gain clarity of the modification degree in future libraries, we introduced a fluorescence-tag in the H2A-tail (figure 3.7). In this manner, we plan to observe the protein *trans*-splicing efficiency for generation of modified H2A-NCP by comparing it with the Cy5 signal of immobilized NCP. In the case of full ligation we expect this ratio to be 2:1.
For efficient ligation, synthetic histone tails as well as recombinant histone core domains of H3 and H2A had to be modified, which resulted in minor alterations in amino acid sequences at the ligation sites in the final, full-length histone. For H3, the final product was H3A29L, as this was not a site for histone PTM nor a negative or positive charge was introduced, we assumed this mutation did not influence our assays. In agreement with this, the binding assay revealed functionality of H3-modified-NCP by selective binding of eCFP-HP1 to H3K9me2-NCP, but not H3K9me2S10ph-NCP and H3um-NCP (figure 3.11). For H2A, protein *trans*-splicing using mini-split intein led to an insertion of four amino acids (GSIE) into the final splice product. We showed that there was no difference in migration in native agarose gel electrophoresis between spliced H2A-NCPs and WT-NCPs, suggesting full integrity of ligated NCPs with a wild type like size (figure 3.5 (B)). Whether they are functional equivalent to native H2A-NCP remains to be tested, as we focused on this study in the development of biochemical assays on H3-NCP library.

4.1.2 Quantification of immobilized H3Δ-NCPs

Quantification of immobilized Cy5-labeled H3Δ-NCPs by in-well fluorescence compared to plate external quantification methods (western blot, absorbance of DNA at 260 nm) resulted in a 2-3 fold difference in detection (figure 3.9 (F) and figure 3.10). This was probably due

to the limited availability of NCPs for spectroscopic detection within the well, while all NCPs were solubilized using SDS containing buffer for western blot. Similarly, the entire NCP immobilization degree was detected by the indirect determination of bound NCPs. It was calculated from the difference in NCP concentration of the loaded and unbound NCP-material. The concentration was determined by the absorbance of DNA at 260 nm (A260), suggesting local detection of Cy5-NCPs by in-well fluorescence as well. This was probably due to a limited excitation spot size of the plate reader (2 mm diameter, TECAN infinite Pro Manual), which possibly did not excite molecules outside this area (e.g. molecules bound to the walls). This was addressed by performing an eCFP-HP1 binding assay on immobilized NCPs and a subsequent release of immobilized Cy5-NCP into solution thereby increasing the amount of detected molecules (figure 3.16). To control for pH and temperature dependent variations of fluorescence intensities[141], reference wells containing either eCFP or Cy5 fluorophore were placed on the same plate (figure 3.16). A slight increase was observed in the amount of detected molecules before and after release of Cy5-NCP and bound CFP-HP1 into the solution. However, this increase did not result in the same amount of immobilized NCP as obtained by DNA absorbance at 260 nm and western blot analysis. As the ratio of eCFP to Cy5 did not change before and after their release into solution and the detected in-well fluorescence was representative for the immobilization degree of NCP in each well (figure 3.16 (A)), we reasoned the fluorescence readout would be an adequate choice for our qualitative binding assays.

However, we could not increase the immobilization degree above 20 pmol per well (8 pmol quantified by in-well Cy5 fluorescence), which was only one sixth of theoretically available binding sites within 50 μL coating volume. This limited the sensitivity of this detection method. Related techniques observing interactions with immobilized probes such as Enzyme-Linked Immunosorbent Assay (ELISA) circumvent the issue of limited sensitivity by the use of enzymes (e.g. horseradish peroxidase). Upon addition of a substrate a colorimetric or chemiluminescent signal can be observed in solution which reflects the entire well content and not just a limited area, thus amplifying the signal[142–147]. In microtiter plate based assays using fluorescence readout, sensitivity is limited to background fluorescence and possible quenching effects by analyte compounds[148]. Thus, in high-throughput assay development the focus turns towards proximity-based techniques such as ALPHAlisa, LANCE[104;106] or

DELFIA (dissociation-enhanced lanthanide fluorescence immunoassay). DELFIA relies on fluorescence compounds that possess a large stokes shift, resulting in wide separation of excitation and emission maxima for time resolved fluorescence detection without background fluorescence by other compounds[149;150]. A study by Schiedel *et al.*[151] describes that the increase of immobilized material by immobilization to magnetic beads instead of plates results in an increase in dynamic range and robustness.
In summary, besides an higher background signal compared to proximity based set ups, in this study the limiting factor for the sensitivity and dynamic range of the here developed binding assay was the immobilization of Cy5-NCP and the not enzymatically amplified signal detection.

4.1.3 Factors introducing variability

To develop a robust assay, it was not only important to increase the signal intensity by immobilizing as many NCPs as possible, but it was even more paramount to guarantee the reproducibility of the binding and activity assays. In the developed assays several factors contributed to library-to-library and plate-to-plate variability. Firstly, the well-to-well variability of NCP coverage determined by in-well Cy5 fluorescence was found to be 15 % for binding assay plates (BA-plates) and 16 % for Flash plates (figure 3.8). This was in part caused by the provided streptavidin coating by the vendor as well as by small experimental variations. In order to minimize the variability introduced through NCP capture, the data was normalized with respect to the H3Δ-NCP content for each well determined by Cy5-in well fluorescence. However, this only took H3Δ-NCP into account, as discussed above, but not the modified H3-NCP which depended on the ligation efficiency for each modification. Thus H3 ligation was a source of library-to-library variation.
Secondly, in eCFP-HP1 binding assays, signal intensity depended strongly on incubation time and wash steps (figure 3.12). Therefore, it was necessary to normalize with respect to an experiment internal standard (H3Δ-NCP). However, this was not sufficient to obtain reproducible eCFP-HP1 binding results for all modified H3-NCP (figure 3.15). Possibly, inherent properties of the HP1 protein accounted for such variability. For example, HP1 proteins are known to dimerize via their C-terminal chromo shadow domains. Recently, it was shown that HP1 dimer dissociation is kinetically trapped on condensed chromatin displaying high local

concentration of H3K9 methylated tails[77]. As the ligation efficiency varied for each modification and for each conducted ligation (figure 3.4), the variability of the H3K9me2 density might be a possible source for the observed differences in H3K9me2 binding. Whether this was the only mechanism causing the variations between the experiments remained to be investigated.

Thirdly, in all microtiter plate based assays, positioning effects within one plate can introduce bias. Therefore, randomization of samples is suggested to avoid any bias introduced by a certain position[152]. For radioactivity based assays using Flash plates variations within and between columns have been reported[140]. Thus we randomized the positions of modifications in each library in order to avoid that kind of bias. However, randomization could contribute to library-to-library variability. With increasing energy of the radiolabel, a cross-talk between neighboring wells could occur, which could accumulate depending on its position within the plate. Although these effects might be small, they still contributed to library-to-library variability. Automation of HAT and kinase assay in addition to increased sample size will probably reduce the occurrence of outliers and provide an even better overview of library-to-library variation, as well as identification of positive and negative effects of modified H3-NCP on binding and enzymatic activity.

4.1.4 Specificity of assays

We found that the selective binding of eCFP-HP1 to H3K9me2 modified NCPs was identified by in-well fluorescence readout and verified this by western blot analysis (figure 3.11). Moreover, signal intensities depended on eCFP-HP1 incubation time and wash steps. The unspecific interaction of eCFP-HP1 with H3um- and H3Δ-NCPs was of concern. Studies[153–155] indicated that HP1 can also bind unmodified mono-nucleosomes which seems to depend on DNA linker length. It is reported that the hinge region of HP1 interacts with DNA of nucleosome core particles. HP1α is found to bind DNA linker with a ratio of 3:1 to H3K9me3-NCP over H3um-NCP whereas the specificity is reduced to 2:1 in the absence of linker DNA[153]. The opposite effect is observed for the HP1 homolog Swi6. Specificity of Swi6 to H3K9me3-NCP over H3um-NCP is reduced by a factor of 5 with increasing linker length (0-47 base pairs)[154]. However, for HP1β the DNA binding effect is reported to be weaker[156]. Additionally, it was shown recently that the unstructured N-terminus of HP1β makes contacts with

the H3 tail and core regions instead of the HP1β hinge region with DNA[77]. These weak but numerous interactions could to a certain degree explain the unspecific interaction of HP1β to H3um-NCPs observed in figure 3.18. However, after optimization of the binding assay we observed specificity of eCFP-HP1 binding H3K9me2 two to four times of eCFP-HP1 binding H3um-NCP (figure 3.18). This was in accordance with the reported specificity of 2 and 5 fold for HP1α and Swi6, respectively[153;154]. Why we observed an excellent specificity between H3um-NCP and H3K9me2-NCP in the very first binding experiment by in-well fluorescence remains an open question (figure 3.11). The dynamic range was wider than in all following binding experiments even after optimization of the binding conditions. In contrast, western blot analysis suggested comparable specificity between the first binding experiment and after assay optimization (figure 3.18), thus some additional fluorescence specific effects must have contributed to the observation.

In order to increase the signal-to-noise ratio, brighter CFP derivatives were used: monomeric CFP and Cerulean. However, this only would work in the absence of unspecific HP1 binding. Otherwise, taking unspecific bindig of HP1 into account, both binding events, specific and unspecific, would lead to increased fluorescence intensity resulting in a similar ratio of modified versus unmodified NCP as we observed in figure 3.18 (C). Unexpectedly, we detected a lower recruitment of Cerulean-HP1 to H3K9me2-NCP by in-well fluorescence compared to eCFP- and mCFP-HP1. In contrast, western blot analysis revealed rather equal recruitment of all three CFP-HP1 derivatives (figure 3.18 (A, B)). One explanation for this discrepancy could be that the chromophore of Cerulean, carrying mutation S72A but no A206K for improved protein folding and solubility, did not fully mature, thus resulting in differences in detection by in-well fluorescence and western blot analysis.

Hence, the issue whether Cerulean could increase the signal-to-noise ratio by its potentially enhanced spectroscopic properties was not entirely solved. Therefore, we suggest to include the A206K mutation for monomeric Cerulean that supports folding during expression for further studies. In need of even brighter fluorophores to push sensitivity of the assay to its limits the use of the up to date brightest GFP derived CFP derivative mCerulean3 or mTurquoise with a quantum yield of 0.8 are possibly a good choice. Whereas Cerulean and eCFP have quantum yields of 0.6 and 0.3, respectively, with comparable extinction coefficients[157;158].

On the other hand, activity assays relied on the detection of incorporated radioactive isotopes by the enzymes GCN5 and Aurora B. The only limiting factor here was how many labels could be incorporated into nucleosomes and how well these signal could be converted into a detectable signal by the scintillant. For the GCN5 assay, the counts were rather low due to the low energy of the β-particle of 14C compared to 32P. As these factors were inherent to the compounds and plates, signal intensity could be enhanced by increasing the immobilized substrate NCP (figure 3.20 (D)). As a result, ratiometric analysis of HAT and Kinase assay revealed a good discrimination between positive (H3um-NCP) and negative (H3Δ-NCP) control resulting in ratios of 13 and 10 for GCN5 and Aurora B assay, respectively. These ratios are comparable to a Flash plate-based HAT inhibitor screen assay on immobilized histone H3. This shows that the increase of immobilized substrate results in good assay window and overall robustness[159].

4.2 Influence of pre-modified NCP on GCN5 and Aurora B activity

Enzymes modifying chromatin interact either directly with chromatin or are recruited to chromatin by other proteins[50]. GCN5 for example acts in a two-step mechanism: at first, it acetylates H3K14, which stabilizes its binding through engaging the bromodomain. This facilitates the second step, acetylation of other sites within H3 and hyperacetylation of H4[60]. We observed no acetylation of the H3Δ-NCP, which was in agreement with the mechanism described above. Furthermore, no acetylation of other histones was observed in the absence of the H3 tail (figure 3.22), which is responsible for tethering GCN5 to the nucleosome according to Cieniewicz *et.al*[60]. With the assay we could observe the overall acetylation degree in dependence of the histone H3 modification patterns, but not the exact histone which was modified. Importantly, we could directly compare the effect of pre-modified H3-NCP on the acetylation rate by GCN5. However, we could not detect the described[56;160;161] overall enhancement of acetylation by H3K4me2/3 or H3S10ph. This was probably due to the different acetylation behavior of GCN5 alone compared to GCN5 in the SAGA or ADA complex[52;160]. Recognition of H3K4me2/3 has been assigned to a complex partner (Sgf29) within the SAGA complex[160;162]. In previous investigations, the influence of H3S10ph on GCN5-mediated

acetylation is found to be controversial[32]. Studies reported both an increasing effect on the acetylation rate or no effect compared to unmodified substrates[91;161;163;164].
For the GCN5 activity assay developed in this work, we observed an enhanced acetylation rate for H3 PTM patterns containing H3K27me2S28ph compared to single phosphorylated modifications at H3S10 (figure 3.22). *In vivo*, H3S28ph and H3K27me3S28ph are linked to transcriptional activation[81;165] and concomitant acetylation of histone H3 and H4 is observed[82;165]. Thus it seemed possible that GCN5 supports transcriptional activation upon phosphorylation of H3K27me3S28 by kinases (Aurora B or MSK1) from the repressive state marked by methylated H3K27.
The introduction of acetylation of H3K4, H3K9 or H3K27, which are targeted by the bromodomain of GCN5, did not increase acetylation compared to the methylated states (H3K4me2 or H3K27me2). This was probably due to the preference of GCN5 for modifying H3K14 and subsequently binding to this site[60]. Surprisingly, H3K9me2 greatly decreased the acetylation rate of GCN5. Although H3K9me2 is known to be located at silenced domains within euchromatic regions and is therefore a good candidate for reducing the affinity of GCN5 to nucleosomes, this effect has not been observed before[43]. Interestingly, in this work decreased acetylation by GCN5 was only observed on single modified NCPs but not when the modification occurred in combination with H3K27me2 or H3K4me2K27me2. In any case, effects of certain H3-NCP-PTM patterns on GCN5 acetylation rates need further evaluation to verify the observation.

In contrast to the GCN5 assay, the activity assay performed with the kinase Aurora B clearly showed that nucleosomes pre-occupied on both phosphorylation sites (H3S10 and H3S28) were not a substrate for Aurora B. Pre-modification of H3S10 led to a reduced phosphorylation activity compared to H3-NCP modification patterns that contained unmodified serines or H3S28ph only. This suggested that Aurora B preferred H3S10 as substrate over H3S28. Both H3S10ph and H3S28ph are reported to be phosphorylated by Aurora B during mitosis and have been described to be crucial for chromosome condensation and segregation. While H3S10ph is observed from late G2 until telophase whereas H3S28ph only occurs between prophase and anaphase, indicating that H3S28ph is regulated independently of H3S10ph, but a mechanism has not been described[70]. Our studies suggested that the discrimina-

tive phosphorylation of H3S28 on pre-phosphorylated H3S10 histone tails was an Aurora B inherent property, which was possibly further regulated by other components.

In conclusion, we developed a powerful tool for determining the impact of histone PTM patterns on the activity of chromatin-modifying enzymes. PTM patterns identified this way provide a good lead for further investigation.

4.3 Features and limitations of binding and activity assays

The assays developed in this study provided several advantages over previously developed PTM screening approaches[88;104;115]. Because of the one-modification-one-well set up, we could detect interactions independent of the use of histone PTM antibodies, whose binding target is known to be prone to inhibition by adjacent PTMs[42]. Our assay, in contrast to antibody-based assays, allowed the widespread, unbiased evaluation of the impact of any combination of PTMs incorporated into the NCP on enzymatic behavior. In theory, the enzymatic activity assay could be extended and performed with any desired enzyme and available radio-labeled substrate, in the way we exemplified with GCN5 and Aurora B. In contrast to the homogenous in-solution activity assay on NCPs developed by Nguyen *et al.*[115], immobilization of the substrate (H3-NCP) allowed assay execution in a few steps, simple separation of the enzyme as well as a surplus radio-labeled substrate after the reaction from immobilized NCP. The remaining, immobilized NCPs can be used for further analysis of *de novo* PTMs.
Extending the assay by enzymatic release of NCP from the plate and analysis of *de novo* modification degree by gel shift experiments[59;166] or by performing the experiment using non-radioactive PTM label donor (AcCoA or ATP) on promising H3-PTM pattern and subsequent analysis by mass spectrometry would identify the *de novo* modification degree and site-dependence on the NCP pre-modification pattern. In a next step, it would be very interesting to study modified nucleosome arrays with our developed system. However, a study by Mittal *et al.*[167] pointed out, that an additional effect needs to be considered. They found a varying acetylation degree of bead-bound tri-nucleosomes. The acetylation degree varies depending on its position with respect to the linkage of the bead. This can mask the effect of pre-modified nucleosome arrays on the activity of enzymes.
In contrast, we were not able to develop a robust binding assay using this experimental set up

because of limited sensitivity and unstable assay performance. Moreover, the signal range of strong binding and no binding was narrow (2-4 fold), thus intermediate binding events would possibly not be recognized. New bead-based detection techniques, which have been implemented successfully for analyzing methyltransferase activity and methyl binding domains on histone peptides and full-length protein using ALPHAlisa and LANCE technology, might provide a broader signal range because of the conditional signal development based on the proximity of bound protein to its target[104–106].

5 Summary and conclusion

Post-translational modifications of histones within nucleosomes regulate cell development, cell maintenance and cellular response to external factors[168]. According to the histone code hypothesis, each biologic reaction is encoded by a specific set of histone PTMs[79]. In order to decipher the histone code, we developed a platform in which ligation-ready nucleosomes can be decorated with histone tails carrying PTMs of choice in a histone type specific manner. In this study, we presented the development of ligation-ready nucleosomes and histone type specific ligation of histone tails to H3 and H2A. For H3, Sortase A mediated ligation was chosen as it has been shown before to function at the histone level. For H2A, protein *trans*-splicing with an optimized mini-split intein (*Ssp* DnaB M86) was used. Ligation ready nucleosome core particle were assembled with H3 and H2A carrying tags which allowed a type selective approach. This meant for H3, truncation of the first 32 amino acids and for H2A, N-terminal removal of the fist 18 amino acids and attachment of the split-intein C-terminal part. Using these ligation strategies for H3 and H2A we were able to generate a NCP library with 36 combinatoric modified H3 and 8 variations of H2A modifications, resulting in a library with a complexity of 288. However, for the development of binding and activity assays only a 36 member H3-NCP library was used.

The interpretation of histone marks that lead eventually to the regulation of cell development, cell maintenance and cellular response is carried out by effector proteins that 'read', 'write' or 'erase' histone PTMs. In order to gain insight in the 'reading' and 'writing' properties in dependence of H3-NCP modifications, we present the stage of development of a binding assay with fluorescence readout in 96-well format. As a 'model' protein was used in here, the well characterized HP1β. In addition, we explored the H3-NCP modification dependent activity of the histone acetyltransferase GCN5 and the kinase Aurora B in an enzymatic activity assay with readout of incorporated radioisotopes.

For the HP1-binding assay, we found specific recruitment of enhanced cyan fluorescent protein labeled HP1 (eCFP-HP1) by H3K9me2 over H3um-NCP in a proof of principle experiment. This was detected by in-well fluorescence measurement and verified by western blot analysis. Experiments on the whole H3-NCP library brought up the question: how can we increase signal intensities and the ratio of eCFP-HP1 specific binding to H3K9me2- over H3um-NCP? This has been addressed by optimization of experimental factors (buffer composition, incubation time, wash steps) and the use of brighter CFP variants. Despite the optimizations in several directions we have been unable to develop a stable and robust binding assay.

The setup of an high-throughput screening of the impact of modified H3-NCP on the activity of GCN5 and Aurora B presents an additional use of the immobilized NCP-library. Noticeable, a stark increase in overall acetylation was observed in the presence of H3S28ph or H3K27me2S28ph containing H3-NCP. This suggests a crucial role of PTMs in fine tuning the enzymatic activity of GCN5. In contrast, for Aurora B we observed that pre-phosphorylated H3-NCPs on both phosphorylation sites (H3S10ph/S28ph) were not a target for Aurora B anymore. In addition, we found that NCPs unmodified at H3S10 were better substrates for Aurora B than H3-NCPs containing pre-modified H3S10ph. This highlights the power of this assay to detect enzyme inherent properties as a function of pre-modified NCPs.

Bibliography

[1] C. Allis, T. Jenuwein, D. Reinberg, and M. Caparros, eds., *Epigenetics*. John Inglis, Cold Spring Harbor Labratory press., 2007.

[2] K. L. Huisinga, B. Brower-Toland, and S. C. R. Elgin, "The contradictory definitions of heterochromatin: transcription and silencing," *Chromosoma*, vol. 115, no. 2, pp. 110–122, 2006.

[3] K. Luger, A. W. Mader, R. K. Richmond, D. F. Sargent, and T. J. Richmond, "Crystal structure of the nucleosome core particle at 2.8[thinsp]a resolution," *Nature*, vol. 389, pp. 251–260, Sept. 1997.

[4] L. Böhm and C. Crane-Robinson, "Proteases as structural probes for chromatin: The domain structure of histones," *Bioscience Reports*, vol. 4, pp. 365–386, 05 1984.

[5] M. Lawrence, S. Daujat, and R. Schneider, "Lateral thinking: How histone modifications regulate gene expression," *Trends in Genetics*, vol. 32, pp. 42–56, 1 2016.

[6] V. Böhm, A. R. Hieb, A. J. Andrews, A. Gansen, A. Rocker, K. Tóth, K. Luger, and J. Langowski, "Nucleosome accessibility governed by the dimer/tetramer interface," *Nucleic Acids Research*, vol. 39, no. 8, pp. 3093–3102, 2011.

[7] N. P. Hazan, T. E. Tomov, R. Tsukanov, M. Liber, Y. Berger, R. Masoud, K. Toth, J. Langowski, and E. Nir, "Nucleosome core particle disassembly and assembly kinetics studied using single-molecule fluorescence," *Biophysical Journal*, vol. 109, pp. 1676–1685, 10 2015.

[8] P. Oudet, M. Gross-Bellard, and P. Chambon, "Electron microscopic and biochemical evidence that chromatin structure is a repeating unit," *Cell*, vol. 4, no. 4, pp. 281–300, 1975.

[9] G. Felsenfeld and M. Groudine, "Controlling the double helix," *Nature*, vol. 421, pp. 448–453, Jan. 2003.

[10] J. D. McGhee, J. M. Nickol, G. Felsenfeld, and D. C. Rau, "Higher order structure of chromatin: Orientation of nucleosomes within the 30 nm chromatin solenoid is independent of species and spacer length," *Cell*, vol. 33, no. 3, pp. 831–841, 1983.

[11] J. T. Finch and A. Klug, "Solenoidal model for superstructure in chromatin," *Proceedings of the National Academy of Sciences*, vol. 73, no. 6, pp. 1897–1901, 1976.

[12] C. L. Woodcock, L. L. Frado, and J. B. Rattner, "The higher-order structure of chromatin: evidence for a helical ribbon arrangement.," *The Journal of Cell Biology*, vol. 99, p. 42, 07 1984.

[13] R. A. Horowitz, D. A. Agard, J. W. Sedat, and C. L. Woodcock, "The three-dimensional architecture of chromatin in situ: electron tomography reveals fibers composed of a continuously variable zig-zag nucleosomal ribbon.," *The Journal of Cell Biology*, vol. 125, p. 1, 04 1994.

[14] Q. Bian and A. S. Belmont, "Revisiting higher-order and large-scale chromatin organization," *Current Opinion in Cell Biology*, vol. 24, pp. 359–366, 6 2012.

[15] W.-L. Wang, L. C. Anderson, J. J. Nicklay, H. Chen, M. J. Gamble, J. Shabanowitz, D. F. Hunt, and D. Shechter, "Phosphorylation and arginine methylation mark histone h2a prior to deposition during xenopus laevis development," *Epigenetics & Chromatin*, vol. 7, no. 1, pp. 1–20, 2014.

[16] K. Murray, "The occurrence of iε-n-methyl lysine in histones," *Biochemistry*, vol. 3, pp. 10–15, 01 1964.

[17] D. M. P. Phillips, "The presence of acetyl groups in histones," *Biochemical Journal*, vol. 87, pp. 258–263, 05 1963.

[18] V. G. Allfrey, R. Faulkner, and A. E. Mmirsky, "Acetylation and methylation of histones and their possible role in the regulation of rna synthesis," *Proceedings of the National Academy of Sciences*, vol. 51, p. 786, 1964.

[19] C. Tse, T. Sera, A. P. Wolffe, and J. C. Hansen, "Disruption of higher-order folding by core histone acetylation dramatically enhances transcription of nucleosomal arrays by rna polymerase iii," *Molecular and Cellular Biology*, vol. 18, pp. 4629–4638, 08 1998.

[20] D. E. Sterner and S. L. Berger, "Acetylation of histones and transcription-related factors," *Microbiology and Molecular Biology Reviews*, vol. 64, no. 2, pp. 435–459, 2000.

[21] B. M. Turner, "Decoding the nucleosome," *Cell*, vol. 75, no. 1, pp. 5–8, 1993.

[22] B. M. Turner, "Histone acetylation and an epigenetic code," *BioEssays*, vol. 22, no. 9, pp. 836–845, 2000.

[23] T. Kouzarides, "Chromatin modifications and their function," *Cell*, vol. 128, pp. 693–705, Feb. 2007.

[24] R. Marmorstein and M.-M. Zhou, "Writers and readers of histone acetylation: Structure, mechanism, and inhibition," *Cold Spring Harbor Perspectives in Biology*, vol. 6, no. 7, 2014.

[25] L. Zeng, Q. Zhang, S. Li, A. N. Plotnikov, M. J. Walsh, and M.-M. Zhou, "Mechanism and regulation of acetylated histone binding by the tandem phd finger of dpf3b," *Nature*, vol. 466, pp. 258–262, 07 2010.

[26] S. Y. Roth, J. M. Denu, and C. D. Allis, "Histone acetyltransferases," *Annu. Rev. Biochem.*, vol. 70, pp. 81–120, June 2001.

[27] Y. Fusauchi and K. IWAI, "Tetrahymena histone h2a. acetylation in the n-terminal sequence and phosphorylation in the c-terminal sequence," *Journal of Biochemistry*, vol. 95, no. 1, pp. 147–154, 1984.

[28] A. Portela and M. Esteller, "Epigenetic modifications and human disease," *Nat Biotech*, vol. 28, pp. 1057–1068, 10 2010.

[29] A. Sawicka and C. Seiser, "Histone h3 phosphorylation –a versatile chromatin modification for different occasions," *Biochimie*, vol. 94, pp. 2193–2201, 11 2012.

[30] S. Wera and B. A. Hemmings, "Serine/threonine protein phosphatases," *Biochemical Journal*, vol. 311, p. 17, 10 1995.

[31] S. D. Taverna, H. Li, A. J. Ruthenburg, C. D. Allis, and D. J. Patel, "How chromatin-binding modules interpret histone modifications: lessons from professional pocket pickers," *Nat Struct Mol Biol*, vol. 14, pp. 1025–1040, Nov. 2007.

[32] A. Sawicka and C. Seiser, "Sensing core histone phosphorylation -a matter of perfect timing," *Biochimica et Biophysica Acta (BBA) - Gene Regulatory Mechanisms*, vol. 1839, pp. 711–718, Aug. 2014.

[33] W. Fischle, B. S. Tseng, H. L. Dormann, B. M. Ueberheide, B. A. Garcia, J. Shabanowitz, D. F. Hunt, H. Funabiki, and C. D. Allis, "Regulation of hp1-chromatin binding by histone h3 methylation and phosphorylation," *Nature*, vol. 438, pp. 1116–1122, Dec. 2005.

[34] C. M. Barber, F. B. Turner, Y. Wang, K. Hagstrom, S. D. Taverna, S. Mollah, B. Ueberheide, B. J. Meyer, D. F. Hunt, P. Cheung, and C. D. Allis, "The enhancement of histone h4 and h2a serine 1 phosphorylation during mitosis and s-phase is evolutionarily conserved," *Chromosoma*, vol. 112, no. 7, pp. 360–371, 2004.

[35] A. J. Ruthenburg, H. Li, D. J. Patel, and C. David Allis, "Multivalent engagement of chromatin modifications by linked binding modules," *Nat Rev Mol Cell Biol*, vol. 8, pp. 983–994, Dec. 2007.

[36] S. Rea, F. Eisenhaber, D. O'Carroll, B. D. Strahl, Z.-W. Sun, M. Schmid, S. Opravil, K. Mechtler, C. P. Ponting, C. D. Allis, and T. Jenuwein, "Regulation of chromatin structure by site-specific histone h3 methyltransferases," *Nature*, vol. 406, pp. 593–599, Aug. 2000.

[37] A. J. Bannister and T. Kouzarides, "Regulation of chromatin by histone modifications," *Cell Res*, vol. 21, pp. 381–395, 03 2011.

[38] X. Cheng, "Structural and functional coordination of dna and histone methylation," *Cold Spring Harbor Perspectives in Biology*, vol. 6, no. 8, 2014.

[39] Y. G. Shi and Y.-i. Tsukada, "The discovery of histone demethylases," *Cold Spring Harbor Perspectives in Biology*, vol. 5, 09 2013.

[40] S. S. Ng, W. W. Yue, U. Oppermann, and R. J. Klose, "Dynamic protein methylation in chromatin biology," *Cellular and Molecular Life Sciences*, vol. 66, pp. 407–422, 02 2009.

[41] C. Martin and Y. Zhang, "The diverse functions of histone lysine methylation," *Nat Rev Mol Cell Biol*, vol. 6, pp. 838–849, 11 2005.

[42] B. A. Garcia, J. Shabanowitz, and D. F. Hunt, "Characterization of histones and their post-translational modifications by mass spectrometry," *Current Opinion in Chemical Biology*, vol. 11, pp. 66–73, 2 2007.

[43] J. C. Rice, S. D. Briggs, B. Ueberheide, C. M. Barber, J. Shabanowitz, D. F. Hunt, Y. Shinkai, and C. D. Allis, "Histone methyltransferases direct different degrees of methylation to define distinct chromatin domains," *Molecular Cell*, vol. 12, pp. 1591–1598, 12 2003.

[44] K. J. Ferrari, A. Scelfo, S. Jammula, A. Cuomo, I. Barozzi, A. Stützer, W. Fischle, T. Bonaldi, and D. Pasini, "Polycomb-dependent h3k27me1 and h3k27me2 regulate active transcription and enhancer fidelity," *Molecular Cell*, vol. 53, pp. 49–62, 1 2014.

[45] A. D. Lorenzo and M. T. Bedford, "Histone arginine methylation," *FEBS Letters*, vol. 585, no. 13, pp. 2024–2031, 2011.

[46] L. J. Walport, R. J. Hopkinson, R. Chowdhury, R. Schiller, W. Ge, A. Kawamura, and C. J. Schofield, "Arginine demethylation is catalysed by a subset of jmjc histone lysine demethylases," *Nature Communications*, vol. 7, pp. 11974 EP –, 06 2016.

[47] C. Wilczek, R. Chitta, E. Woo, J. Shabanowitz, B. T. Chait, D. F. Hunt, and D. Shechter, "Protein arginine methyltransferase prmt5-mep50 methylates histones h2a and h4 and the histone chaperone nucleoplasmin in xenopus laevis eggs," *J Biol Chem*, vol. 286, 2011.

[48] S. L. Schreiber and B. E. Bernstein, "Signaling network model of chromatin," *Cell*, vol. 111, pp. 771–778, 12 2002.

[49] B. D. Strahl and C. D. Allis, "The language of covalent histone modifications," *Nature*, vol. 403, pp. 41–45, Jan. 2000.

[50] G. J. Narlikar, H.-Y. Fan, and R. E. Kingston, "Cooperation between complexes that regulate chromatin structure and transcription," *Cell*, vol. 108, pp. 475–487, 2 2002.

[51] J. E. Brownell, J. Zhou, T. Ranalli, R. Kobayashi, D. G. Edmondson, S. Y. Roth, and C. Allis, "Tetrahymena histone acetyltransferase a: A homolog to yeast gcn5p linking histone acetylation to gene activation," *Cell*, vol. 84, pp. 843–851, Mar. 1996.

[52] P. A. Grant, A. Eberharter, S. John, R. G. Cook, B. M. Turner, and J. L. Workman, "Expanded lysine acetylation specificity of gcn5 in native complexes," *Journal of Biological Chemistry*, vol. 274, no. 9, pp. 5895–5900, 1999.

[53] M.-H. Kuo and C. D. Allis, "Roles of histone acetyltransferases and deacetylases in gene regulation," *Bioessays*, vol. 20, no. 8, pp. 615–626, 1998.

[54] K. G. Tanner, R. C. Trievel, M.-H. Kuo, R. M. Howard, S. L. Berger, C. D. Allis, R. Marmorstein, and J. M. Denu, "Catalytic mechanism and function of invariant glutamic acid 173 from the histone acetyltransferase gcn5 transcriptional coactivator," *Journal of Biological Chemistry*, vol. 274, no. 26, pp. 18157–18160, 1999.

[55] B. P. Hudson, M. A. Martinez-Yamout, H. Dyson, and P. E. Wright, "Solution structure and acetyl-lysine binding activity of the gcn5 bromodomain1," *Journal of Molecular Biology*, vol. 304, pp. 355–370, Dec. 2000.

[56] A. Clements, A. N. Poux, W.-S. Lo, L. Pillus, S. L. Berger, and R. Marmorstein, "Structural basis for histone and phosphohistone binding by the gcn5 histone acetyltransferase," *Molecular Cell*, vol. 12, pp. 461–473, 8 2003.

[57] W. Lo, E. R. Gamache, K. W. Henry, D. Yang, L. Pillus, and S. L. Berger, “Histone h3 phosphorylation can promote tbp recruitment through distinct promoter‚Äêspecific mechanisms,” *The EMBO Journal*, vol. 24, p. 997, 02 2005.

[58] C. Tse, E. I. Georgieva, A. B. Ruiz-Garcia, R. Sendra, and J. C. Hansen, “Gcn5p, a transcription-related histone acetyltransferase, acetylates nucleosomes and folded nucleosomal arrays in the absence of other protein subunits,” *Journal of Biological Chemistry*, vol. 273, pp. 32388–32392, 12 1998.

[59] A. E. Ringel, A. M. Cieniewicz, S. D. Taverna, and C. Wolberger, “Nucleosome competition reveals processive acetylation by the saga hat module,” *Proceedings of the National Academy of Sciences*, vol. 112, no. 40, pp. E5461–E5470, 2015.

[60] A. M. Cieniewicz, L. Moreland, A. E. Ringel, S. G. Mackintosh, A. Raman, T. M. Gilbert, C. Wolberger, A. J. Tackett, and S. D. Taverna, “The bromodomain of gcn5 regulates site specificity of lysine acetylation on histone h3,” *Molecular & Cellular Proteomics*, vol. 13, no. 11, pp. 2896–2910, 2014.

[61] M. Carmena and W. C. Earnshaw, “The cellular geography of aurora kinases,” *Nat Rev Mol Cell Biol*, vol. 4, pp. 842–854, 11 2003.

[62] S. Ruchaud, M. Carmena, and W. C. Earnshaw, “Chromosomal passengers: conducting cell division,” *Nat Rev Mol Cell Biol*, vol. 8, pp. 798–812, 10 2007.

[63] F. Sessa, M. Mapelli, C. Ciferri, C. Tarricone, L. B. Areces, T. R. Schneider, P. T. Stukenberg, and A. Musacchio, “Mechanism of aurora b activation by incenp and inhibition by hesperadin,” *Molecular Cell*, vol. 18, pp. 379–391, Apr. 2005.

[64] M. Carmena, M. Wheelock, H. Funabiki, and W. C. Earnshaw, “The chromosomal passenger complex (cpc): from easy rider to the godfather of mitosis,” *Nat Rev Mol Cell Biol*, vol. 13, pp. 789–803, Dec. 2012.

[65] A. Frangini, M. Sjöberg, M. Roman-Trufero, G. Dharmalingam, V. Haberle, T. Bartke, B. Lenhard, M. Malumbres, M. Vidal, and N. Dillon, “The aurora b kinase and the polycomb protein ring1b combine to regulate active promoters in quiescent lymphocytes,” *Molecular Cell*, vol. 51, pp. 647–661, 9 2013.

[66] J. A. Endicott, M. E. M. Noble, and L. N. Johnson, “The structural basis for control of eukaryotic protein kinases,” *Annual Review of Biochemistry*, vol. 81, pp. 587–613, 2016/08/18 2012.

[67] V. M. Bolanos-Garcia, “Aurora kinases,” *The International Journal of Biochemistry & Cell Biology*, vol. 37, pp. 1572–1577, 8 2005.

[68] I. M. Cheeseman, “Phospho-regulation of kinetochore-microtubule attachments by the aurora kinase ipl1p,” *Cell*, vol. 111, pp. 163–172, 2002.

[69] A. E. Kelly, C. Ghenoiu, J. Z. Xue, C. Zierhut, H. Kimura, and H. Funabiki, “Survivin reads phosphorylated histone h3 threonine 3 to activate the mitotic kinase aurora b,” *Science*, vol. 330, no. 6001, pp. 235–239, 2010.

[70] H. Goto, Y. Yasui, E. A. Nigg, and M. Inagaki, “Aurora-b phosphorylates histone h3 at serine28 with regard to the mitotic chromosome condensation,” *Genes to Cells*, vol. 7, no. 1, pp. 11–17, 2002.

[71] Y. Yasui, T. Urano, A. Kawajiri, K.-i. Nagata, M. Tatsuka, H. Saya, K. Furukawa, T. Takahashi, I. Izawa, and M. Inagaki, "Autophosphorylation of a newly identified site of aurora-b is indispensable for cytokinesis," *Journal of Biological Chemistry*, vol. 279, no. 13, pp. 12997–13003, 2004.

[72] J. C. Eissenberg and S. C. R. Elgin, "Hp1a: a structural chromosomal protein regulating transcription," *Trends in Genetics*, vol. 30, pp. 103–110, 3 2014.

[73] E. J. Richards and S. C. R. Elgin, "Epigenetic codes for heterochromatin formation and silencing: Rounding up the usual suspects," *Cell*, vol. 108, pp. 489–500, 2 2002.

[74] M. S. Lechner, D. C. Schultz, D. Negorev, G. G. Maul, and F. J. Rauscher III, "The mammalian heterochromatin protein 1 binds diverse nuclear proteins through a common motif that targets the chromoshadow domain," *Biochemical and Biophysical Research Communications*, vol. 331, pp. 929–937, 6 2005.

[75] F. Hediger and S. M. Gasser, "Heterochromatin protein 1: don't judge the book by its cover!," *Current Opinion in Genetics & Development*, vol. 16, pp. 143–150, 4 2006.

[76] J. C. Eissenberg and S. C. Elgin, "The hp1 protein family: getting a grip on chromatin," *Current Opinion in Genetics & Development*, vol. 10, pp. 204–210, 4 2000.

[77] K. Hiragami-Hamada, S. Soeroes, M. Nikolov, B. Wilkins, S. Kreuz, C. Chen, I. A. De La Rosa-Velazquez, H. M. Zenn, N. Kost, W. Pohl, A. Chernev, D. Schwarzer, T. Jenuwein, M. Lorincz, B. Zimmermann, P. J. Walla, H. Neumann, T. Baubec, H. Urlaub, and W. Fischle, "Dynamic and flexible h3k9me3 bridging via hp1[beta] dimerization establishes a plastic state of condensed chromatin," *Nat Commun*, vol. 7, 04 2016.

[78] T. Hirota, J. J. Lipp, B.-H. Toh, and J.-M. Peters, "Histone h3 serine 10 phosphorylation by aurora b causes hp1 dissociation from heterochromatin," *Nature*, vol. 438, pp. 1176–1180, 12 2005.

[79] T. Jenuwein and C. D. Allis, "Translating the histone code," *Science*, vol. 293, no. 5532, pp. 1074–1080, 2001.

[80] A. J. Ruthenburg, C. D. Allis, and J. Wysocka, "Methylation of lysine 4 on histone h3: Intricacy of writing and reading a single epigenetic mark," *Molecular Cell*, vol. 25, pp. 15–30, 1 2007.

[81] S. S. Gehani, S. Agrawal-Singh, N. Dietrich, N. S. Christophersen, K. Helin, and K. Hansen, "Polycomb group protein displacement and gene activation through msk-dependent h3k27me3s28 phosphorylation," *Molecular Cell*, vol. 39, pp. 886–900, 9 2010.

[82] P. N. I. Lau and P. Cheung, "Histone code pathway involving h3 s28 phosphorylation and k27 acetylation activates transcription and antagonizes polycomb silencing," *Proceedings of the National Academy of Sciences*, vol. 108, pp. 2801–2806, 02 2011.

[83] B. A. Garcia, C. M. Barber, S. B. Hake, C. Ptak, F. B. Turner, S. A. Busby, J. Shabanowitz, R. G. Moran, C. D. Allis, and D. F. Hunt, "Modifications of human histone h3 variants during mitosis," *Biochemistry*, vol. 44, pp. 13202–13213, 10 2005.

[84] W. Fischle, Y. Wang, and C. David Allis, "Binary switches and modification cassettes in histone biology and beyond," *Nature*, vol. 425, pp. 475–479, Oct. 2003.

[85] A. J. Ruthenburg, H. Li, T. A. Milne, S. Dewell, R. K. McGinty, M. Yuen, B. Ueberheide, Y. Dou, T. W. Muir, D. J. Patel, and C. D. Allis, "Recognition of a mononucleosomal histone modification pattern by bptf via multivalent interactions," *Cell*, vol. 145, pp. 692–706, 5 2011.

[86] B. J. Wilkins, N. A. Rall, Y. Ostwal, T. Kruitwagen, K. Hiragami-Hamada, M. Winkler, Y. Barral, W. Fischle, and H. Neumann, "A cascade of histone modifications induces chromatin condensation in mitosis," *Science*, vol. 343, no. 6166, pp. 77–80, 2014.

[87] P. Voigt, G. LeRoy, W. J. Drury III, B. M. Zee, J. Son, D. B. Beck, N. L. Young, B. A. Garcia, and D. Reinberg, "Asymmetrically modified nucleosomes," *Cell*, vol. 151, pp. 181–193, 9 2012.

[88] E. Shema, D. Jones, N. Shoresh, L. Donohue, O. Ram, and B. E. Bernstein, "Single-molecule decoding of combinatorially modified nucleosomes," *Science*, vol. 352, pp. 717–721, 05 2016.

[89] P. Dawson, T. Muir, I. Clark-Lewis, and S. Kent, "Synthesis of proteins by native chemical ligation," *Science*, vol. 266, pp. 776–779, Nov. 1994.

[90] P. E. Dawson and S. B. H. Kent, "Synthesis of native proteins by chemical ligation," *Annual Review of Biochemistry*, vol. 69, pp. 923–960, 2016/08/31 2000.

[91] M. A. Shogren-Knaak, C. J. Fry, and C. L. Peterson, "A native peptide ligation strategy for deciphering nucleosomal histone modifications," *Journal of Biological Chemistry*, vol. 278, pp. 15744–15748, May 2003.

[92] M. Q. Xu and F. B. Perler, "The mechanism of protein splicing and its modulation by mutation.," *The EMBO Journal*, vol. 15, pp. 5146–5153, 10 1996.

[93] Y. Li, "Split-inteins and their bioapplications," *Biotechnology Letters*, vol. 37, no. 11, pp. 2121–2137, 2015.

[94] J. H. Appleby, K. Zhou, G. Volkmann, and X.-Q. Liu, "Novel split intein for trans-splicing synthetic peptide onto c terminus of protein," *Journal of Biological Chemistry*, vol. 284, no. 10, pp. 6194–6199, 2009.

[95] Y. David, M. Vila-Perelló, S. Verma, and T. W. Muir, "Chemical tagging and customizing of cellular chromatin states using ultrafast trans-splicing inteins," *Nat Chem*, vol. 7, pp. 394–402, May 2015.

[96] J. H. Appleby-Tagoe, I. V. Thiel, Y. Wang, Y. Wang, H. D. Mootz, and X.-Q. Liu, "Highly efficient and more general cis- and trans-splicing inteins through sequential directed evolution," *Journal of Biological Chemistry*, vol. 286, pp. 34440–34447, Sept. 2011.

[97] C. Ludwig, M. Pfeiff, U. Linne, and H. D. Mootz, "Ligation of a synthetic peptide to the n terminus of a recombinant protein using semisynthetic protein trans-splicing," *Angewandte Chemie International Edition*, vol. 45, no. 31, pp. 5218–5221, 2006.

[98] H. Mao, S. A. Hart, A. Schink, and B. A. Pollok, "Sortase-mediated protein ligation: A new method for protein engineering," *J. Am. Chem. Soc.*, vol. 126, pp. 2670–2671, Feb. 2004.

[99] K. Piotukh, B. Geltinger, N. Heinrich, F. Gerth, M. Beyermann, C. Freund, and D. Schwarzer, "Directed evolution of sortase a mutants with altered substrate selectivity profiles," *J. Am. Chem. Soc.*, vol. 133, pp. 17536–17539, Oct. 2011.

[100] N. Nady, J. Min, M. S. Kareta, F. Chédin, and C. H. Arrowsmith, "A spot on the chromatin landscape? histone peptide arrays as a tool for epigenetic research," *Trends in Biochemical Sciences*, vol. 33, pp. 305–313, 7 2008.

[101] R. Frank, "The spot-synthesis technique: Synthetic peptide arrays on membrane supports—principles and applications," *Journal of Immunological Methods*, vol. 267, pp. 13–26, 9 2002.

[102] A. ESPEJO, J. CÔTÉ, A. BEDNAREK, S. RICHARD, and M. T. BEDFORD, "A protein-domain microarray identifies novel protein–protein interactions," *Biochemical Journal*, vol. 367, p. 697, 11 2002.

[103] J. Kim, J. Daniel, A. Espejo, A. Lake, M. Krishna, L. Xia, Y. Zhang, and M. T. Bedford, "Tudor, mbt and chromo domains gauge the degree of lysine methylation," *EMBO reports*, vol. 7, p. 397, 01 2006.

[104] N. Gauthier, M. Caron, L. Pedro, M. Arcand, J. Blouin, A. Labonté, C. Normand, V. Paquet, A. Rodenbrock, M. Roy, N. Rouleau, L. Beaudet, J. Padrós, and R. Rodriguez-Suarez, "Development of homogeneous nonradioactive methyltransferase and demethylase assays targeting histone h3 lysine 4," *Journal of Biomolecular Screening*, vol. 17, no. 1, pp. 49–58, 2012.

[105] A. M. Quinn, A. Allali-Hassani, M. Vedadi, and A. Simeonov, "A chemiluminescence-based method for identification of histone lysine methyltransferase inhibitors," *Molecular BioSystems*, vol. 6, no. 5, pp. 782–788, 2010.

[106] A. Kawamura, A. Tumber, N. R. Rose, O. N. F. King, M. Daniel, U. Oppermann, T. D. Heightman, and C. Schofield, "Development of homogeneous luminescence assays for histone demethylase catalysis and binding," *Analytical Biochemistry*, vol. 404, pp. 86–93, 9 2010.

[107] A. L. Garske, G. Craciun, and J. M. Denu, "A combinatorial h4 tail library for exploring the histone code," *Biochemistry*, vol. 47, pp. 8094–8102, 08 2008.

[108] A. L. Garske, S. S. Oliver, E. K. Wagner, C. A. Musselman, G. LeRoy, B. A. Garcia, T. G. Kutateladze, and J. M. Denu, "Combinatorial profiling of chromatin binding modules reveals multisite discrimination," *Nat Chem Biol*, vol. 6, pp. 283–290, Apr. 2010.

[109] M. S. Eram, E. Kuznetsova, F. Li, E. Lima-Fernandes, S. Kennedy, I. Chau, C. H. Arrowsmith, M. Schapira, and M. Vedadi, "Kinetic characterization of human histone h3 lysine 36 methyltransferases, ash1l and setd2," *Biochimica et Biophysica Acta (BBA) - General Subjects*, vol. 1850, pp. 1842–1848, 9 2015.

[110] M. Nikolov, A. Stützer, K. Mosch, A. Krasauskas, S. Soeroes, H. Stark, H. Urlaub, and W. Fischle, "Chromatin affinity purification and quantitative mass spectrometry defining the interactome of histone modification patterns," *Molecular & Cellular Proteomics*, vol. 10, no. 11, 2011.

[111] M. Mann, “Functional and quantitative proteomics using silac,” *Nat Rev Mol Cell Biol*, vol. 7, pp. 952–958, 12 2006.

[112] T. Bartke, M. Vermeulen, B. Xhemalce, S. C. Robson, M. Mann, and T. Kouzarides, “Nucleosome-interacting proteins regulated by dna and histone methylation,” *Cell*, vol. 143, pp. 470–484, 10 2010.

[113] R. Noberini, G. Sigismondo, and T. Bonaldi, “The contribution of mass spectrometry-based proteomics to understanding epigenetics,” *Epigenomics*, vol. 8, pp. 429–445, 2016/08/30 2015.

[114] P. N. I. Lau and P. Cheung, “Elucidating combinatorial histone modifications and crosstalks by coupling histone-modifying enzyme with biotin ligase activity,” *Nucleic Acids Research*, vol. 41, no. 3, p. e49, 2013.

[115] U. T. T. Nguyen, L. Bittova, M. M. Müller, B. Fierz, Y. David, B. Houck-Loomis, V. Feng, G. P. Dann, and T. W. Muir, “Accelerated chromatin biochemistry using DNA-barcoded nucleosome libraries,” *Nature Methods*, vol. 11, pp. 834–840, Jul 2014.

[116] L. Wang, C. Mizzen, C. Ying, R. Candau, N. Barlev, J. Brownell, C. D. Allis, and S. L. Berger, “Histone acetyltransferase activity is conserved between yeast and human gcn5 and is required for complementation of growth and transcriptional activation.,” *Molecular and Cellular Biology*, vol. 17, no. 1, pp. 519–27, 1997.

[117] J. Sambrook and D. W. Russel, *Molecular Cloning*. Cold Spring Harbor Laboratory Press, 3 ed., 2001.

[118] J. Sambrook and D. W. Russell, “Preparation and transformation of competent e. coli using calcium chloride,” *Cold Spring Harbor Protocols*, vol. 2006, no. 1, p. pdb.prot3932, 2006.

[119] J. Sambrook and D. W. Russell, “Agarose gel electrophoresis,” *Cold Spring Harbor Protocols*, vol. 2006, no. 1, p. pdb.prot4020, 2006.

[120] M. F. Carey, C. L. Peterson, and S. T. Smale, “Pcr-mediated site-directed mutagenesis,” *Cold Spring Harbor Protocols*, vol. 2013, no. 8, p. pdb.prot076505, 2013.

[121] A. N. Vallejo, R. J. Pogulis, and L. R. Pease, “Pcr mutagenesis by overlap extension and gene soe,” *Cold Spring Harbor Protocols*, vol. 2008, no. 2, p. pdb.prot4861, 2008.

[122] P. Lowary and J. Widom, “New dna sequence rules for high affinity binding to histone octamer and sequence-directed nucleosome positioning,” *Journal of Molecular Biology*, vol. 276, pp. 19–42, Feb. 1998.

[123] C. Mülhardt, *Einige grundlegende Methoden*, pp. 12–46. Heidelberg: Spektrum Akademischer Verlag, 2009.

[124] E.Gasteiger, C. Hoogland, A. Gattiker, S. Duvaud, M. Wilkins, R. Appel, and A. Bairoch, *The Proteomics Protocols Handbook*, ch. Protein Identification and Analysis Tools on the ExPASy Server, pp. 571–607. Humana Press, 2005.

[125] R. J. Simpson, “Sds-page of proteins,” *Cold Spring Harbor Protocols*, vol. 2006, no. 1, p. pdb.prot4313, 2006.

[126] R. J. Simpson, “Staining proteins in gels with coomassie blue,” *Cold Spring Harbor Protocols*, vol. 2007, no. 4, p. pdb.prot4719, 2007.

[127] H. Towbin, T. Staehelin, and J. Gordon, “Electrophoretic transfer of proteins from polyacrylamide gels to nitrocellulose sheets: procedure and some applications.,” *Proceedings of the National Academy of Sciences of the United States of America*, vol. 76, pp. 4350–4354, 09 1979.

[128] K. Luger, T. J. Rechsteiner, A. J. Flaus, M. M. Y. Waye, and T. J. Richmond, “Characterization of nucleosome core particles containing histone proteins made in bacteria1,” *Journal of Molecular Biology*, vol. 272, pp. 301–311, 9 1997.

[129] P. Dyer, R. Edayathumangalam, C. White, Y.Bao, S.Chakravarthy, U. Muthurajan, and K. Luger, *Chromatin and Chromatin Remodeling Enzymes 'Reconstitution of Nucleosome Core Particle from recombinant Histones and DNA'*, vol. 375. Elsevier Academic Press, 2004.

[130] L. Papula, *Mathematik für Ingenieure und Naturwissenschaftler*, vol. 3. Vieweg + Teubner Verlag, 2011.

[131] A. Stützer, S. Liokatis, A. Kiesel, D. Schwarzer, R. Sprangers, J. Söding, P. Selenko, and W. Fischle, “Modulations of dna contacts by linker histones and post-translational modifications determine the mobility and modifiability of nucleosomal h3 tails,” *Molecular Cell*, vol. 61, pp. 247–259, 1 2016.

[132] A. Thåström, P. T. Lowary, H. R. Widlund, H. Cao, M. Kubista, and J. Widom, “Sequence motifs and free energies of selected natural and non-natural nucleosome positioning dna sequences1,” *Journal of Molecular Biology*, vol. 288, pp. 213–229, 4 1999.

[133] P. Weber, D. Ohlendorf, J. Wendoloski, and F. Salemme, “Structural origins of high-affinity biotin binding to streptavidin,” *Science*, vol. 243, p. 85, 01 1989.

[134] K. Luger, T. J. Rechsteiner, and T. J. Richmond, “Preparation of nucleosome core particle from recombinant histones,” *Methods in Enyzmology*, vol. 304, 1999.

[135] M. A. Rizzo, G. H. Springer, B. Granada, and D. W. Piston, “An improved cyan fluorescent protein variant useful for fret,” *Nat Biotech*, vol. 22, pp. 445–449, 04 2004.

[136] R. B. Mujumdar, L. A. Ernst, S. R. Mujumdar, C. J. Lewis, and A. S. Waggoner, “Cyanine dye labeling reagents: Sulfoindocyanine succinimidyl esters,” *Bioconjugate Chemistry*, vol. 4, pp. 105–111, 03 1993.

[137] N. C. Shaner, P. A. Steinbach, and R. Y. Tsien, “A guide to choosing fluorescent proteins,” *Nat Meth*, vol. 2, pp. 905–909, 12 2005.

[138] P. A. Grant, L. Duggan, J. Côté, S. M. Roberts, J. E. Brownell, R. Candau, R. Ohba, T. Owen-Hughes, C. D. Allis, F. Winston, S. L. Berger, and J. L. Workman, “Yeast gcn5 functions in two multisubunit complexes to acetylate nucleosomal histones: characterization of an ada complex and the saga (spt/ada) complex.,” *Genes & Development*, vol. 11, no. 13, pp. 1640–1650, 1997.

[139] C. Crosio, G. M. Fimia, R. Loury, M. Kimura, Y. Okano, H. Zhou, S. Sen, C. D. Allis, and P. Sassone-Corsi, “Mitotic phosphorylation of histone h3: Spatio-temporal regulation by mammalian aurora kinases,” *Molecular and Cellular Biology*, vol. 22, pp. 874–885,

Oct. 2001.

[140] A. Mádi, L. Kárpáti, A. Kovács, L. Muszbek, and L. Fésüs, "High-throughput scintillation proximity assay for transglutaminase activity measurement," *Analytical Biochemistry*, vol. 343, pp. 256–262, 8 2005.

[141] G.-J. Kremers, J. Goedhart, E. B. van Munster, and T. W. J. Gadella, "Cyan and yellow super fluorescent proteins with improved brightness, protein folding, and fret förster radius,," *Biochemistry*, vol. 45, pp. 6570–6580, 05 2006.

[142] Y. Arita, S. Kihara, N. Ouchi, M. Takahashi, K. Maeda, J.-i. Miyagawa, K. Hotta, I. Shimomura, T. Nakamura, K. Miyaoka, H. Kuriyama, M. Nishida, S. Yamashita, K. Okubo, K. Matsubara, M. Muraguchi, Y. Ohmoto, T. Funahashi, and Y. Matsuzawa, "Paradoxical decrease of an adipose-specific protein, adiponectin, in obesity," *Biochemical and Biophysical Research Communications*, vol. 257, no. 1, pp. 79–83, 1999.

[143] E. Engvall and P. Perlmann, "Enzyme-linked immunosorbent assay (elisa) quantitative assay of immunoglobulin g," *Immunochemistry*, vol. 8, no. 9, pp. 871–874, 1971.

[144] D. O. Cohen, S. Duchin, M. Feldman, R. Zarivach, A. Aharoni, and D. Levy, "Engineering of methylation state specific 3xmbt domain using elisa screening," *PLoS ONE*, vol. 11, pp. e0154207–, 04 2016.

[145] K.-Y. Lee, K. Ito, R. Hayashi, E. P. I. Jazrawi, P. J. Barnes, and I. M. Adcock, "Nf-κb and activator protein 1 response elements and the role of histone modifications in il-1β-induced tgf-β1 gene transcription," *The Journal of Immunology*, vol. 176, pp. 603–615, 01 2006.

[146] W. Lai, Q. Wei, J. Zhuang, M. Lu, and D. Tang, "Fenton reaction-based colorimetric immunoassay for sensitive detection of brevetoxin b," *Biosensors and Bioelectronics*, vol. 80, pp. 249–256, 6 2016.

[147] R. de la Rica and M. M. Stevens, "Plasmonic elisa for the detection of analytes at ultralow concentrations with the naked eye," *Nat. Protocols*, vol. 8, pp. 1759–1764, 09 2013.

[148] P. Gribbon and A. Sewing, "Fluorescence readouts in hts: no gain without pain?," *Drug Discovery Today*, vol. 8, pp. 1035–1043, Nov. 2003.

[149] M. L. Schmitt, K. I. Ladwein, L. Carlino, J. Schulz-Fincke, D. Willmann, E. Metzger, P. Schilcher, A. Imhof,Äâ, R. Schüle, W. Sippl, and M. Jung, "Heterogeneous antibody-based activity assay for lysine specific demethylase 1 (lsd1) on a histone peptide substrate," *Journal of Biomolecular Screening*, vol. 19, no. 6, pp. 973–978, 2014.

[150] K. Dobslaff and T. Zuchner, "Application of time-resolved fluorescence for imaging-based multisample and multianalyte detection in single microtiter wells," *Analytical and Bioanalytical Chemistry*, vol. 406, no. 28, pp. 7205–7212, 2014.

[151] M. Schiedel, M. Marek, J. Lancelot, B. Karaman, I. Almlöf, J. Schultz, W. Sippl, R. J. Pierce, C. Romier, and M. Jung, "Fluorescence-based screening assays for the nad+-dependent histone deacetylase smsirt2 from schistosoma mansoni," *Journal of Biomolecular Screening*, vol. 20, no. 1, pp. 112–121, 2015.

[152] C. Roselle, T. Verch, and M. Shank-Retzlaff, “Mitigation of microtiter plate positioning effects using a block randomization scheme,” *Analytical and Bioanalytical Chemistry*, vol. 408, no. 15, pp. 3969–3979, 2016.

[153] Y. Mishima, M. Watanabe, T. Kawakami, C. D. Jayasinghe, J. Otani, Y. Kikugawa, M. Shirakawa, H. Kimura, O. Nishimura, S. Aimoto, S. Tajima, and I. Suetake, “Hinge and chromoshadow of hp1αparticipate in recognition of k9 methylated histone h3 in nucleosomes,” *Journal of Molecular Biology*, vol. 425, pp. 54–70, 1 2013.

[154] D. Canzio, E. Y. Chang, S. Shankar, K. M. Kuchenbecker, M. D. Simon, H. D. Madhani, G. J. Narlikar, and B. Al-Sady, “Chromodomain-mediated oligomerization of hp1 suggests a nucleosome-bridging mechanism for heterochromatin assembly,” *Molecular Cell*, vol. 41, pp. 67–81, 1 2011.

[155] T. Zhao, T. Heyduk, C. D. Allis, and J. C. Eissenberg, “Heterochromatin protein 1 binds to nucleosomes and dna in vitro,” *Journal of Biological Chemistry*, vol. 275, pp. 28332–28338, 09 2000.

[156] F. Munari, S. Soeroes, H. M. Zenn, A. Schomburg, N. Kost, S. Schröder, R. Klingberg, N. Rezaei-Ghaleh, A. Stützer, K. A. Gelato, P. J. Walla, S. Becker, D. Schwarzer, B. Zimmermann, W. Fischle, and M. Zweckstetter, “Methylation of lysine 9 in histone h3 directs alternative modes of highly dynamic interaction of heterochromatin protein hhp1$\beta$with the nucleosome,” *Journal of Biological Chemistry*, vol. 287, pp. 33756–33765, 09 2012.

[157] M. L. Markwardt, G.-J. Kremers, C. A. Kraft, K. Ray, P. J. C. Cranfill, K. A. Wilson, R. N. Day, R. M. Wachter, M. W. Davidson, and M. A. Rizzo, “An improved cerulean fluorescent protein with enhanced brightness and reduced reversible photoswitching,” *PLoS ONE*, vol. 6, pp. e17896–, 03 2011.

[158] J. Goedhart, L. van Weeren, M. A. Hink, N. O. E. Vischer, K. Jalink, and T. W. J. Gadella, “Bright cyan fluorescent protein variants identified by fluorescence lifetime screening,” *Nat Meth*, vol. 7, pp. 137–139, 02 2010.

[159] F. Turlais, A. Hardcastle, M. Rowlands, Y. Newbatt, A. Bannister, T. Kouzarides, P. Workman, and G. Aherne, “High-throughput screening for identification of small molecule inhibitors of histone acetyltransferases using scintillating microplates (flashplate),” *Analytical Biochemistry*, vol. 298, pp. 62–68, Nov. 2001.

[160] C. Bian, C. Xu, J. Ruan, K. K. Lee, T. L. Burke, W. Tempel, D. Barsyte, J. Li, M. Wu, B. O. Zhou, B. E. Fleharty, A. Paulson, A. Allali‚ÄêHassani, J. Zhou, G. Mer, P. A. Grant, J. L. Workman, J. Zang, and J. Min, “Sgf29 binds histone h3k4me2/3 and is required for saga complex recruitment and histone h3 acetylation,” *The EMBO Journal*, vol. 30, pp. 2829–2842, 06 2011.

[161] W.-S. Lo, R. C. Trievel, J. R. Rojas, L. Duggan, J.-Y. Hsu, C. Allis, R. Marmorstein, and S. L. Berger, “Phosphorylation of serine 10 in histone h3 is functionally linked in vitro and in vivo to gcn5-mediated acetylation at lysine 14,” *Molecular Cell*, vol. 5, pp. 917–926, June 2000.

[162] M. Vermeulen, H. C. Eberl, F. Matarese, H. Marks, S. Denissov, F. Butter, K. K. Lee, J. V. Olsen, A. A. Hyman, H. G. Stunnenberg, and M. Mann, “Quantitative interaction

proteomics and genome-wide profiling of epigenetic histone marks and their readers," *Cell*, vol. 142, pp. 967–980, 9 2010.

[163] C. FRY, M. SHOGREN-KNAAK, and C. PETERSON, "Histone h3 amino-terminal tail phosphorylation and acetylation: Synergistic or independent transcriptional regulatory marks?," *Cold Spring Harbor Symposia on Quantitative Biology*, vol. 69, pp. 219–226, 2004.

[164] S. Liokatis, A. Stützer, S. J. Elsässer, F.-X. Theillet, R. Klingberg, B. van Rossum, D. Schwarzer, C. D. Allis, W. Fischle, and P. Selenko, "Phosphorylation of histone h3 ser10 establishes a hierarchy for subsequent intramolecular modification events," *Nat Struct Mol Biol*, vol. 19, pp. 819–823, 08 2012.

[165] A. Sawicka, D. Hartl, M. Goiser, O. Pusch, R. R. Stocsits, I. M. Tamir, K. Mechtler, and C. Seiser, "H3s28 phosphorylation is a hallmark of the transcriptional response to cellular stress," *Genome Research*, vol. 24, no. 11, pp. 1808–1820, 2014.

[166] D. Shechter, H. L. Dormann, C. D. Allis, and S. B. Hake, "Extraction, purification and analysis of histones," *Nat. Protocols*, vol. 2, pp. 1445–1457, 06 2007.

[167] C. Mittal, M. J. Blacketer, and M. A. Shogren-Knaak, "Nucleosome acetylation sequencing to study the establishment of chromatin acetylation," *Analytical Biochemistry*, vol. 457, pp. 51–58, 7 2014.

[168] C. D. Allis and T. Jenuwein, "The molecular hallmarks of epigenetic control," *Nat Rev Genet*, vol. 17, pp. 487–500, 08 2016.

Appendix

Additional information and figures

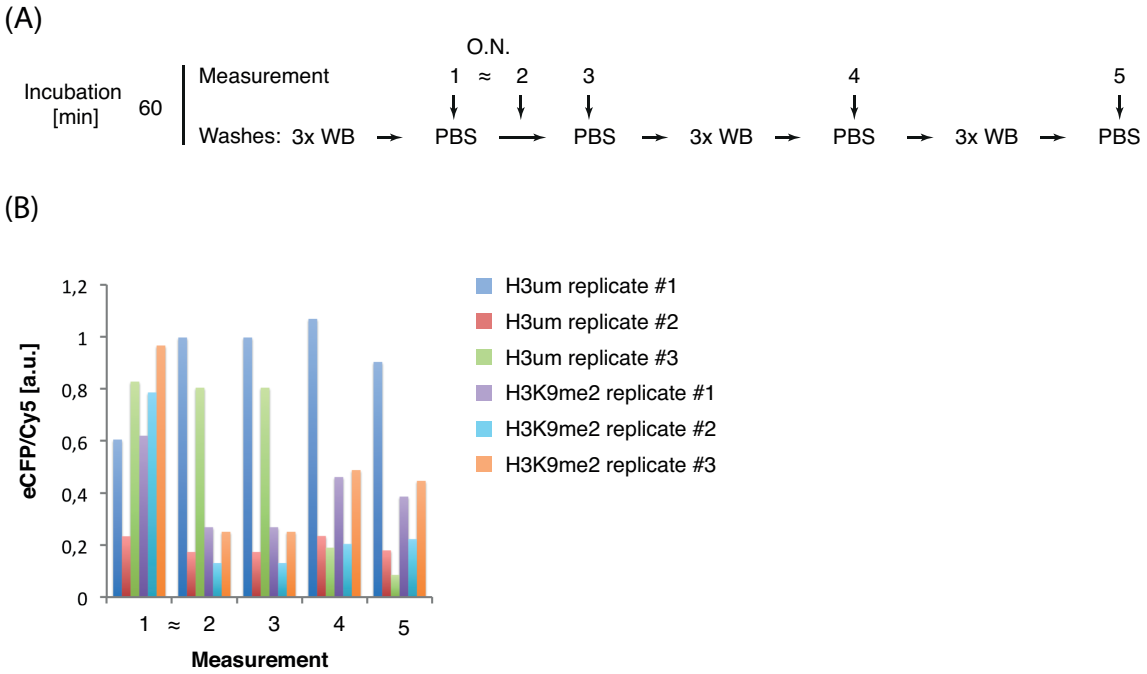

Figure 5.1: Impact of wash steps on eCFP-HP1 incubation with H3um- and H3K9me2-NCP for 60 min

(A) Schematic representation of experimental set up: eCFP-HP1 was removed after 60 min of incubation with n=3 wells per incubation time. Fluorescence measurement took place in PBS with high salt and detergent containing wash steps in between, as indicated. (B) Influence of washes on eCFP-HP1 recruitment normalized with respect to NCP content for all replicates with 60 min incubation time. The replicate H3um #1 shows resistance to all wash steps, thus this replicate was removed from analysis.

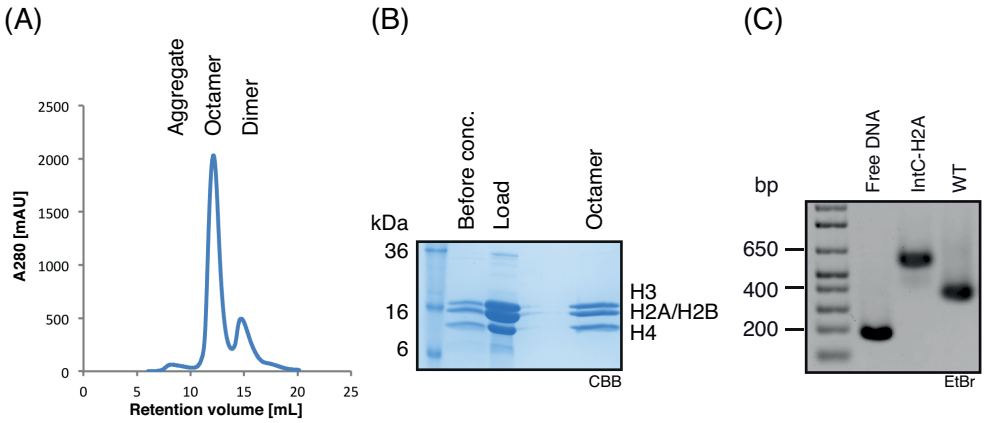

Figure 5.2: Assembly of wild type octamer and NCP

(A) Elution profile of size exclusion chromatography using HiLoad Superdex200 10/300 PG column for the purification of *in vitro* assembled wild type histone octamer. (B) Analysis of octamer input before concentration and after concentration (Load) for injection onto the column, pooled octamer fractions were analyzed by SDS-PAGE and subsequent CBB staining. (C) Native agarose gel electrophoresis of wWT- and IntC-H2A-NCP stained with EtBr.

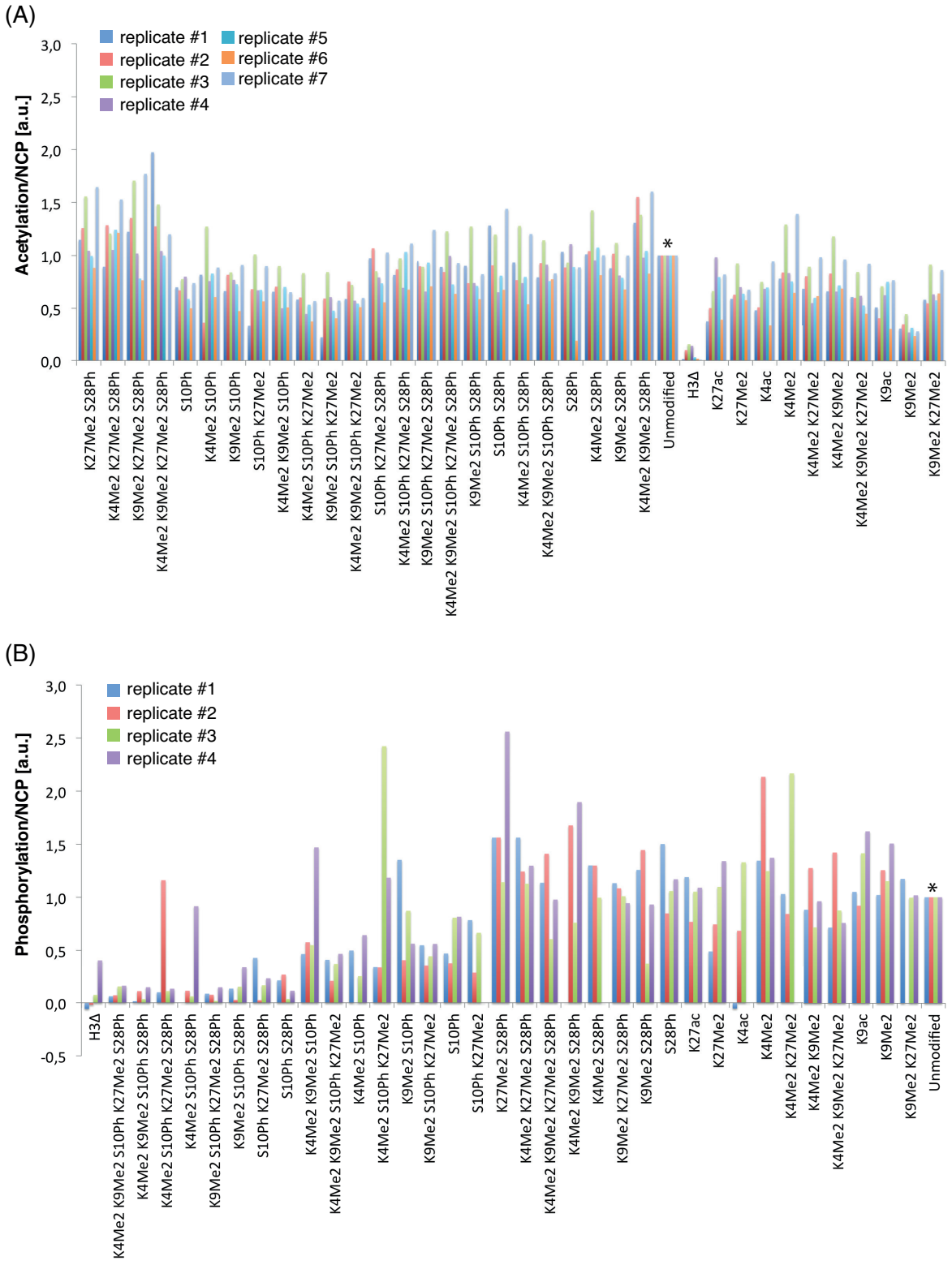

Figure 5.3: Replicates of HAT and kinase assay
All replicates of HAT (A) and kinase (B) assay normalized to H3um-NCP (Unmodified, $*$).